



UNIVERSITÀ DELLA CALABRIA

Facoltà di Farmacia
e Scienze della Nutrizione e della Salute

Dottorato di Ricerca in
METODOLOGIE PER LO SVILUPPO DI MOLECOLE DI
INTERESSE FARMACOLOGICO *XXIII ciclo*
S.S.D. CHIM/08

*Design and Quality control of drugs of natural and synthetic
origin.*

Coordinator
Prof. Bartolo Gabriele

Supervisor
Prof. Gaetano Ragno

Ph.D. Student
Filomena Oliverio

Anno Accademico 2009/2010

Index

Introduction	4
1. Prediction of photosensitivity of 1,4-dihydropyridine antihypertensives by quantitative structure property relationship	5
1.1. Photodegradation Tests	8
1.2. Studied Drugs And Experimental Methodology	9
1.3. Descriptors	10
1.4. Software	12
1.5. Results and Discussion	13
1.6. Conclusions	29
For more details:	30
2. Different photodegradation behavior of barnidipine under natural and forced irradiation	37
2.1. Drug and Experimental Methodology	39
2.2. Results and Discussion	43
2.3. Conclusions	63
For more details:	64
3. A chemometric model for assessment of real drug photodegradation from forced test	67
3.1. Drugs and Photodegradation Kinetics	70
3.2. Results and Discussion	70
3.3. Multivariate Model	78
3.4. Conclusions	86
For more details:	87
4. Kinetic studies of nitrofurazone photodegradation by multivariate curve resolution applied to UV-spectral data	88
4.1. Drug and Experimental Procedure	91
4.2. Chemometric Techniques	93
4.3. Results and Discussion	98
4.4. Conclusions	112
For more details:	113
5. Application of multivariate curve resolution (MCR) to the spectrophotometric study of the melatonin photodegradation	118
5.1. Drug and Experimental Procedures	120
5.2. Applied Chemometry	121
5.3. Results and Discussion	126
For more details:	134
6. Multivariate calibration techniques applied to derivative spectroscopy data for the analysis of pharmaceutical mixtures	138
6.1. Drugs and Experimental Method	141
6.2. Chemometric Techniques	143
6.3. Results and Discussion	146
6.4. Conclusions	167

For more details:.....	169
7. Artificial neural network combined with principal component analysis (ANN-PCA) for resolution of complex pharmaceutical formulations ..	174
7.1. Chemometric Techniques	177
7.2. Drug and Experimental Method	180
7.3. Results and Discussion	182
For more details:.....	196
8. Naproxen as a Photoactive Probe within Liposomes Microenvironment. Retarded Photooxidation by Included Cholesterol.	
.....	200
8.1. Drug and Experimental Procedures	202
8.2. Results and Discussion	206
8.3. Conclusions	215
For more details:.....	216

Introduction

Proper storage of drugs is important to maintain the characteristics throughout the period of validity indicated on the package. Stability is an essential requirement because the drugs could have a loss in the expected pharmacological activity. According to the Italian Pharmacopoeia, "A drug is considered stable when, in a given period of time, its essential properties do not change or change within tolerable limits, if stored in a suitable vessel, under defined temperature, humidity and exposure to light."

In 1987, a detailed guidance on the stability study of new active products has been issued. It was prepared by the International ICH (International Conference on Harmonization) and is currently implemented in Europe, Japan, Canada and USA, and at least subject to consultation with other countries. The guidelines provide a general indication on the requirements for stability testing, but leave enough flexibility to meet the variety of different scientific situations and characteristics of various materials to be evaluated.

Light has been recognized as one of the most important external factors in drug instability and new compounds are regularly added to the list of photolabile drugs. The first effect from the photodegradation of most of drugs consists in the loss of their pharmacological activity, but several cases involving the formation of toxic degradation products are known.

So, my interest during the three years of PhD has been directed towards the photostability of drugs with particular

attention to the 1,4-dihydropyridines, a class of calcium antagonists used against hypertension and angina.

The last period of work has been dedicated to the quality assurance of drugs and pharmaceutical formulations. Chemometric algorithms and spectrophotometric analysis were applied in order to perform the monitoring of drugs, and the photostabilization of drugs by incorporating them in liposomal matrices. This part of the work was developed during one year of foreign stage spent at the Universidad Politecnica de Valencia (Instituto de Tecnologia Quimica), Spain.

1. Prediction of photosensitivity of 1,4-dihydropyridine antihypertensives by quantitative structure property relationship

Quantitative Structure-Property Relationships (QSPR) techniques help to establish a correlation between the molecular structures and chemical or chemical-physics properties of a congeneric series. In the last years, QSPR approach has been investigated in various fields of chemistry, biochemistry, pharmacy and environmental chemistry [1]. In the modern pharmaceutical chemistry, the prediction of required properties of new molecules plays a very important role throughout the overall drug design. The up-to-date techniques pursue this target by means of a mathematical model. A QSPR relationship can be used to identify the parameters affecting a specific property of the molecules or to predict the same property for other molecules belonging to the series [2-3].

Elaboration of a reliable and robust experimental relationship represents the real core in a QSPR analysis [4]. An empirical equation in a QSPR model is generally expressed as:

$$f(P) = \sum_{i=1, j=1}^{i=n, j=m} a_{ij} D_{ij} + b$$

where P is the property of interest; a_{ij} and b are the regression coefficients, D_{ij} are parameters characterizing each molecular structure of the series, named descriptors [5].

The selection of the descriptors represents an essential step in improving the quality of the model. This choice has become more

and more demanding because of the high number of descriptors proposed in literature [6]. The most common descriptors are constitutional or topological parameters explaining the number of carbon atoms or the chemical bonds in the molecules. Another important series of chemical descriptors, namely quantum descriptors, define the electronic and geometric properties of the molecules and their interactions [5]. Recently, a quantum chemical approach has been used to determine energetic information of the molecules and, in particular, to define the minimum energy configuration [3].

In a QSPR elaboration, it is difficult to establish as well if a chemical group can lead a significant variation on the different properties in a congeneric series. Moreover, it is daring to take as a reference the data of analogue works in literature because a substituent can give an important effect into a class of compounds and have no effect in another class [4]. The continuous development of chemometric techniques has represented in the last years a very important support to the elaboration of QSPR models. Principal Component Analysis (PCA), Partial Least Squares (PLS) and Analysis of Variance (ANOVA) have proved to be very useful tools in testing a high number of variables and then in selecting those that significantly influence the system. This approach has permitted the building of complex QSPR models, characterized by high prediction power [7-14].

In our work, a set of nine 1,4-dihydropyridine (1,4-DHP) antihypertensive drugs, Amlodipine (AML), Felodipine (FEL), Lercanidipine (LER), Nisoldipine (NIS), Nitrendipine (NIT),

Nicardipine (NIC), Nifedipine (NIF), Manidipine (MAN), Nimodipine (NIM) has been submitted to a QSPR study. 1,4-DHP drugs are calcium antagonist agents largely used in the treatment of cardiovascular disorders, above all hypertension and cardiac arrhythmias [15-18]. Unfortunately, a feature common of all compounds of this class is the high photosensitivity. Light catalyzes their oxidation to pyridine derivatives, lacking in therapeutic effect [19-23] and, in some cases, to secondary photoproducts [24-26]. Aromatization of 1,4-DHP has also attracted considerable attention recently because it has been demonstrated that metabolism of those drugs involves an analogous cytochrome P-450 catalyzed oxidation in the liver [27].

Our work aims at defining a correlation between the photodegradation rate of 1,4-DHP drugs and their chemical structure by means of QSPR modeling. The successful application of the model in predicting the light sensitivity of related compounds, or in designing new congeners with a potential high photostability, represents the final target.

Contributes about the application of QSPR analysis to photodegradation studies have been published. An interesting QSPR model for predicting the photodegradation rate of chlorinated polycyclic aromatic hydrocarbons has been proposed [28]. A set of quantum chemical descriptors has been adopted to develop QSPR models for estimation of photodegradation half-lives of persistent organic pollutants [28-29]. Structural descriptors have been used to build a QSPR relationship used in the study of photolysis mechanisms [30].

Quantitative Structure-Activity Relationship (QSAR) analysis has been applied to the 1,4-DHP class to establish the calcium channel antagonist activity as a function of some theoretically derived descriptors [31-32]. In particular, the binding of the molecules to the receptor has been expressed by topology, hydrophobicity and surface area descriptors [32].

The our QSPR study was supported by multivariate regression techniques, because of their ability in computing a high number of variables. In particular, a PCA elaboration followed by PLS regression was applied to both experimental and calculated data with the aim to select a number of predictors furnishing the most useful information to define a well-fitted multivariate model.

With the aim to use homogeneous results in the model building, the photodegradation process was standardized, by performing light exposure according to the international rules [33].

1.1. Photodegradation Tests

Absorption spectra were registered on the λ range of 190 – 450 nm in a 10 mm quartz cell by means of a Perkin-Elmer Lambda 40P Spectrophotometer at the following conditions: scan rate 1 nm s⁻¹; time response 1 s; spectral band 1 nm. The software UV Winlab 2.79.01 (Perkin-Elmer) was used for spectral acquisition and elaboration.

Drugs photodegradation was carried out according to the “Guide for the Photostability Testing of New Drug Substances and Products” recommended by the International Conference on Harmonization of Technical Requirements for Registration of

Pharmaceuticals for Human Use [33].

Light exposure was performed in a light cabinet Suntest CPS+ (Heraeus, Milan, Italy), equipped with a Xenon lamp. The apparatus was fitted up with an electronic device for irradiation and temperature measuring and controlling inside the box. The system was able to closely simulate sunlight and to appropriately select spectral regions by interposition of filters.

1.2. Studied Drugs And Experimental Methodology

The study has been performed by using a set of nine drugs for elaboration of the QSPR model and then other two drugs for the validation study. A series of standard solutions of each analyte in ethanol was prepared and used to set up the calibration curves. These relationships were used to carry out the drug concentration. Solute concentration was within the range 5.0–50.0 µg/ml for all the compounds. The drug solutions (20 µg/ml), in a quartz cuvette perfectly stoppered, were directly light irradiated in a λ range between 300 and 800 nm, by means of a glass filter, according to the ID65 standard of the ICH rules; the power was maintained to 350 W/m², corresponding to a light dose of 21 kJ/min·m², at the constant temperature of 25 °C. The UV spectra, just after preparation (t = 0) and at the following times: 2, 5, 8, 10, 15, 20, 30, 45, 60, 90, 120, 180, 300 min, were recorded.

The irradiation conditions were maintained to a moderate level because of the high sensitivity of the drugs to light, allowing

so to obtain a more accurate control on the photodegradation processes.

1.3. Descriptors

A large number of molecular descriptors in setting the calibration set were screened using multivariate techniques. PLS analysis was adopted to select the descriptors significantly correlated with the photosensitivity of the studied molecules. Six descriptors, representative of the chemical features, emerged as the most responsible for the photosensitivity of the studied drugs: molecular volume (MV), hydrophobic constant of Hansch-Fujita (π_x), polar surface area (PSA), H bond donors (HDon), H bond acceptors (HAcc) and Octanol/Water Partition Coefficient (XlogP).

1.3.1. Molecular volume (MV)

The volume of a molecule has a clearly conventional character and it is used sometimes as a molecular index in QSAR equations [34]. MV can also be employed as a measure of molecular similarity and help in understanding the steric requirements of a receptor.

1.3.2. Hydrophobic constant of Hansch-Fujita (π_x)

The hydrophobic constant of Hansch-Fujita describes the contribution of a substituent to the lipophilicity of a compound and is defined as:

$$\pi_x = \log P(RX) - \log P(RH)$$

where R is the molecular residue and X is the substituent. $\pi_H = 0$ is the hydrophobic constant for hydrogen and it is used as referent. This predictor has a positive value if the substituent is hydrophobic and a negative value if the substituent is hydrophilic [35]. This constant must be also calculated for the entire molecule because it is influenced by the overall hydrophobicity from the compound. The sum of the π_X constants of the substituents in a molecule represents the global descriptor of hydrophobicity for a molecule [36].

1.3.3. Polar surface area (PSA)

PSA of a molecule is used according with the approach developed by Ertl et al. [37] and it is defined as the surface sum over of polar atoms. This molecular descriptor explains the electrostatic and polarization interactions between the solute and the solvent. All the interactions are obviously weak interactions such as higher-multipole interaction, dipole and induced-dipole ones. So, PSA can be considered an important electrostatic descriptor during a QSPR study to understand the charge distribution of the molecules and use this information to project new drugs with desired properties [34].

1.3.4. H bond donors (HDon) and H bond acceptors (HAcc)

Different hydrogen bond donors and acceptors are two important parameters introduced by Lipinski et al. [38] to describe molecular properties important for a drug's pharmacokinetics in

the human body. The availability to form H bonds is an important parameter to define the physic-chemical properties of a drug.

1.3.5. Octanol/Water partition coefficient (XlogP)

logP is a quantitative descriptor of lipophilicity and estimates the propensity of a neutral compound to differentially dissolve in two immiscible phases. It is usually referred to the octanol-water partition coefficient (P), expressed as logarithmic ratio. Hansch's work has started a series of studies about the biological activity varying in relation to the hydrophobic character of a molecule [39-40]. Nowadays, logP is commonly used in QSAR studies and drug design since it relates to drug absorption, bioavailability, metabolism, and toxicity. The calculation of the logP is implemented following the XlogP approach developed by Wang et al. [41]. The XlogP method is an atom-additive method that calculates the octanol/water partition coefficient of neutral organic molecules by summing up atom-based and substructure-based (correction factors) contributions.

1.4. Software

The theoretical descriptors from the chemical structure of the compounds were calculated by means of the Adriana.Code 2.0 software (Molecular Networks GmbH Computerchemie, Erlangen, Germany). This software executes the calculation of physic-chemical descriptors through empirical models for the influence of atoms in molecules and mathematical transformation techniques.

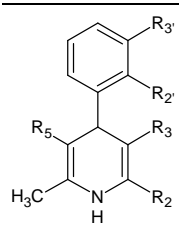
The substituent descriptors were calculated by ACD/ChemSketch 10.0 software (Advanced Chemistry Development, Inc., Toronto, Canada). This software is able to present and manipulate the molecular structure and allows to directly access the electronic substituent constants like hydrophobic constant of Hansch-Fujita and molecular volume.

PLS analysis was performed by application of the algorithms supported by the software “The Unscrambler 9.7” (Camo Process As., Oslo, Norway). This software also allowed to optimize the calibration models and develop validation procedures.

1.5. Results and Discussion

Table 1 summarizes the different chemical groups in the studied drugs. Most of these drugs furnish the pyridine by-product as the only photodegradation product, according with a first-order degradation kinetics [20,42-46]. Nevertheless, after a variable time from this oxidation, secondary photoproducts come from degradation of some molecules as NIF [25], LER [47] and NIS [48].

Table 1. Chemical substituents on the dihydropyridine structures



Drug	R ₂	R ₃	R ₅	R _{2'}	R _{3'}
AML	CH ₂ OCH ₂ CH ₂ NH ₂	COOC ₂ H ₅	COOCH ₃	Cl	H
FEL	CH ₃	COOC ₂ H ₅	COOCH ₃	Cl	Cl
LER	CH ₃	COOC(CH ₃) ₂ CH ₂ N(CH ₃)CH ₂ CH ₂ CH(Ph) ₂	COOCH ₃	H	NO ₂
MAN	CH ₃	COOCH ₂ CH ₂ -piperazin- CH(Ph) ₂	COOCH ₃	H	NO ₂
NIC	CH ₃	COO(CH ₂) ₂ N(CH ₃) CH ₂ Ph	COOCH ₃	H	NO ₂
NIF	CH ₃	COOCH ₃	COOCH ₃	NO ₂	H
NIM	CH ₃	COOCH ₂ CH ₂ OCH ₃	COOCH(CH ₃) ₂	H	NO ₂
NIS	CH ₃	COOCH ₂ CH(CH ₃) ₂	COOCH ₃	NO ₂	H
NIT	CH ₃	COOC ₂ H ₅	COOCH ₃	H	NO ₂

1.5.1. Photodegradation kinetics

As a first step of the work, the drugs were subjected to forced photodegradation under the standard conditions above reported. The sequence of the UV spectra during light irradiation was recorded for each drug solution (20.0 µg/ml). The most of the drugs resulted completely degraded after ten minutes of light irradiation. In contrast, AML and FEL degraded at all after two hours.

A gradual decrease of the maximum peak in the zone 350-370 nm, that is a typical signal of the 1,4-DHP structure, and a contemporary increase of a new peak in the zone 260-280 nm, characteristic for the pyridinic structure, was observed for all the

compounds. The residual concentration of the drugs was calculated by using the absorbance measurement of the peaks between 350-370 nm, because of the insignificant absorbance of the degradation products after 330 nm. Effectively, also the main secondary photoproducts from some compounds don't have absorbance in this region [49-50].

Nevertheless, in order to obtain data as homogeneous as possible for the QSPR modeling, the spectral data used in calibration were limited to a degradation equivalent to a third of the starting concentration (33.33%). Within the examined times, all the products showed to follow a first order kinetics. Therefore the absorbance data until the time ($t_{0.33}$) necessary to reach this degradation percentage were collected.

A good linearity was obtained by plotting the logarithm of absorbances as a function of time, in agreement with the following equation:

$$\log \%A = -k \cdot t + 2$$

where %A is the percentage of residual absorbance, k the photodegradation rate constant, t the time (s), 2 is the logarithm of starting absorbance (100%).

Table 2 summarizes the degradation kinetics parameters calculated for the drug investigated. The data were carried out from three replicate analyses for each sample and very low variance was measured in all the cases.

Table 2. Photodegradation kinetics parameters

Drug	k	R²	t_{0.33}	log t_{0.33}
AML	-1.10e-05	0.9991	15 982	4.203
FEL	-1.60e-05	0.9992	11 027	4.042
LER	-9.38e-05	0.9827	608	2.783
MAN	-2.73e-04	0.9884	85	1.926
NIC	-2.08e-03	0.9985	218	2.338
NIF	-8.08e-04	0.9957	170	2.230
NIM	-9.77e-04	1.0000	30	1.474
NIS	-5.90e-03	0.9954	98	1.992
NIT	-1.49e-03	0.9963	106	2.024

t is expressed as seconds

1.5.2. Selection of descriptors

QSPR modeling needed to choose the variables affecting the drugs photodegradation. The selection of the descriptors responsible of significant variations in the molecular properties represents a key step in a multivariate modeling. This choice has to be carefully performed, because excluding descriptors carrying useful information from the system may lead to misleading results in building the model. At the same time, an indiscriminate use of a higher number of predictors could increase random noise and lower the robustness of the model [51-52].

Since the number of known descriptors is very high and a full selection procedure is practically unfeasible, some methods for simplification have been developed. One of the techniques for reducing full search procedure is the multilinear regression, based on a stepwise forward selection through extension of the

correlation to new descriptors until a statistic parameter becomes better than that previously calculated.

In the present study, PLS algorithm was applied to analyze the interactions between photosensitivity and descriptors. PLS has proved to be able in defining the relationship between dependent variables and predictor variables, but also to reduce the number of the descriptors [14]. The root mean square error of prediction (RMSEP) was adopted as a discriminating criterion in PLS calibration and the correlation coefficient R^2 was used to evaluate the model fitting. Usually, a R^2 value higher than 0.3 can be considered statistically meaningful, a value greater than 0.5 is indicative for a good model and a value over 0.8 proves an excellent correlation.

A screening of the descriptors was made by focusing just those describing constitutional, electrostatic and geometrical ones in consideration of the electronic and steric aspects of the aromatization reaction [53-54]. This reaction has been the subject of several studies [55-57], due to its technological and biological importance. The chemical-physical properties of the substituents on both the benzene and dihydropyridine moieties were investigated, because they characterize the various 1,4-DHP drugs. All descriptors were calculated on the neutral species.

A series of electronic descriptors relative to the entire molecules or geometrical and hydrophobic descriptors for the chemical substituents gave significant correlation with the drug photosensitivity. In particular, by applying the PLS procedure, the molecular descriptors PSA, HDon, HAcc and XlogP, relative to the

global chemical structures, were selected. Among the variables describing the chemical substituents, the geometrical descriptor MV and the hydrophobic descriptor π_x , showed the most significant influence on photodegradation. Each drug was so described by fourteen independent descriptors.

The logarithm of the time necessary to cause a degradation of a third for each compound ($\log t_{0.33}$) was used as dependent variable. The calibration set listing the values of $\log t_{0.33}$ and the descriptors relative to all the compounds is reported in Table 3.

Table 3. Calibration set

Drug	log t_{0.33}	MVR₂	πR₂	MVR₃	πR₃	MVR₅	πR₅	MVR_{2'}	πR_{2'}	MVR_{3'}	πR_{3'}	HDon	HAcc	PSA	XlogP
AML	4.204	73.84	-0.80	67.28	0.51	50.78	-0.02	25.67	0.59	0.00	0.00	3.00	7.00	99.88	1.84
FEL	4.043	30.79	0.46	67.28	0.51	50.78	-0.02	25.67	0.59	25.67	0.59	1.00	5.00	64.63	3.73
LER	2.784	30.79	0.46	298.17	4.78	50.78	-0.02	0.00	0.00	27.06	-0.27	1.00	9.00	113.69	6.41
MAN	1.927	30.79	0.46	274.03	2.47	50.78	-0.02	0.00	0.00	27.06	-0.27	1.00	10.00	116.93	4.78
NIC	2.338	30.79	0.46	168.25	1.88	50.78	-0.02	0.00	0.00	27.06	-0.27	1.00	9.00	113.69	3.54
NIF	2.231	30.79	0.46	50.78	-0.02	50.78	-0.02	27.06	-0.27	0.00	0.00	1.00	8.00	110.45	1.95
NIM	1.475	30.79	0.46	90.15	-0.44	84.17	0.85	0.00	0.00	27.06	-0.27	1.00	9.00	119.68	2.66
NIS	1.993	30.79	0.46	100.67	1.39	50.78	-0.02	27.06	-0.27	0.00	0.00	1.00	8.00	110.45	3.03
NIT	2.025	30.79	0.46	67.28	0.51	50.78	-0.02	0.00	0.00	27.06	-0.27	1.00	8.00	110.45	2.38

1.5.3. QSPR model

The calibration set, based on the values of $\log t_{0.33}$ (Y variable) as a function of fourteen molecular descriptors (X variables), was used to elaborate the QSPR model by means of PLS analysis.

PLS provided to perform interdependent PCA decomposition of the original data in both X and Y matrices in which new variables, called principal components or factors, were calculated as linear combinations of the old ones.

PCA transformed the original data matrix in a new matrix of scores (T) and loadings (P):

$$X = TP^T + E_X \quad (E_X = X - X_{\text{model}})$$

$$Y = UQ^T + E_Y \quad (E_Y = Y - Y_{\text{model}})$$

where E is the difference between the measured and calculated X and Y values.

The principal components are sorted by decreasing information content so that most of the information is preserved in the first few ones. Each principal component was extracted from the independent variables and simultaneously maximally correlated with the variance of the dependent variable [58-60].

The model was validated by full-cross procedure, adopting a leave-one-out procedure, and satisfactory statistical results were carried out. Values of 0.3984 and 0.8453 for RMSEP and R^2 were obtained, respectively, associated with an optimized number of five principal components. At this moment, the selected descriptors demonstrated to furnish useful information for the model building.

1.5.4. Photosensitivity prediction of external samples

An independent validation was performed by applying the defined QSPR model to two 1,4-DHP drugs external to the calibration set. The tested compounds were Barnidipine (BAR) and Cilnidipine (CIL), recently commercialized. These drugs were subjected to stressed photodegradation under the same stressing conditions adopted for the calibration samples and the relative values of $t_{0.33}$ were measured. Table 4 lists the chemical substituents and the descriptor values relative to both the molecules.

Table 4. Prediction set

<i>Chemical substituents</i>															
	R₂	R₃					R₅					R_{2'}	R_{3'}		
BAR	CH ₃	COO-pyrrolidin-CH ₂ Ph					COOCH ₃					H	NO ₂		
CIL	CH ₃	COOCH ₂ CH ₂ OCH ₃					COOCH ₂ CH=CHPh					H	NO ₂		
<i>Predictors</i>															
	log t_{0.33}	MVR₂	πR₂	MVR₃	πR₃	MVR₅	πR₅	MVR_{2'}	πR_{2'}	MVR_{3'}	πR_{3'}	HDon	HAcc	PSA	XlogP
BAR	2.20	30.79	0.46	171.85	1.67	50.78	-0.02	0.00	0.00	27.06	-0.27	1.00	9.00	113.69	3.09
CIL	2.02	30.79	0.46	90.15	-0.44	136.14	2.34	0.00	0.00	27.06	-0.27	1.00	9.00	119.68	4.08

When the photodegradation rate of these samples was predicted by the QSPR model, unsatisfactory statistical results were unfortunately obtained. Errors not below 8% on the $t_{0.33}$ value for BAR was carried out, but the results were particularly incorrect for CIL, whose relative errors were about 26%. The failure of the model was supposed to be caused by bad information within the data provided by the used descriptors. All the X variables don't clearly contributed with useful information to build a robust model.

An optimization was so necessary to improve as much as possible the prediction ability of the model. For this aim, the full-cross validation was coupled with the Martens' Uncertainty Test [61], which allowed the identification of perturbing samples or variables and then a further focusing of the most significant X-variables (Fig. 1). The weight of each descriptor in the model building was so considered, so that those furnishing useful information were single out [62-63]. This procedure provided to identify the descriptors MV and π , both for the substituent R₅, as "bad-descriptors", responsible of useless or noising information. So the overall contribute of the substituent R₅ to the model was removed and the model was rebuilt on twelve descriptors.

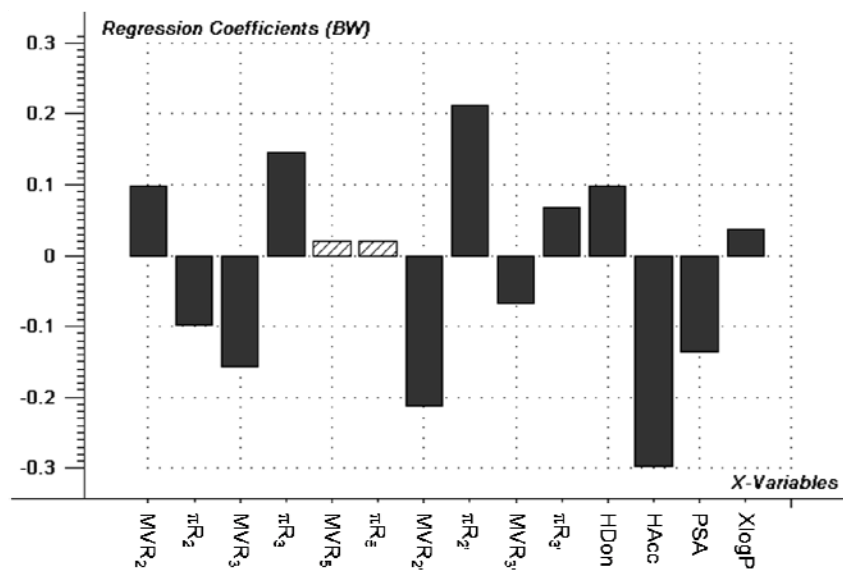


Figure 1. Weight of the descriptors by Martens' Uncertainty Test. PLS procedure carried out the following model equation:

The new model was:

$$\log t_{0,33} = 8.737e-03 \text{ MVR}_2 - 0.299 \pi R_2 - 7.872e-04 \text{ MVR}_3 + 0.162 \pi R_3 - 0.182 \text{ MVR}_{2'} + 0.295 \pi R_{2'} - 2.316e-02 \text{ MVR}_{3'} + 3.743e-02 \pi R_{3'} + 0.188 \text{ HDon} - 0.222 \text{ HAcc} - 1.499e-02 \text{ PSA} + 5.839e-03 \text{ XlogP} + 10.773$$

When internal validation was computed on the optimized model, values of 0.3616 for RMSEP and 0.8727 for R², respectively, were obtained, even demonstrating an improved prediction ability of the ultimate model. Application of this model to the prediction samples gave successful results with relative errors of 2.5% and 12.62% for BAR and CIL, respectively. The measured and predicted photodegradation data of the training set were plotted in fig. 2. The relative values for the external samples

were also depicted in this graph. These results demonstrated that the optimization step notably improved the reliability and robustness of the model. The optimal number of principal components, calibrated for twelve selected descriptors, resulted equal to four, as it is evident in the graphic of fig. 3, showing the residual variance.

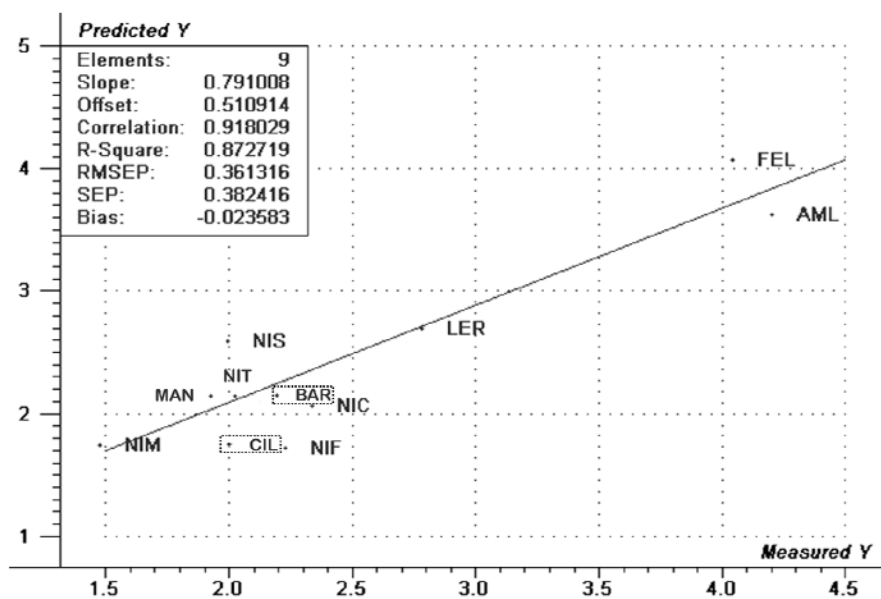


Figure 2. Plot of predicted vs. measured photodegradation rate for 1,4-DHP drugs. The external Figure samples are marked.

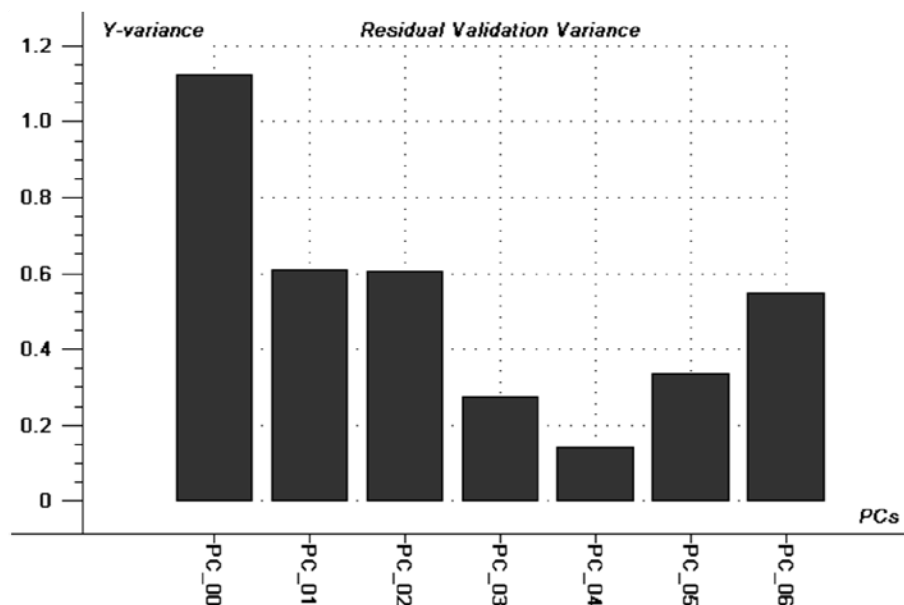
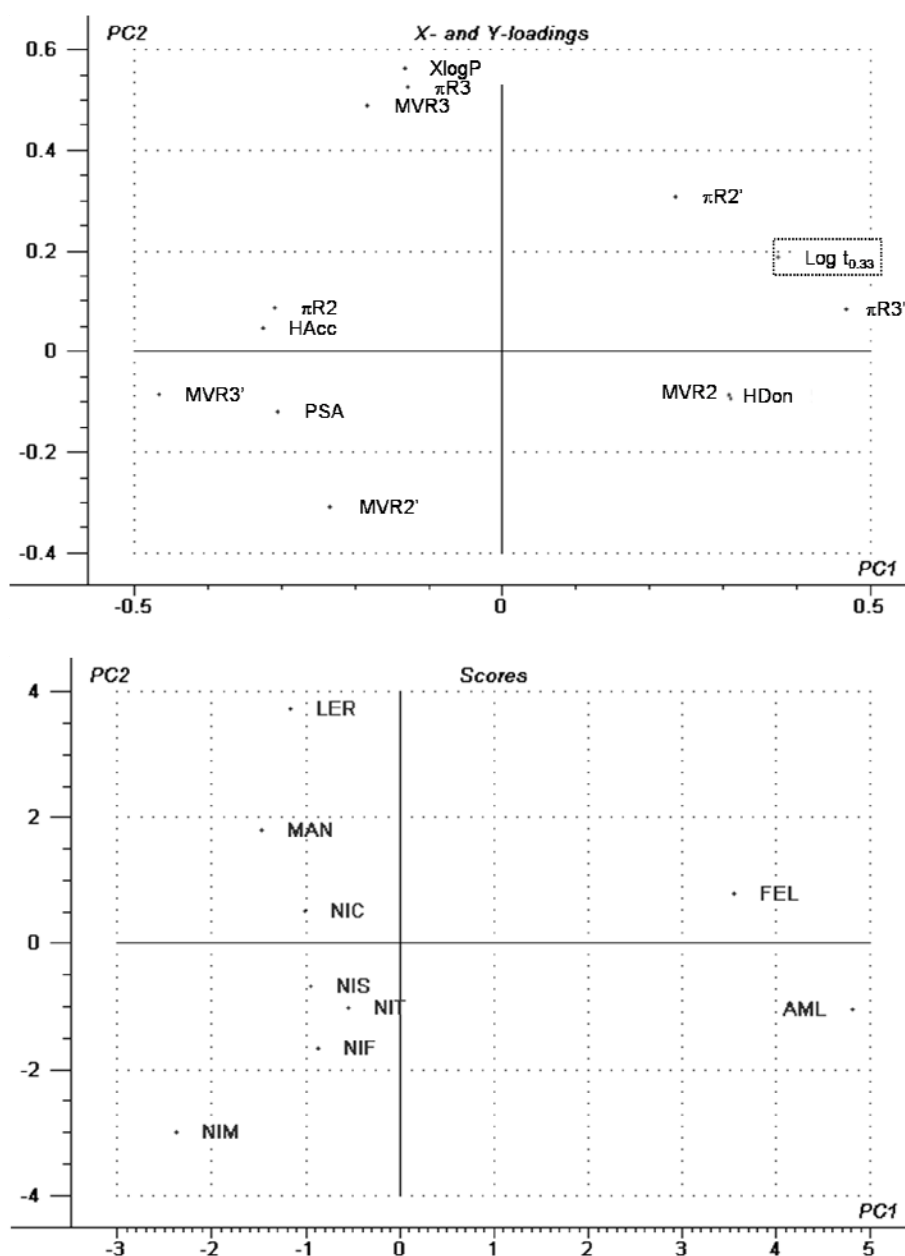


Figure 3. Residual variance from validation of the model vs. Principal Components.

Fig. 4 and 5 showed the graphical reports of “Scores” and “X- and Y-Loadings”, respectively. Score graph showed the distribution of the 1,4-DHPs into the model space (PC1 vs PC2), distributed according to X and Y variables. This graph helped to determine which variables were responsible for differences between samples. The drugs to the right of the score plot had a large value for variables to the same sector of the loading plot, and a small value for variables to the left of the loading plot; the most stable 1,4-DHPs were accordingly situated in same direction of log $t_{0.33}$.



Figures 4 and 5. Score plot, X- and Y- Loading plot of the optimized QSPR model.

1.5.5. Design of photostable dihydropyridine molecules

The study of the model equation and of the validation report permitted to evaluate the weight of the used predictors on the photostability of the drugs. The molecular descriptors HAcc and PSA should be maintained low. The value of HDon has to be high, whereas the value of XlogP is less influential. The substituents R₂' and R₃' should be small, since a low value of MV presents a discrete significance in increasing stability. At the same time, photostability is decreased if these groups have hydrophilic features. In fact, the presence of a nitro group on the 2' position assists an intramolecular disproportionation reaction, followed by aromatization of the pyridinic ring [64]. Analogously, a low value of MV is necessary, while a hydrophobicity feature seems unimportant. On the contrary, the R₂ substituent should have large volume and hydrophilic characteristics.

1.6. Conclusions

In conclusion, we have built a QSPR model correlating the photostability of the 1,4-DHP drugs with global and structural fragment descriptors. The influence of different substituents on both benzene and pyridinic rings has been evaluated in terms of hydrophobic, electronic and steric parameters. The model has demonstrated a good prediction ability when applied on congeneric drugs not enclosed in the calibration modeling. The value of 0.8727 for the correlation coefficient R^2 , obtained from the model validation, showed that the model has good predictive ability and robustness for estimating the photodegradation rates of 1,4-DHP drugs. The proposed model could be applied to new compounds not covered by the original data sets.

In addition, some rules have been derived from the model, which may be used by pharmaceutical chemists as a guideline on the contribution of the chemical substituents on photosensitivity of 1,4-DHP molecules. These rules could be used to identify novel 1,4-DHP structures characterized by high light stability.

For more details:

- [1] A. Toropov, K. Nesmerak, I.Jr. Raska, K. Waisser, K. Palat, *Comput. Biol. Chem.* 30 (2006) 434-437.
- [2] I.Jr. Raska, A. Toropov, *Eur. J. Med. Chem.* 41 (2006) 1271-1278.
- [3] P. Thanikaivelan, V. Subramanian, J. Rao Raghava, Unni Nair Balachandran, *Chem. Phys. Lett.* 323 (2000) 59-70.
- [4] R. Poneca, L. Amat, R. Carbó-Dorca, *J. Comput.-Aided Mol. Design* 13 (1999) 259-270.
- [5] J.D. Dyekjær, S.Ó. Jónsdóttir, *Carbohydr. Res.* 339 (2004) 269-280.
- [6] K. Baumann, *Trends Anal. Chem.* 18 (1999) 36-46.
- [7] A.L. de Queiroz Baddini, S. Presentin Cardoso, E. Hollauer, J.A. da Cunha Ponciano Gomesc, *Electrochim. Acta* 53 (2007) 434-446.
- [8] L. Du-Cuny, J. Huwyler, M. Wiese, M. Kansy, *Eur. J. Med. Chem.* 43 (2008) 501-512.
- [9] L. Li, S. Xie, H. Cai, X. Bai, Z. Xue, *Chemosphere* 72 (2008) 1602-1606.
- [10] A. Niazi, S. Jameh-Bozorgi, D. Nori-Shargh, *J. Hazard. Mater.* 151 (2008) 603-609.

- [11] S. Riahi, M. Reza Ganjali, P. Norouzi, F. Jafari, *Sens. Actuators B: Chem.* 132 (2008) 13-19.
- [12] C. Sârbu, C. Onișor, M. Posa, S. Kevresan, K. Kuhajda, *Talanta* 75 (2008) 651-657.
- [13] S. Wold, M. Sjöström, L. Eriksson, *Chemom. Intell. Lab. Syst.* 58 (2001) 109-130.
- [14] Q. Zhang, J. Huang, G. Yu, *Prog. Nat. Sci.* 18 (2008) 867-872.
- [15] T. Godfraind, S. Salomone, *Cardiovasc. Drug Ther.* 10 (1996) 439-446.
- [16] T.F. Krzemiński, D. Hudziak, A.W. Sielańczyk, M. Porc, A. Kędzia, *Vasc. Pharmacol.* 49 (2008) 91-96.
- [17] B.N. Singh, *Br. J. Clin. Pharmacol.* 21 (1986) 109- 122.
- [18] B.N. Singh, K. Nademanee, *Am. J. Cardiol.* 59 (1987) B153-B162.
- [19] V. Marinkovic, D. Agbaba, K. Karljickovic-Rajic, J. Comor, D. Zivanov-Stakic, *Il Farmaco* 55 (2000) 128-133.
- [20] G. Ragno, E. Cione, A. Garofalo, G. Genchi, G. Ioele, A. Risoli, A. Spagnoletta, *Int. J. Pharm.* 265 (2003) 125-132.
- [21] K. Takahashi, H. Noda, A. Noda, *Kyushu Yakugakkai Kaiho* 47 (1993) 37-43.

- [22] T. Yan, Y. Wu, J. Zhao, H. Nie, F. Yuan, H. Tang, S. Jin, Yaowu Fenxi Zazhi 9 (1989) 10-12.
- [23] P.K.F. Yeung, S.J. Mosher, P.T. Pollak, J. Pharm. Biom. Anal. 7 (1991) 565-571.
- [24] P. De Filippis, E. Bovina, L. Da Ros, J. Fiori, V. Cavrini, J. Pharm. Biom. Anal. 27 (2002) 803-812.
- [25] Y. Kawabe, H. Nakamura, E. Hino, S. Suzuki, J. Pharm. Biom. Anal. 47 (2008) 618-624.
- [26] J. Mielcarek, M. Stobiecki, R. Frański, J. Pharm. Biom. Anal. 24 (2000) 71-79.
- [27] R.H. Böcker, F.P. Guengerich, J. Med. Chem. 29 (1986) 1596-1603.
- [28] J. Niu, L. Wang, Z. Yang, Ecotoxicol. Environ. Saf. 66 (2007) 272-277.
- [29] J. Niu, Z. Shen, Z. Yang, X. Long, G. Yu, Chemosphere 64 (2006) 658-665.
- [30] J. Chen, X. Quan, F. Yang, W.J.G.M. Peijnenburg, Sci. Total Environ. 269 (2001) 163-170.
- [31] M.C.A. Costa, A.S. Gaudio, Y. Takahata, J. Mol. Struct. (Theochem) 394 (1997) 291-300.

- [32] B. Hemmateenejad, R. Miri, M. Akhond, M. Shamsipur, *Chemom. Intell. Lab. Syst.* 64 (2002) 91-99.
- [33] ICH Harmonized Tripartite Guideline, Photostability Testing of New Drug Substance and Products, Fed. Register 62 (1996) 27115-27122.
- [34] J. Ghasemi, S. Saaidpour, *Anal. Chim. Acta* 604 (2007) 99-106.
- [35] W. Li, I. Kubo, *Bioorg. Med. Chem.* 12 (2004) 701-713.
- [36] R. Todeschini, *Introduzione alla Chemiometria*, EdiSES, Napoli, 1998.
- [37] P. Ertl, B. Rohde, P. Selzer, *J. Med. Chem.* 43 (2000) 3714-3717.
- [38] C.A. Lipinski, F. Lombardo, B.W. Dominy, P.J. Feeney, *Adv. Drug Delivery Rev.* 23 (1997) 3-25.
- [39] T. Djaković-Sekulić, M. Ačanski, N. Perišić-Janjić, *J. Chromatogr. B.* 766 (2001) 67-75.
- [40] L.C. Tavares, A. Tavares do Amaral, *Bioorg. Med. Chem.* 12 (2004) 1377-1381.
- [41] R. Wang, Y. Gao, L. Lai, *Perspect. Drug Discovery Des.* 19 (2000) 47-66.
- [42] X.Z. Qin, J. De Marco, D.P. Ip, *J. Chromatogr. A* 707 (1995) 245-254.

- [43] G. Ragno, M. Veronico, C. Vetuschi, *Int. J. Pharm.* 99 (1993) 351-355.
- [44] G. Ragno, M. Veronico, C. Vetuschi, *Int. J. Pharm.* 119 (1995) 115-119.
- [45] G. Ragno, C. Vetuschi, *Die Pharmazie* 53 (1998) 628-631.
- [46] G. Ragno, F. Aiello, A. Garofalo, G. Ioele, M.S. Sinicropi, *Il Farmaco* 58 (2003) 909-915.
- [47] A.B. Baranda, R.M. Alonso, R.M. Jiménez, W. Weinmann, *Forensic Sci. Int.* 156 (2006) 23-34.
- [48] C. Vetuschi, G. Ragno, M. Veronico, A. Risoli, A. Giannandrea, *Anal. Lett.* 35 (2002) 1327-1339.
- [49] V. Marinkovic, D. Agbaba, K. Karljickovic-Rajic, J. Comor, D. Zivanov-Stakic, *Il Farmaco* 55 (2000) 128-133.
- [50] L. J. Núñez-Vergara, S. Bollo, J. Fuentealba, J. C. Sturm, J. A. Squella, *Pharm. Res.* 19 (2002) 522-529.
- [51] R.B. Darlington, *Regression and linear models*, McGraw-Hill, New York, 1990.
- [52] J. Neter, W. Wasserman, M.H. Kutner, *Applied linear regression models* (2nd ed.), Homewood, IL: Irwin, 1989.

[53] S. Dehghanpour, M.M. Heravi, F. Derikvand, *Molecules* 12 (2007) 433-438.

[54] H.R. Memerian, M. Abdoli-Senejani, D. Döpp, *J. Chinese Chem. Soc.* 54 (2007) 131-139.

[55] R. Alajarin, P. Jordan, J.J. Vaquero, J. Alvarez-Builla, *Synthesis* 4 (1995) 389-391.

[56] L. Chai, Y. Zhao, Q. Sheng, Z. Liu, *Tetrahedron Lett.* 47 (2006) 9283-9285.

[57] M. Filipan-Litvić, M. Litvić, V. Vinković, *Bioorg. Med. Chem.* 16 (2008) 9276-9282.

[58] Z. Rezaei, B. Hemmateenejad, S. Khabnadideh, M. Gorgia, *Talanta* 65 (2005) 21-28.

[59] J. Navalon, R. Blanc, M. del Olmo, J.L. Vilchez, *Talanta* 48 (1999) 469-475.

[60] M.L. Luis, J.M.G. Fraga, A.I. Jiménez, F. Jiménez, O. Hernández, J.J. Arias, *Talanta* 62 (2004) 307-316.

[61] A.M.C. Davies, Uncertainty testing in PLS regression, *Spectrosc. Europe* 13 (2001) 16-19.

[62] M. De Luca, F. Oliverio, D. Ioele, G.P. Husson, G. Ragno, *Int. J. Environ. Anal. Chem.* 88 (2008) 1087-1105.

[63] G. Ragno, M. De Luca, G. Ioele, *Microchem. J.* 87 (2007) 119-127.

[64] B.K. Logan, K.S. Patrick, *J. Chromatogr.* 529 (1990) 175-181.

2. Different photodegradation behavior of barnidipine under natural and forced irradiation

Barnidipine (BAR) [3-(3R)-1-benzylpyrrolidin-3-yl-5-methyl-2,6-dimethyl-4-(3-nitrophenyl)-1,4-dihydropyridine-3,5-dicarboxylate] is one of a new generation of 1,4-dihydropyridine calcium-channel blockers [1], widely used against hypertension and angina [2-6].

The 1,4-dihydropyridine antihypertensives are well-known photosensitive drugs. The most common photodegradation pathway is the oxidation to the pyridine derivatives, lacking any therapeutic effect [7-12]. This degradation mechanism has recently attracted considerable attention because it has been demonstrated that metabolism of those drugs involves an analogous cytochrome P-450 catalyzed oxidation in the liver [13]. Some 1,4-dihydropyridine drugs undergo a more complex degradation with the formation of secondary photoproducts [14-16].

In literature there are no studies about photodegradation kinetics of BAR. In a recent publication, the influence of its chemical substituents on photosensitivity has been discussed [7]. Details on the photodegradation mechanism still remain unclear as well as the sequential degradation steps that may take place. Usually, the prediction of the photochemical behavior of a molecule is a very complex problem [17], because the photodegradation mechanism depends not only on the structure but also on experimental conditions.

In the present work, the photodegradation behavior of BAR under stressing light and natural light was evaluated and the relative degradation pathways and kinetics under these irradiation conditions were compared. Photodegradation was conducted in accordance with the recommendations of the “Guide for the Photostability Testing of New Drug Substances and Products” developed by the International Conference on Harmonization (ICH) [18]. This guideline addresses the evaluation of stability data that should be submitted in registration applications for new drugs and associated drug products and provides recommendations on establishing re-test periods and shelf lives. The guideline refers light testing as an integral part of the global evaluation for stability data to be performed. Testing should demonstrate that light exposure does not result in unacceptable changes and be performed on pure drug and drug products. Photostability tests should evaluate the overall photosensitivity of a drug for method development purposes and degradation pathway elucidation and then provide the information necessary for handling, packaging, and labelling. Detailed articles on the ICH guideline and its application have been published [19-21].

In order to avoid different testing procedures, the guideline gives an accurate definition of the light sources to be adopted. In this work, the stressing tests were conducted by means of a cabinet equipped with a Xenon lamp, in accordance with one of the light sources reported in the guide. Degradation in natural conditions was conducted under daylight and direct sunlight.

BAR photodegradation was monitored by HPLC and zero-crossing derivative spectrophotometry. Adoption of the spectrophotometric analysis was justified by the easy recording of the spectra and the rapid interpretation of the data, which makes this technique very attractive for routine uses. Zero-crossing is a powerful technique for the quantitative assay of the components of a mixture, particularly effective when a wide peaks overlapping is present in the corresponding zero-order spectrum [22-27].

HPLC analysis allowed to evaluate in detail the formation of all the photoproducts and hypothesize the sequential degradation steps that may take place during the light exposure under natural and forced conditions. The study of the photochemical properties of BAR were useful to understand the transient species produced after light absorption. An analytical method based on zero-crossing derivative spectrophotometry was also developed to be used as a routine quality control for BAR and its pharmaceutical formulations.

2.1. Drug and Experimental Methodology

BAR was obtained from extraction from the specialty Libradin® 20.0 mg (Sigma-Tau S.p.A., Italy). The content of five capsules was pulverized in a mortar and the equivalent to one capsule was suspended in ethanol in a 20 ml volumetric flask. The suspension was sonicated for 10 min and then filtered through a PTFE 0.45 µm membrane to obtain a stock solution of 1 mg/ml.

The pyridine by-product (BOX) was obtained by exposing under daylight the BAR stock solution in a 20 ml quartz volumetric

flask for five hours. Purity and identity of the photoproduct were confirmed by HPLC-DAD analysis.

Zero-to-fourth order derivative spectra were registered on the λ range of 200 – 450 nm in a 10 mm quartz cell, by means of a Perkin-Elmer Lambda 40P spectrophotometer at the following conditions: scan rate 1 nm/s; time response 1 s; spectral band 1 nm. The software UV Winlab 2.79.01 (Perkin-Elmer) was used for spectral acquisition and elaboration.

HPLC analysis was carried out by using a HP 1100 pump fitted with a diode array detector G1315B (Agilent Technologies) and a Rheodyne 7725 manual injector. The LC column was a C18 Gemini (Phenomenex), 250 x 4.6 mm x 5 μ m. The mobile phase consisted of acetonitrile–phosphate buffer (pH 7) (75:25, v/v) at room temperature. The mobile phase was filtered through a 0.45 μ m nylon membrane under vacuum. The mobile phase was pumped isocratically at a flow rate of 1 ml/min during analysis. The injection volume was 5 μ l.

Gas-chromatographic (GC–MS) analysis was performed by using a gaschromatograph Agilent 6890N with a Mass Selective Detector Agilent 5973. The GC conditions were as follows: column, HP capillary (30 m x 0.25 mm I.D.), 250 nm film thickness; injection port temperature, 250 °C, carrier gas, helium; flow-rate 0.3-0.6 ml/min; column temperature, programmed from 60 – 280 °C at 13 °C/min, initial time 3 min, final time 54 min.

Forced photodegradation was conducted in a light cabinet Suntest CPS+ (Heraeus, Milan, Italy), equipped with a Xenon lamp. The apparatus was fitted up with an electronic device for

irradiation and temperature measuring and controlling inside the box. The system was able to select spectral regions by interposition of filters. In the present study, samples were irradiated in a λ range between 300 and 800 nm, by means of a glass filter, according to the ID65 standard of ICH rules.

The steady state fluorescence experiments were carried out on a spectrofluorometer system (Photon Technology International, Birmingham, NJ), equipped with a monochromator in the wavelength range of 200-900 nm. The solutions were placed in 10 mm quartz cells with a septum cap.

The Laser Flash Photolysis (LFP) experiments were conducted by using a Q-switched Nd:YAG (neodymium-doped yttrium aluminium garnet) laser coupled to a turn-key mLFP-miniaturized equipment from Luzchem (Ottawa, ON, Canada). Samples were prepared in acetonitrile and purged with nitrogen for 10 min in a 10 mm fluorescence quartz cell, then sealed with a septum before irradiation at 355 nm. The single pulse was of about 17 ns and the energy was below 100 mJ/pulse.

Standard solutions of the pure products BAR and BOX in ethanol were prepared and used to set up the spectrophotometric calibration curves. BAR concentration was within the range 5.0 - 50.0 $\mu\text{g/ml}$ and BOX in the range 0.2 - 50.0 $\mu\text{g/ml}$. A second set of standard mixtures within the above reported concentrations were prepared, with BOX percentage value between 1 and 50%. These samples were used to validate the elaborated methods.

For HPLC analysis, a series of standard solutions in ethanol with both BAR and BOX within the range 20.0 – 400.0 µg/ml were prepared to set up the calibration curves.

The content of five capsules was pulverized and the equivalent to one capsule was suspended in ethanol in a 20.0 ml volumetric flask. The suspension was sonicated for 10 min and then filtered through a PTFE 0.45 µm membrane. Samples for UV analysis were obtained after serial dilution 1:100 (10^2) of this filtrate with ethanol and analyzed. For HPLC assay, samples were obtained by diluting 1 ml of the filtrate to 10.0 ml with ethanol.

To minimize BAR photodegradation, all laboratory experiments were carried out in a dark room under the illumination of a red lamp (60 Watt), kept at a distance of about 2 m.

The stressing tests were performed on a series of BAR solutions in quartz cells perfectly stoppered and irradiated in the light cabinet, according to the ID65 standard of the ICH rules. The irradiation power was sequentially fixed at 250, 350, 450, 550 and 650 W/m² (corresponding to 15, 21, 27, 33 and 39 kJ/m²min of irradiance, respectively) at a constant temperature of 25 °C. Samples with BAR concentration of 20.0 and 200.0 µg/ml were assayed by spectrophotometry and HPLC, respectively, without further treatment. Both the techniques were performed just after preparation (t= 0 min) and every minute until 100 min.

These forced conditions were also applied to test the stability of the pharmaceutical formulation. The content of two capsules was evenly distributed along one of the internal surfaces of a quartz cell and analyzed at various intervals during light exposure

until twenty hours. The samples for analysis were prepared as above described for the sample for UV analysis.

Degradation under natural light was performed on ethanol solutions with the same concentrations used in the forced degradation. The samples were exposed to direct sunlight and diffuse light coming from the surrounding sky dome or reflected off adjacent surfaces (daylight). The analyses were made at the following times: 0, 1, 5, 10, 15, 20 and then every 10 min until 100 min.

2.2. Results and Discussion

2.2.1. Kinetics of BAR photodegradation

In accordance with the recommendations of ICH guideline, a series of ethanol solutions of BAR 20.0 µg/ml were subjected to forced photodegradation under the standard conditions above reported. Figure 1 shows, as an example, the sequence of spectra collected during a degradation experiment with a irradiation power set at 250 W/m².

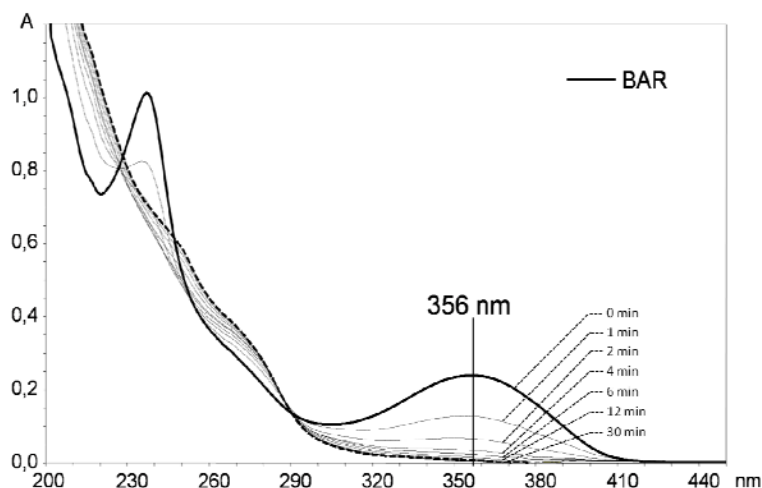


Figure 1. Spectral sequence of BAR solution 20.0 µg/ml degraded under light at 250 W/m².

BAR degradation was monitored through the gradual disappearance of the maximum peak at 356 nm, that is the typical signal of the 1,4-dihydropyridine structure. A contemporary increase of a new peak in the zone 260 - 280 nm, characteristic of the pyridinic group, demonstrated the oxidation of the dihydropyridinic ring, in agreement with the common degradation occurring for the drugs belonging to this class [7-8]. However, the absence of clear isosbestic points suggested the formation of secondary products. In fact, an isosbestic point should be present whenever there is only a single by-product overlying the parent product. The lack of such a point consequently indicates the existence of multiple by-products [28, 29].

A clear influence of the irradiation power on the degradation rate was shown during the first six minutes of irradiation by plotting the residual concentrations of BAR against the degradation time (Fig. 2).

Different photodegradation behavior of barnidipine under natural and forced irradiation

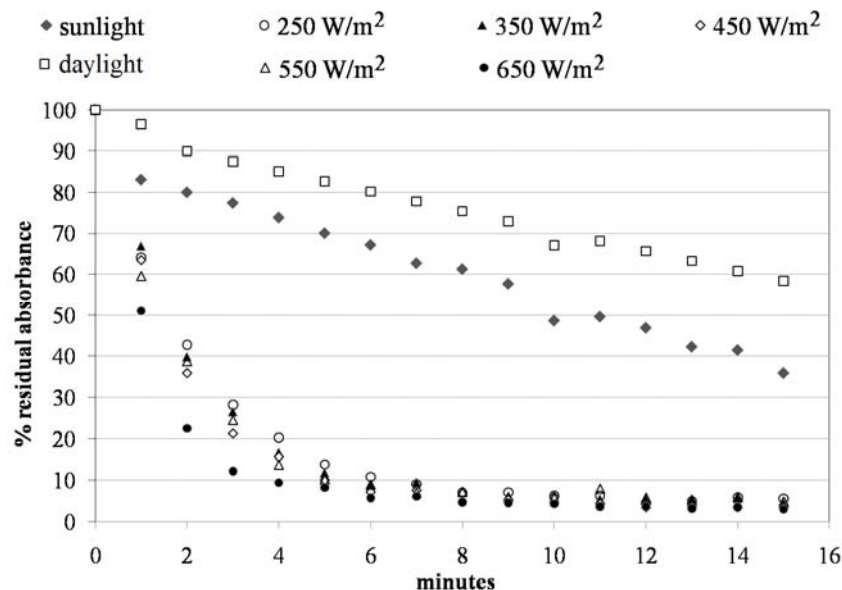


Figure 2. Photodegradation profiles of BAR under natural light and forced light at different power irradiation.

After this time, a degradation of about 90% was calculated under whatever irradiation power. The forced tests induced a degradation following a second-order kinetics, with the formation of two or more products [30]. When the values of concentration percentage (BAR%) were plotted against the degradation time, straight lines with slope k_2 and intercept 0.01 were obtained, according to the following equation:

$$1/\text{BAR}\% = k_2 \cdot t + 0.01$$

where BAR% is the percentage of the residual drug concentration, k_2 the photodegradation rate constant, t the time (min) and 0.01 is the reciprocal value of the starting concentration percentage (100%). Table 1 lists the parameters describing the photodegradation kinetics for all the samples. The calculated degradation rates resulted higher than those of other congener

drugs and comparable to that of Nifedipine, the prototype compound of the 1,4-dihydropyridine class [7].

Table 1. Kinetic parameters of photodegradation under different irradiation sources and power values

Forced irradiation			Natural irradiation		
W/m ²	K ₂	R ²	Source	K ₁	R ²
250	0.0125	0.9227	sunlight	0.0236	0.9723
350	0.0130	0.9292	daylight	0.0150	0.9923
450	0.0189	0.9477			
550	0.0207	0.8925			
650	0.0243	0.9549			

This relevant sensitivity of BAR to light led us to check the behaviour of the drug when exposed under natural lighting. A full knowledge about the intrinsic photochemical characteristics of a so unstable drug seemed in fact essential to set up efficient manufacturing or formulation.

For this aim, two ethanol solutions of BAR 20.0 µg/ml in quartz cells were exposed to direct sunlight and daylight, respectively. The experiments were replicated three times on different days, to take into account the variability of weather, but not significant differences were detected. The concentration of BAR during these degradation tests was plotted against the exposure time, giving the curves reported in figure 2. In this case, the degradation process had followed a first-order kinetics, according to the solely formation of the pyridine by-product. The persistence of isosbestic points in both the spectral sequences

confirmed this hypothesis. A good linearity was obtained by plotting the logarithm of the residual drug concentration as a function of time, in agreement with the equation:

$$\log \text{BAR}\% = -k_1 \cdot t + 2$$

where BAR% is the percentage of residual concentration, k_1 the photodegradation rate constant, t the time (min), 2 the logarithm of the starting concentration (100%). The kinetic parameters describing the degradation process under natural light are also reported in Table 1.

Photodegradation rate of the samples exposed to direct sunlight was significantly higher than the samples kept under daylight. The different degradation pathways that BAR showed when exposed to natural or forced light was confirmed by HPLC-DAD analysis, as described in the next paragraph.

Results obtained from our investigation highlighted a clear disagreement between natural and artificial exposure, making critical the definition of appropriate analytical methods to be used in the control quality of BAR and its pharmaceutical formulations. These results suggested that data from the forced degradation cannot be automatically extended to degradation occurring under real conditions. The assessment of photostability under natural light seems all the more necessary in the presence of highly photosensitive drugs presenting degradation pathways depending on the light source.

2.2.2 HPLC study of forced photodegradation of BAR

The forced photodegradation test had revealed a complex degradation process with the formation of several photoproducts, in contrast with the degradation under natural light leading to the pyridine derivative only. Therefore, a HPLC-DAD study was conducted to investigate the pathway occurring in the degradation process. Chromatographic analysis was executed by using the conditions above described. The study was performed by exposing an ethanol solution of 200.0 µg/ml BAR to artificial light. The sample was analyzed by HPLC just after the preparation and at different times during light exposure until a total time of 100 min.

Different photodegradation behavior of barnidipine under natural and forced irradiation

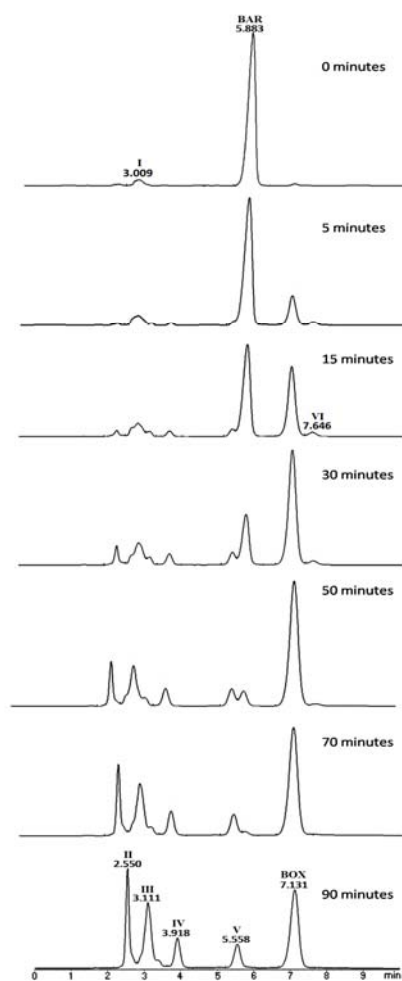


Figure 3. Chromatograms recorded at sequential times of an ethanol solution of BAR 200.0 $\mu\text{g/ml}$ exposed to stressing light irradiation.

A low value of radiant power (250 W/m^2) was chosen to perform the forced degradation study, because of the high sensitivity to light of BAR. The chromatograms recorded at sequential times were assembled in fig. 3. A very low amount of a secondary product, with RT 3.009 (I), is already initially present as an impurity of BAR. The absence of any characteristic peak after

210 nm in the UV spectrum of this compound indicated that it did not derive from drug degradation.

During the stressing test, the BAR signal (RT 5.883) rapidly decreased with the contemporary formation of a first degradation product with RT 7.131, corresponding to the pyridine by-product BOX, as confirmed by its UV spectrum. The formation of other five secondary products was evident after only 15 minutes of light irradiation, positioned at 2.550 (II), 3.111 (III), 3.918 (IV), 5.558 (V) and 7.646 (VI) min, respectively. The graph in figure 4 reports the plotting of the chromatographic peak areas for the parent drug and its main photoproducts against time.

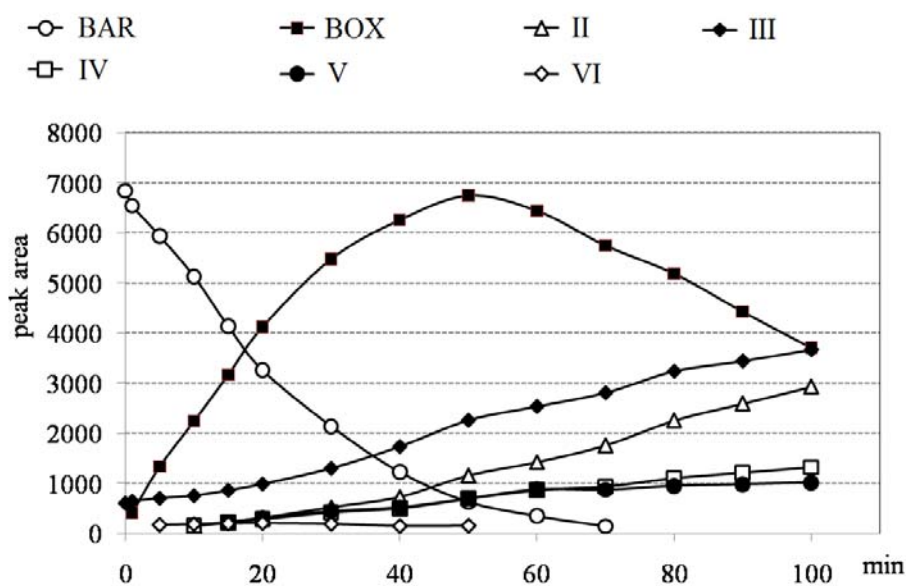


Figure 4. Kinetic profiles of the products involved in the photodegradation of BAR 200.0 µg/ml exposed to stressing light irradiation.

It is evident the high photodecomposition rate of BAR, with a halving of its concentration after only 19 min and a complete

disappearance after 70 min. The corresponding increase of BOX resulted constant until about 50 min, afterwards it decreased with the simultaneous increase of the secondary degradation products II, III, IV and V. In contrast, the product VI seemed only an intermediate degradation product, as it disappears after about 50 min. These results suggested a first degradation step in which BAR was oxidized to the pyridinic form which in turn underwent a more complex degradation process leading to the formation of different secondary by-products. Effectively, all these secondary photoproducts presented no absorbance above 320 nm, confirming so the saturation of the dihydropyridinic ring in their molecular structures [31, 32]. The UV spectra of all the products involved in the chromatographic analysis are shown in figure 5.

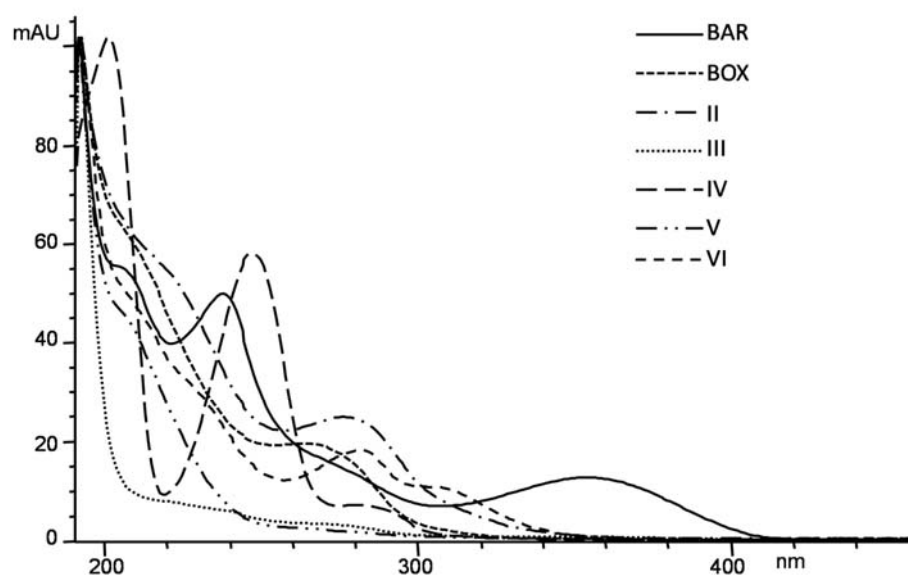


Figure 5. Pure spectra of BAR and relative photoproducts obtained in the photodegradation of BAR 20.0 $\mu\text{g/ml}$ exposed to stressing light irradiation.

The exact identification of the photoproducts was attempted by means of GC–MS analysis, but their low concentration and easy degradability at high temperatures made this study very difficult. The photo-exposed solutions of 200.0 µg/ml BAR in ethanol were subjected to GC–MS analysis using the above reported conditions. The mass spectra were recorded providing information on the molecular weight and structure of the analytes.

MS spectrum of BAR and a representative scheme of the fragmentation pattern, are shown in fig. 6 and 7, respectively.

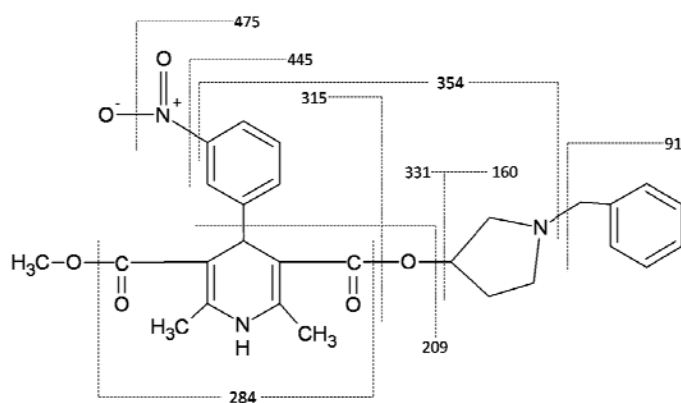


Figure 6. MS spectrum of BAR.

Different photodegradation behavior of barnidipine under natural and forced irradiation

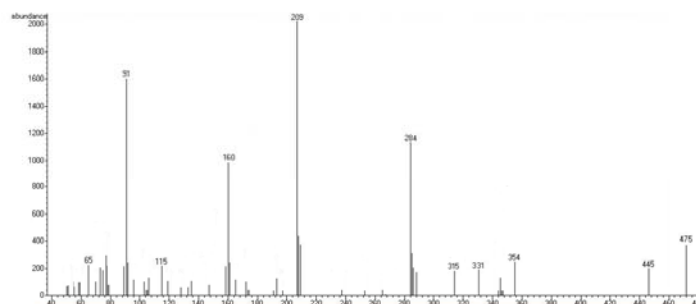


Figure 7. Scheme of the fragmentation pattern.

This fragmentation was also found for some photoproducts. The photoreactive centres, on which the main modifications take place, were found to be the dihydropyridinic ring, the nitro group and the benzylic group on the side chain. In particular, the dihydropyridinic moiety was rapidly oxidized to give the pyridinic by-product (BOX). The subsequent products derived then from further degradation of this molecule, as depicted in fig. 8.

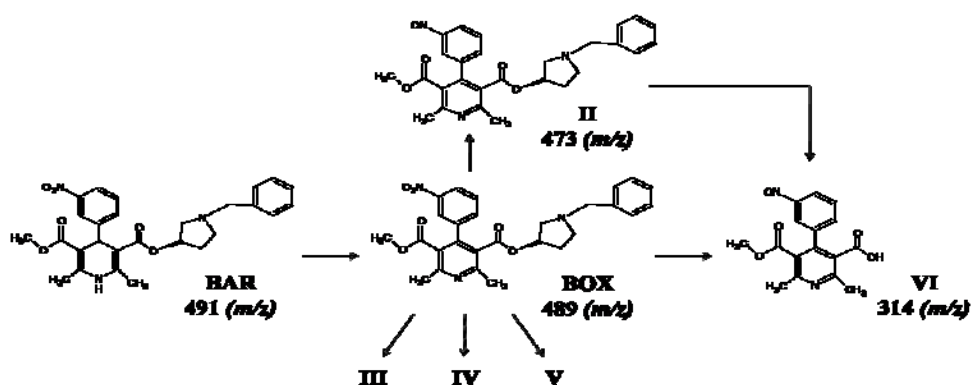


Figure 8. Scheme of photodegradation pathway.

The nitro group was converted in nitroso to furnish the photoproduct II; MS data of the product VI were in accordance with the loss of the benzyl-pyrrolidinic group in the side chain with the contemporary reduction of the nitro group in nitroso. Characterization with the same reliability of the photoproducts III, IV and V products was not possible and their identification is still under investigation. Effectively, these results are in agreement with those already reported in literature in the photodegradation pathways of some congeners [33, 34].

The influence of the nitro group on the photodegradation process is deeply discussed in other studies [7, 35]. The probably formation of a metabolite of BAR with loss of the benzylic substituent has been also reported [36].

In contrast, the chromatographic study on the BAR solutions exposed to natural light demonstrated a simplest photodegradation process. Fig. 9 shows the chromatograms recorded at sequential times for the sample kept under daylight.

The principal degradation process was the aromatization process of the drug to give the pyridinic photoproduct BOX. The formation of the secondary photoproducts II, III, IV and V, observed during the forced degradation, was detected only after about 1 hour of light exposure but their concentration remained under a value of 5-6%, with respect to BAR, throughout the entire experiment. The photoproduct VI was never revealed.

Different photodegradation behavior of barnidipine under natural and forced irradiation

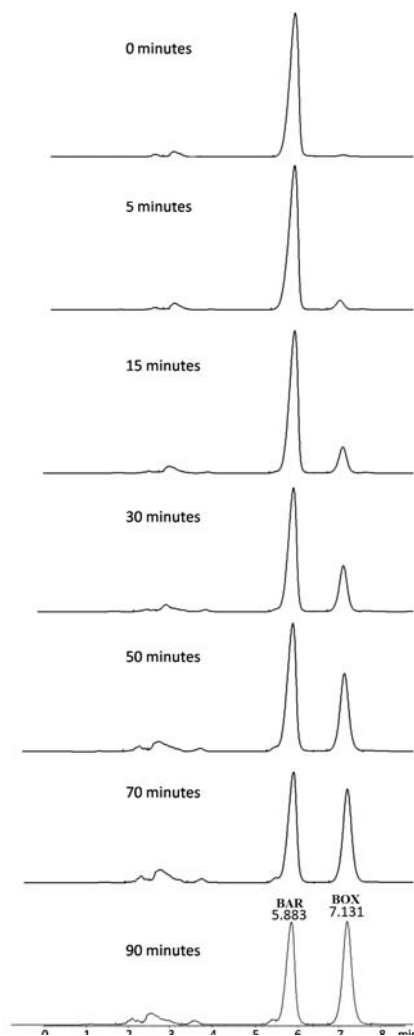


Figure 9. Chromatograms recorded at sequential times of an ethanol solution of BAR 200.0 $\mu\text{g/ml}$ exposed to daylight.

Exposure of an analogous BAR sample to direct sunlight showed the same qualitative results with a moderate increase of the degradation rate.

2.2.3 Photochemical study

Characterization of a photodegradation process through the study of the transient species, their lifetime and the course between precursor and products, is a crucial way to understand the potential photo-toxicity of a drug and the causes determining it. The transient species can be monitored by using emission (luminescence technique) and absorption (laser flash photolysis) techniques.

The phototoxic effects of 1,4-dihydropyridines are well known [37]. A very important feature of the photodegradation of these drugs involves the probable formation of singlet oxygen that can modify or destroy tissues causing significant damages [38] and loss of therapeutic activity. A contribute to understand the general mechanism of photo-oxidation of Nimodipine and Felodipine has been reported by Pizarro et al. [39] Later, Fasani et al. [40] proposed a general scheme for the photochemistry of 1,4-dihydropyridines. Actually, no photochemical studies are present about the drugs of last generation belonging to this class.

In order to investigate the mechanism of the fast degradation of BAR, the drug was submitted to the steady state photolysis study. BAR solutions (23.8 $\mu\text{g/ml}$) with maximum absorbance 0.3 were irradiated at a monochromatic light fixed at λ_{exc} 356 nm. The samples were prepared in both ethanol and acetonitrile, but the photoreaction resulted not significantly affected by the medium. The spectra showed the characteristic UV visible features of the 1,4-dihydropyridines. The generated photoproduct was due to the

loss of two hydrogen atoms, in position 1 and 4, of the dihydropyridinic moiety to give a pyridinic by-product.

No detectable fluorescence of BAR due to a singlet excited state was observed at room temperature. This state was probably deactivated by the fast intramolecular electron transfer from the dihydropyridinic ring to the substituted phenyl ring, yielding a zwitterionic radical as an intermediary species. The same mechanism has been proposed for congeners of BAR [40]. Besides, the presence of a nitro group on the phenyl ring plays an important role in this mechanism. In fact, it increases the charge delocalization during excitation and promotes the formation of a zwitterionic radical. A 1,4-dihydropyridine drug is so quickly oxidized to pyridinic byproduct thanks to both ionization and deprotonization.

Likewise, a triplet state due to an intersystem crossing (ISC) was not identified. Transition from the initial lowest excited singlet to the triplet state and from the triplet back to the ground state is surely accelerated by the nitro group, in a similar way to many aromatic compounds. This is in agreement with previous studies on other dihydropyridinic drugs [41].

2.2.4 Assay of BAR and pyridine photoproduct by derivative spectrophotometry

Despite the results obtained from the forced degradation revealed the formation of a large number of products, degradation under natural conditions showed a single product and traces of the others. So a simple and reliable method to be applied in the routine

quality control of BAR and its pharmaceutical formulations was defined, able to determine simultaneously the drug and its main pyridinic photoproduct, produced from usual exposure to light.

Actually, BAR concentration resulted proportional to the absorbance measurement of the maximum peak at 356 nm, because of the insignificant absorbance of the degradation product at that wavelength. Unfortunately, the absorption spectrum of a mixture of the two components showed no specific signal for BOX, whose spectrum is even fully overlapped by the BAR spectrum.

Therefore the derivative spectra (first to fourth-order) of the binary mixture were checked to select a suitable spectrum to be used for the simultaneous determination of the components. Derivative techniques in spectroscopy often offer a powerful tool for a resolution enhancement, when signal overlap or interference exists. Several specific signals were singled out for the two components in the spectra of different derivative orders but the first-order derivative spectra seemed to be the most suitable for analytical aim. In fig. 10, the 1st-order derivative spectra of BAR and BOX, both presenting a 20.0 µg/ml concentration, are plotted.

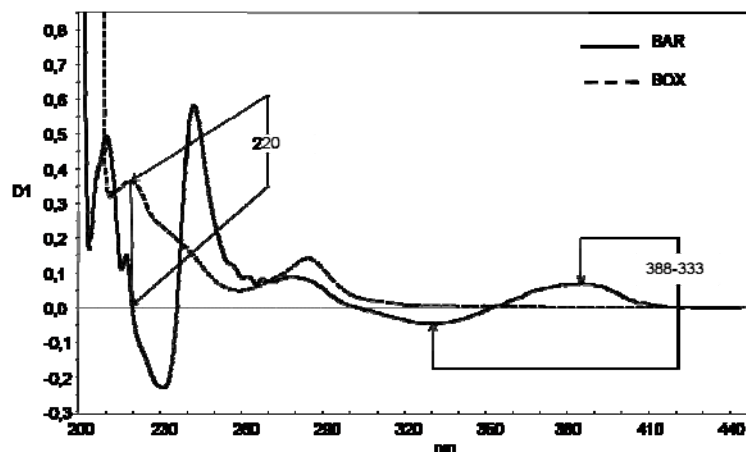


Figure 10. First-order derivative spectra of BAR and BOX ethanol solutions.

BAR concentration was carried out by using the peak-through ${}^1D_{333-388}$ whose absorbance was exclusively due to the drug. Because of the absence of specific signals of BOX, its determination was performed through a zero-crossing approach. This technique states that the absorbance measured to a specific wavelength in a derivative spectrum exactly corresponds to the concentration of one component in a mixture, when the absorbance curves of the remaining components cross the abscissa axis.

Several suitable signals in the BAR-BOX mixture fitted such a requirement. In particular, the spectral line of BAR crossed the X-axis at 220, 237 and 304 nm, where the absorbance values reflected the concentration of the photoproduct only. Previous studies reported that the accuracy in a zero-crossing application increased when a signal corresponding to a maximum in the spectrum was used [42]. On the contrary, the results carried out by signals placed on peak shoulders resulted less accurate and precise.

BOX concentration was so carried out by considering just the peak at 220 nm that corresponds to a maximum signal of the photoproduct spectrum. Analogous signals could be singled out in higher derivative order spectra, but the rising of the instrumental noise prevented an accurate analysis.

The equation parameters calculated for determination of BAR or BOX concentration (independent variables) are reported in table 2. These relationships were applied to assay the samples of the prediction set.

An independent HPLC-DAD method was simultaneously developed to check the results obtained by the spectrophotometric analysis. Calibration curves for the BAR and BOX were constructed in the range 50.0 - 400.0 $\mu\text{g/ml}$ and obtained by applying a least squares linear regression to the concentration values carried out by chromatograms at the retention time (RT) of 5.98 and 7.08 min, respectively. The relative equation parameters, with BAR or BOX concentrations as independent variables, are reported in Table 2. Results from application of both UV derivative and HPLC methods were collected in terms of accuracy (% recovery) and precision (relative standard deviation RSD) and listed in table 2.

Different photodegradation behavior of barnidipine under natural and forced irradiation

Table 2. Equation parameters and statistical results for determination of BAR and BOX, as independent variables.

Analytical method	Analyte µg/ml	Signal Abs/Area	Slope	Intercept	R ²	% recovery	RSD
Zero-order derivative	BAR	356 nm	0.0130	-0.0095	0.9989	98.37	1.46
First-order derivative	BAR	388-333 nm	0.0058	-0.0031	0.9989	97.56	2.18
First-order derivative	BOX	220 nm	0.0185	-0.0203	0.9984	96.11	3.22
HPLC	BAR	5.98 min	33.958	6.0248	0.9969	97.67	2.52
HPLC	BOX	7.08 min	47.800	56.783	0.9999	96.43	3.84

Different photodegradation behavior of barnidipine under natural and forced irradiation

The content of BOX in raw material was found to be approximately 3% after eight hours under daylight. The pharmaceutical formulations of BAR were analogously tested but they showed high stability under both natural or stressing conditions. The data were carried out from three replicate analyses and very low variance was measured in all experiments. In particular the pharmaceutical capsules showed a decrease of BAR concentration of 3.2 and 5.4% after 38 hours of exposure to natural and artificial light, respectively. The capsules resulted well protected when enwrapped by the packaging material.

2.3. Conclusions

The work demonstrated the difference in the photodegradation pathway occurred when the antihypertensive barnidipine is exposed to natural or stressing irradiation. A HPLC procedure was developed to investigate the degradation processes. The drug, with a feature common to all compounds of the dihydropyridinic class, when exposed to sunlight or daylight was oxidized to the corresponding pyridinic derivative. In contrast, exposure to stressing light by Xenon lamp caused a more complex photodegradation process with the formation of several photoproducts in addition to the pyridinic by-product. In this case, BAR was subjected to the aromatization of the 1,4-dihydropyridine moiety, reduction to the nitroso-derivatives and N –debenzylation on the side chain as major photodegradation reactions.

A method for the simultaneous determination of BAR and pyridinic photoproduct, produced from usual exposure to light, was developed by derivative spectrophotometry, useful as a routine quality control of the drug formulations. The whole procedure required only a simple and rapid sample preparation with a negligible light exposure when applied to pharmaceuticals. The spectrophotometric results were confirmed by HPLC as a reference procedure. The results reported in this work could be useful to identify precautionary measures needed in manufacturing or in formulation of the drug products.

For more details:

- [1] W.S. Huh, Y.S. Kim, J.S. Han, S.G. Kim, S.B. Kim, J.S. Park, M. Yamamoto, *Curr. Therap. Res.* 61 (2000) 395-405.
- [2] P. D'Elia, F. De Matteis, S. Dragoni, A. Shah, G. Sgaragli, M. Valoti, *Europ. J. Pharm.* 614 (2009) 7-13.
- [3] J. García del Pozo, E. Ramos Sevillano, F.J. de Abajo, R. Mateos Camposc, *Rev. Esp. Cardiol.* 57 (2004) 241-249.
- [4] K. Kimura, N. Suzuki, N. Mise, S. Oba, K. Miyashita, A. Tojo, Y. Hirata, A. Goto, M. Omata, *Curr. Therap. Res.* 59 (1998) 826-834.
- [5] H.C. Park, K.H. Kwon, H.J. Noh, I.H. Lee, S.W. Kang, K.H. Choi, S.K. Ha, H.Y. Lee, D.S. Han, M. Yamamoto, *Curr. Therap. Res.* 61 (2000) 927-937.
- [6] G. Rossetti, S. Pizzocri, F. Brasca, M. Pozzi, L.M. Beltrami, G.B. Bolla, R. Famiani, B. Caimi, S. Omboni, F. Magrini, S. Carugo, Open-Label, Pilot Study, *Curr. Therap. Res.* 69 (2008) 192-206.
- [7] G. Ioele, M. De Luca, F. Oliverio, G. Ragno, *Talanta* 79 (2009) 1418-1424.
- [8] V. Marinkovic, D. Agbaba, K. Karljickovic-Rajic, J. Comor, D. Zivanov-Stakic, *Il Farmaco* 55 (2000) 128-133.
- [9] G. Ragno, E. Cione, A. Garofalo, G. Genchi, G. Ioele, A. Risoli, A. Spagnoletta, *Int. J. Pharm.* 265 (2003) 125-132.

Different photodegradation behavior of barnidipine under natural and forced irradiation

- [10] K. Takahashi, H. Noda, A. Noda, Kyushu Yakugakkai Kaiho 47 (1993) 37-43.
- [11] A.L. Zanocco, L. Diaz, M. Lopez, L.J. Nunez-Vergara, J.A. Squella, J. Pharm. Sci. 81 (1992) 920-924.
- [12] P.K.F. Yeung, S.J. Mosher, P.T. Pollak, J. Pharm. Biomed. Anal. 7 (1991) 565-571.
- [13] R.H. Böcker, F.P. Guengerich, J. Med. Chem. 29 (1986) 1596-1603.
- [14] P. De Filippis, E. Bovina, L. Da Ros, J. Fiori, V. Cavrini, J. Pharm. Biomed. Anal. 27 (2002) 803-812.
- [15] Y. Kawabe, H. Nakamura, E. Hino, S. Suzuki, J. Pharm. Biomed. Anal. 47 (2008) 618-624.
- [16] L.J. Núñez-Vergara, C. Sunkel, J.A. Squella, J. Pharm. Sci. 83 (1994) 502-507.
- [17] W.H. Horspool, P.S. Song, Handbook of organic photochemistry and photobiology, CRC Press, Boca Raton, Florida, USA, 1995.
- [18] ICH Harmonized Tripartite Guideline, Photostability Testing of New Drug Substance and Products, Fed. Register. 62 (1996) 27115-27122.
- [19] D. E. Moore, Photostability of drugs and drug formulations, edited H. H. Tønnesen, CRC Press, New York, 41, 2004.

Different photodegradation behavior of barnidipine under natural and forced irradiation

- [20] H. H. Tønnesen, Photostability of drugs and drug formulations, CRC Press, New York, 2004.
- [21] S. W. Baertschi, K. M. Alsante, H. H. Tonnesen, J. Pharm. Sci. 99 (2010) 2934-2940.
- [22] E. Dinç, D. Baleanu, J. Pharm. Biomed. Anal. 31 (2003) 969-978.
- [23] E. Dinç, G. Kökdil, F. Onur, J. Pharm. Biomed. Anal. 26 (2001) 769-778.
- [24] V.G. Dabbene, M.C. Briñón, M.M. De Bertorello, J. Pharm. Sci. 83 (1994) 1617-1621.
- [25] K. Karljikovic-Rajic, D. Novovic, V. Marinkovic, D. Agbaba, J. Pharm. Biomed. Anal. 32 (2003) 1019-1027.
- [26] N.B. Pappano, Y.C. De Micalizzi, N.B. Debattista, F.H. Ferretti, Talanta 44 (1997) 633-639.
- [27] R.C. Tena, M.A.R. Delgado , M.J. Sanchez, F.G. Montelongo, Talanta 44 (1997) 673-683.
- [28] S.E. Anderson, G.L. Nyberg, Appl. Surface Sci. 22-23 (1985) 325-337.
- [29] M. W. Abdel Aziz, M. H. Ekram M., A.G. Azza, J. Pharm. Biomed. Anal. 12(7) (1994) 951-954.

Different photodegradation behavior of barnidipine under natural and forced irradiation

- [30] K.A. Connors, *Chemical Kinetics, the study of reaction rates in solution*, VCH Publishers, New York, 1991.
- [31] O. Mitsunobu, S. Matsumoto, M. Wada, H. Masuda, *B. Chem. Soc. Jpn* 45(5) (1972) 1453-1457.
- [32] I.A. Majeed, W.J. Murray, D.W. Newton, S. Othman, W.A. Al-Turk, *J. Pharm. Pharmacol.* 39 (1987) 1044-1046.
- [33] J. Fiori, R. Gotti, C. Bertucci, V. Cavrini, *J. Pharm. Biomed. Anal.* 41 (2006) 176-181.
- [34] A.B. Baranda, R.M. Alonso, R.M. Jiménez, W. Weinmann, *Forensic Sci. Int.* 156 (2006) 23-34.
- [35] C. Vetuschi, G. Ragno, M. Veronico, A. Gianandrea, *Anal. Lett.* 35 (2002) 1327-1339.
- [36] M. Pawula, D. Watson, T. Teramura, T. Watanabe, S. Higuchi, K.N. Cheng, *Chromatogr. B* 719 (1998) 113-123.
- [37] S. Onoue, N. Igarashi, Y. Yamauchi, N. Murase, Y. Zhou, T. Kojima, S. Yamada, Y. Tsuda, *Eur. J. Pharm. Sci.* 33(3) (2008) 262-270.
- [38] C. Schweitzer, R. Schmidt, *Chem. Rev.* 103 (2003) 1685-1757.
- [39] N. Pizarro, G. Günther, L.J. Núñez-Vergara, *J. Photochem. Photobiol. A: Chem.* 189 (2007) 23-29.
- [40] E. Fasani, A. Albini, M. Mella, *Tetrahedron* 64 (2008) 3190-3196.

Different photodegradation behavior of barnidipine under natural and forced irradiation

[41] E. Fasani, M. Fagnoni, D. Dondi, A. Albini, *J. Org. Chem.* 71 (2006) 2037-2045.

[42] G. Ragno, G. Ioele, M. De Luca, A. Garofalo, F. Grande, A. Risoli, *J. Pharm. Biomed. Anal.* 42 (2006) 39-45.

3. A chemometric model for assessment of real drug photodegradation from forced test

The Institute ICH (International Conference on Harmonization) has developed guidelines for the study of photodegradation of the drugs [1]. These rules must be applied by using accelerated photodegradation studies with artificial sources, to by-pass studies of degradation in which the sun is used as light source.

The intensity of sunlight can vary considerably and depend on day time, weather conditions and seasons. So, a light-sensitive drug when exposed to light in winter presents a longer degradation time compared to an exposure in the summer. Also the high summer temperatures can promote and then catalyze chemical reactions of decomposition, together the intensity of light.

For companies, it is important to know the real degradation time of the drugs when they are exposed to the solar light. For this reason the main goal of our work was to standardize the accelerated stability study and to know the relationship between the artificial light source and the natural light intensity. So, it should be possible to reproduce the photodegradation process that should take place under solar irradiation in the laboratory without the long times necessary for the sunlight exposition.

We attempted to develop a multivariate mathematical model able to describe a complete degradation of a drug, by linking degradation data from stressing and real sunlight. In order to

standardize the process, some matrices whose photodegradation process was already reported in the literature.

Furthermore, it was decided to choose substances soluble in the same solvent, to ensure a more straightforward application spectrophotometric analysis. In order to respect all these requirements, the selected drug were nitrofurazone, amiloride and melatonin.

Nitrofurazone (5-nitro-2-furaldehyde semicarbazone) (NFZ) is a urinary antiseptic broad spectrum activity against most gram-positive and gram-negative microorganisms.

The process of photodegradation of nitrofurazone, follows the chemical degradation of heterocycles having nitro groups [2]. In particular, when exposed to light, this structure undergoes isomerization and fragmentation of the bond N-N with the formation of the azine group.

Amiloride (3,5-diamino-(diaminometilene)-6-carboxamide-cloropirazin monocloroidrato) (AML) is the most powerful pyrazine derivatives with diuretic and natriuretic activity and moderate anti-hypertensive effect is due to action at the level of the distal tubule where blocks the sodium-potassium exchange by inducing an increase and a reduction in natriuria potassiuria. Amiloride also has a modest antihypertensive activity, including the diuretic action often proves useful in the resolution of water retention.

In literature the process of the amiloride photodegradation in aqueous solution is described [3]. The analysis of UV spectra of the drug after exposure to the light reveals the presence of

isosbestic points to 250 and 320 nm, suggesting a single transformation of the chromophore in the early stages of irradiation.

Melatonin (N - acetyl - 5 - metossitriptamina) (MT) is a natural hormone secreted by the pineal gland (epiphysis) present in all living forms. It is synthesized and secreted by the pineal gland at night, and in the body decreases with advancing aging. This molecule seems to resynchronize the body, keeping intact neuroendocrine system, hormones and immune system.

In an article published a study has reported on the photodegradation of melatonin in methanol solution exposed to an irradiation chamber of Xenon arc lamp (150 W) for three months and analyzed by HPLC for the quantification and NMR for the characterization of photo products. In this study, a possible mechanism of photodegradation of melatonin is proposed [4].

Since chemometrics is normally applied to solve systems in chemistry presenting datasets very large and highly complex, involving hundreds to tens of thousands of variables, and hundreds to millions of cases or observations.

The application of the statistical technique ANOVA (Analysis of Variance), which is able to evaluate the effects continuous or not of several independent variables, was firstly used in order to establish if the data are useful to build the model. In a successive step a PLS model was build for each drug.

3.1. Drugs and Photodegradation Kinetics

Stressed conditions were obtained by exposing the drugs under the light of the cabinet Suntest CPS+ (Heraeus, Milan, Italy), equipped with a Xenon lamp. The apparatus was fitted up with an electronic device for irradiation and temperature measuring and controlling inside the box. The system was able to closely simulate sunlight and to appropriately select spectral regions by interposition of filters. In particular, for the study, the filter UV glass was chosen in order to reproduce solar light .

For the exposition at solar and artificial light, the samples were prepared in ethanol. For the irradiation in natural conditions the days in which the light had characteristics similar to the artificial light were chosen.

Spectrophotometric measurements were performed using an Agilent 8453 Diode Array spectrophotometer (Agilent Technologies. USA). The absorption spectra were recorded in the wavelength range 190 - 1100 nm in a 10 mm quartz cell, under the following conditions: integration time of 0.5 seconds, range 1 nm.

Standard solution for each drug were prepared in ethanol at the concentration of 20 µg/ml except for NFZ that was prepared at the concentration of 40 µg/ml because of its high photosensitivity.

3.2. Results and Discussion

3.1. Photodegradation experiments

The photodegradation tests were performed by using the light cabinet Suntest CPS. The reference power for stressed tests were

250, 350, 450 and 550 W/m². The exposition of samples to natural light was performed after collecting a big amount of data in order to characterize the main parameters of the sunlight, namely illuminance (lux) and irradiation power (W/m²). Solutions of each drug at the concentration of 20 µg/ml were subdued to natural and artificial light. For each drug spectral data from stressed and natural conditions were recorded and the photodegradation process characterized. Photodegradation kinetics were also defined for all the irradiation conditions.

Spectral sequences of the drug in all conditions are showed in the following figures. For NFZ, the absorbance values were detected at a wavelength of 362 nm, at which the drug has an absorption maximum (Fig. 1)

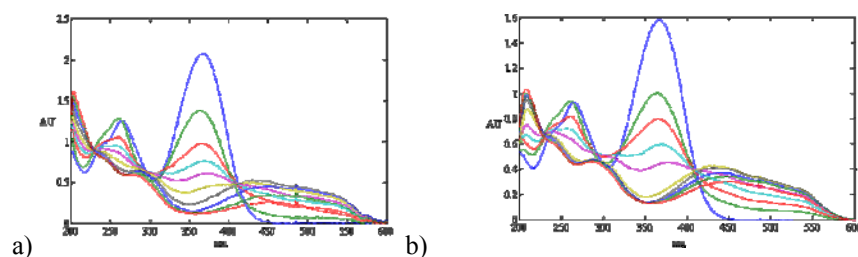


Figure 1. NFZ photodegradation spectra under sunlight (a) and artificial light (b).

From these data the residual concentration of the drug, the value of absorbance (logSun) and the logarithm of the percentage residual (log% sun) (Table 1) were calculated.

Table 1. Photodegradation data for NFZ

Time (min)	Power (W/m ²)	lux (lx)x10 ⁴	lux/Watt (lm/W)	E_{Tot.} (KJ/m ²)	Abs (AU)	Logdeg%
0	0	0	0	0	1,647	2,000
1	677	10,49	154,95	40,62	1,560	1,976
3	655	10,43	159,24	119,22	1,385	1,924
7	665	10,46	157,29	278,82	1,179	1,854
13	679	10,48	154,34	523,26	1,040	1,800
16	678	10,42	153,69	645,30	0,968	1,769
25	684	10,51	153,65	1014,66	0,757	1,662
35	645	10,58	164,03	1401,66	0,533	1,510
50	687	10,61	154,44	2019,96	0,391	1,376
70	677	10,23	151,11	2832,36	0,156	0,976

The same parameters were calculated for the degradation in the Suntest in order to obtain the data useful to understand the photodegradation kinetics of the drug under forced conditions. The kinetics were calculated assuming the variable Y "log deg%" versus the X variable "Time" (Fig 2).

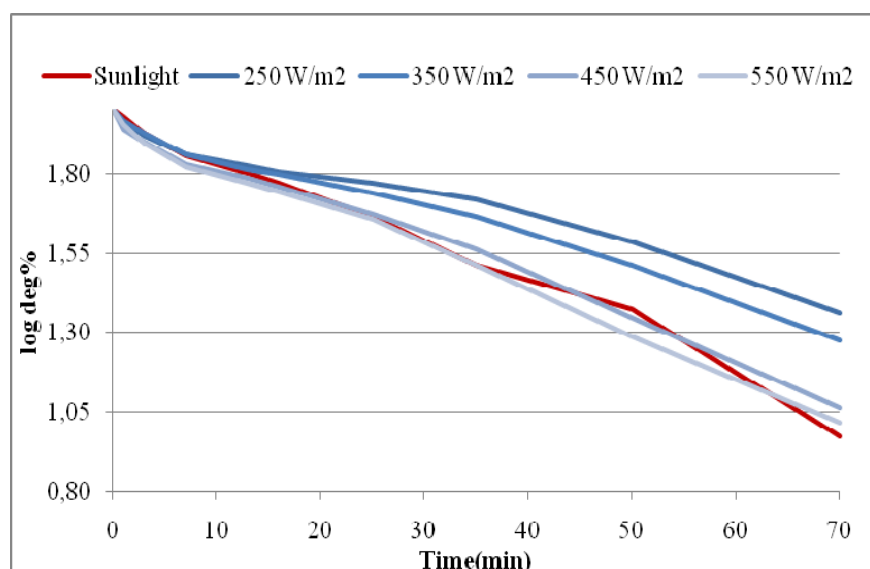


Figure 2. Photodegradation kinetics of NFZ under studied conditions.

The following table shows the kinetic equations of the drug (Table 2).

Table 2. Kinetic equations of NFZ degradation

SUN	$\log \text{ deg\%} = -1,36\text{E-}02\text{X} + 1,894$ $R^2 = 0,998$
250 W/m ²	$\log \text{ deg\%} = -8,05\text{E-}03\text{X} + 1,957$ $R^2 = 0,972$
350 W/m ²	$\log \text{ deg\%} = -9,48\text{E-}03\text{X} + 1,963$ $R^2 = 0,985$
450 W/m ²	$\log \text{ deg\%} = -1,24\text{E-}02\text{X} + 1,957$ $R^2 = 0,990$
550 W/m ²	$\log \text{ deg\%} = -1,33\text{E-}02\text{X} + 1,957$ $R^2 = 0,993$

The kinetics of degradation of nitrofurazone in each of the tested conditions follows a linear path. The energy of sunlight has an effect equivalent to a capacity of between 550-650 W/m².

When the amiloride solution was exposed to natural and artificial light the following spectra and kinetic profile were obtained (Figg. 3 and 4):

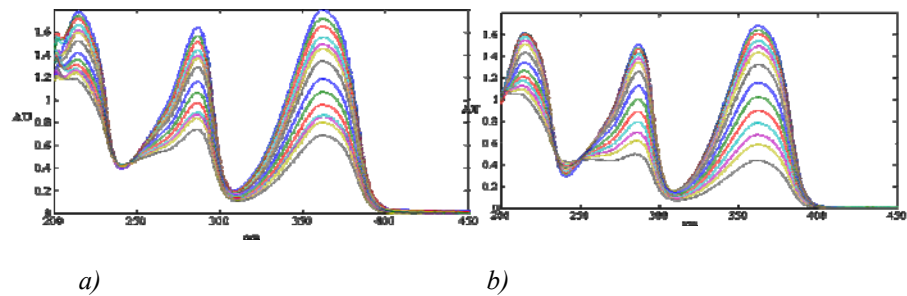
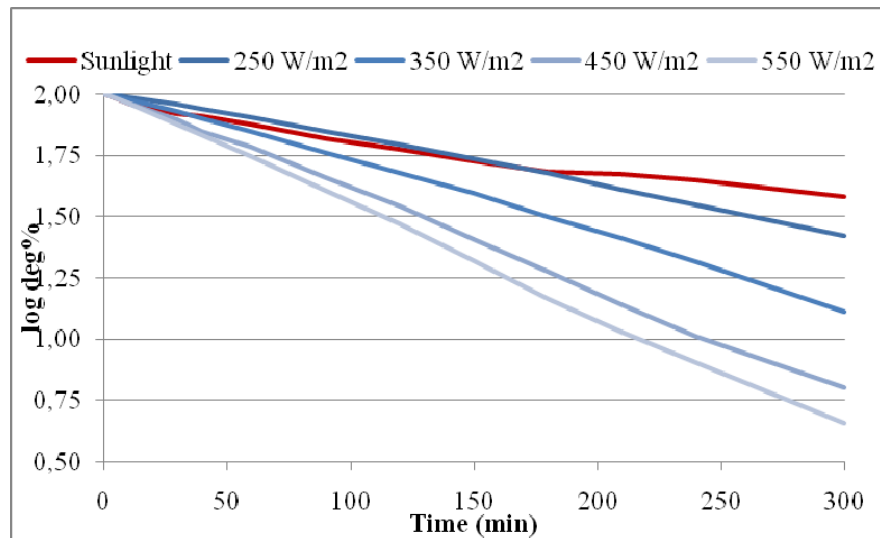


Figure.3. *AML photodegradation spectra under sunlight (a) and artificial light (b).*

The absorption maximum at 362 nm was used to calculate the percentage of residual Amiloride because this signal has a high value of absorption and therefore provides low errors.

Figure 4. Photodegradation kinetics of AML under studied conditions.



The degradation kinetics followed a linear trend in all exposure conditions. The mathematical equations of photodegradation are showed in the table 3.

SUN	$\log \text{deg}\% = -1,39\text{E-}03\text{X} + 1,965$ $R^2 = 0,974$
250 W/m ²	$\log \text{deg}\% = -1,92\text{E-}03\text{X} + 2,012$ $R^2 = 0,998$
350 W/m ²	$\log \text{deg}\% = -2,90\text{E-}03\text{X} + 2,012$ $R^2 = 0,998$
450 W/m ²	$\log \text{deg}\% = -4,07\text{E-}03\text{X} + 2,011$ $R^2 = 0,999$
550 W/m ²	$\log \text{deg}\% = -4,58\text{E-}03\text{X} + 2,008$ $R^2 = 0,999$

Table 3. Kinetic equations of AML degradation

Melatonin is a photosensitive substance, but the reaction kinetics is slower than the other two matrices analyzed. It required 12 hours of light exposure to surely evaluate the degradation products. Melatonin has two absorption maxima at 278 and 223 nm. To calculate the remaining percentage of drug, the 223 wavelength was chosen because the degradation kinetics resulted more linear.

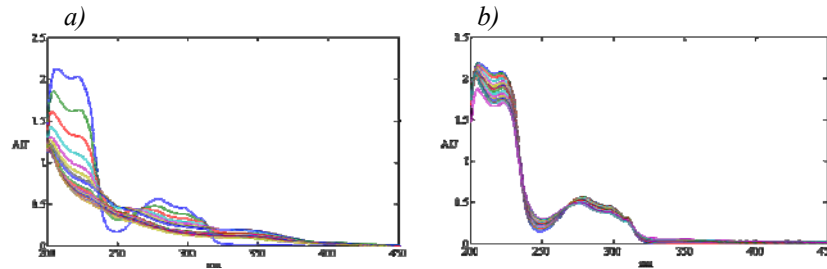


Figure 5. *MT photodegradation spectra under sunlight (a) and artificial light (b).*

Melatonin is degraded according to a first-order kinetics only if exposed to direct solar radiation, while it follows a linear kinetic when using Suntest, under all conditions of radiant energy, only in the first time of irradiation (Fig. 6). The mathematical equations of photodegradation are showed in the table 4.

Figure 6. *Photodegradation kinetics of MT under studied conditions.*

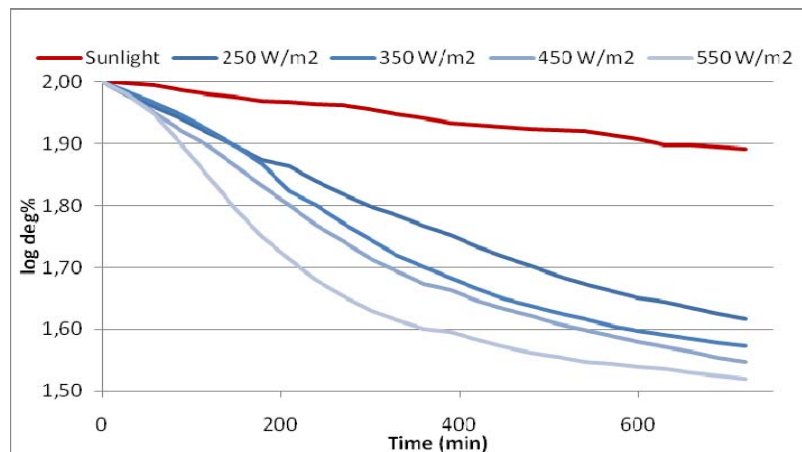


Table 4. Kinetic equations of ML degradation

SUN	$\log\%A = -1,54E-04X + 1,9986$ $R^2 = 0,9928$
250 W/m ²	$\log\%A = -6,21E-04X + 1,9923$ $R^2 = 0,9975$
350 W/m ²	$\log\%A = -8,71E-04X + 2,0141$ $R^2 = 0,9937$
450 W/m ²	$\log\%A = -1,59E-03X + 2,0104$ $R^2 = 0,9974$
550 W/m ²	$\log\%A = -9,62E-04X + 2,0047$ $R^2 = 0,9985$

1.2. Calculation of light parameters

A study to measure the irradiance or lux (lux = lumen/m²) from sun by using a light meter and Suntest sources was conducted, where lumen is the unit of the luminous flux. The measurements showed that the lux of the Suntest had higher values than sun and the same was for the luminous efficiency, which is the ratio between light output and irradiance power of the source. By using these parameters it was possible to build a table describing the characteristics of different light sources and so understand the behavior of a drug during photodegradation.

The values of luminous efficiency measured for sunlight and Suntest, under various conditions, are shown in the following table (Table 5).

Table 5. *Light source parameters*

<i>Source</i>	<i>Power</i> <i>W/m²</i>	<i>Lux</i> <i>Lx = lm/m² x10⁴</i>	<i>Luminous efficiency</i> <i>lm/W</i>
Sun	402 – 805	5,02 – 12,57	124,88 – 156,15
250 W/m ²	250	18,43	736,20
350 W/m ²	350	28,39	811,11
450 W/m ²	450	38,98	866,32
550 W/m ²	550	49,69	903,38

3.3. Multivariate Model

After collecting all the data, a multivariate method based on PLS (Partial Least Squares) modeling, has been defined. The model was able to extrapolate a real degradation of a drug from a forced degradation test.

The first step in building the model is the establishment of the calibration set: an amount of n objects (or procedures), whose predictors X and responses Y are known. The following table shows schematically the composition of the arrays of data included in the calibration set: (Table 6)

Table 6. Calibration set

		<i>X Variables</i>			<i>Y variable</i>
<i>Drug</i>	<i>Light source</i>	<i>Time (min)</i>	<i>E (KJ/m²)</i>	<i>L/WxE (lm/W)x(KJ/m²)</i>	<i>Logdeg%</i>
Nitrofurazone	Sunlight	0–70	0–2832	0-151,11xE	0<Y≤2
	250W	0–70	0–1050	737,20xE	0<Y≤2
	350W	0–70	0–1470	811,11xE	0<Y≤2
	450W	0–70	0–1890	866,32xE	0<Y≤2
	550W	0–70	0–2310	903,38xE	0<Y≤2
Amiloride	Sunlight	0–300	0-1032	0-124,88xE	0<Y≤2
	250W	0–300	0–4500	736,20xE	0<Y≤2
	350W	0–300	0–6300	811,11xE	0<Y≤2
	450W	0–300	0–8100	866,32xE	0<Y≤2
	550W	0–300	0–9900	903,38xE	0<Y≤2
Melatonin	Sunlight	0–720	0–2704	0-149,21xE	0<Y≤2
	250W	0–720	0–1081	736,20xE	0<Y≤2
	350W	0–720	0–1502	811,11xE	0<Y≤2
	450W	0–720	0–1944	866,32xE	0<Y≤2
	550W	0–720	0–2376	903,38xE	0<Y≤2

The data arrays enclose different parameters with different units and scales. With the aim to homogenize the data and allow their processing in the subsequent step it was necessary to normalize the arrays, by using the method of standard deviation (1/DS).

1.2.1. ANOVA analysis

In order to test the significance of data and selected variables, the Analysis of Variance (ANOVA), was performed on all the three matrices [5]. ANOVA is a test widely used and is based on the statistical assumptions of independence, normality and homoscedasticity of the experimental responses. It is a collection of statistical models, and their associated procedures, in which the observed variance in a particular variable is partitioned into components attributable to different sources of variation. The origin of functional ANOVA is linked to the seminal works of Hoeffding in the 1940's [6]. Rabitz and Alis (1999) introduce an alternative generalization of functional ANOVA, called high dimensional model representation (HDMR) theory [7]. They prove the functional ANOVA decomposition through the dissection of the linear space to which the function belong. In this work we used ANOVA to verify that all the matrices can be used to construct a multivariate model ($p < 0,005$) [8].

The data obtained from ANOVA analysis are shown in the Table 7.

Table 7. ANOVA analysis

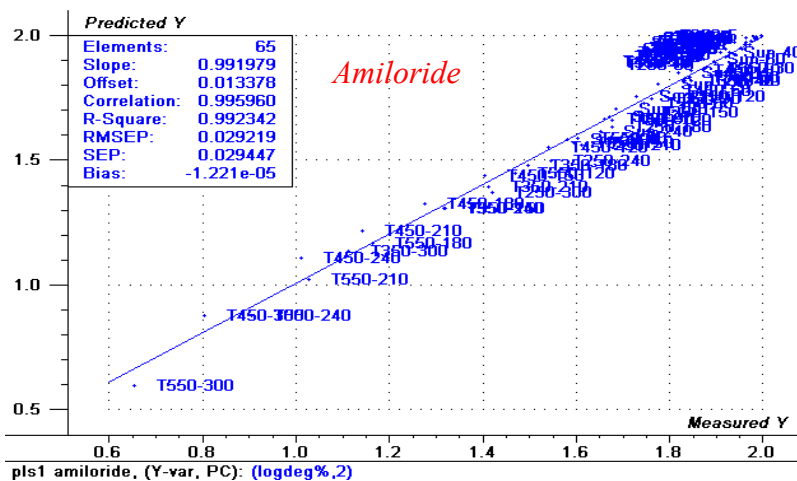
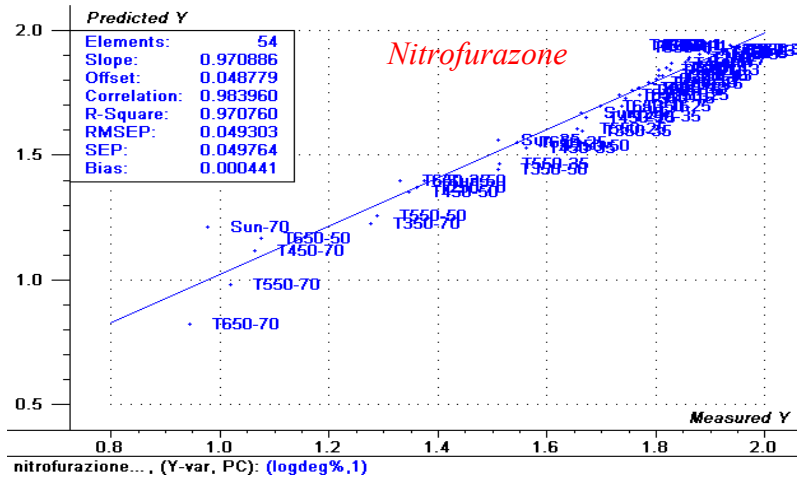
Nitrofurazone	SS	DF	MS	F-ratio	p-value	B-coefficients	STDerr
Model	4,057	3	1,352	1,01E+03	0,0000		
Error	6,69E-02	50	1,34E-03				
Adjusted Total	4,124	53	7,78E-02				
Variable							
Intercept	66,615	1	66,615	4,98E+04	0,0000	1,66	7,44E-03
Time	4,66E-02	1	4,66E-02	34,85	0,0000	-3,25E-03	5,50E-04
E*L/W	6,03E-02	1	6,03E-02	45,064	0,0000	-1,01E-07	1,51E-08
E Tot	0,217	1	0,217	162,239	0,0000	-2,22E-04	1,74E-05
Amiloride							
Summary							
Model	6,842	3	2,281	3,47E+03	0,0000		
Error	4,02E-02	61	6,58E-04				
Adjusted Total	6,882	64	0,108				
Variable							
Intercept	74,024	1	74,024	1,13E+05	0,0000	1,669	4,98E-03
Time	5,84E-03	1	5,84E-03	8,869	0,0042	-2,59E-04	8,70E-05
E*l/w	1,77	1	1,77	2,69E+03	0,0000	-1,31E-07	2,52E-09
E Tot	2,90E-02	1	2,90E-02	44,107	0,0000	-1,78E-05	2,68E-06
Melatonin							
Summary							
Model	0,713	3	0,238	1,70E+03	0,0000		
Error	1,05E-02	75	1,40E-04				
Adjusted Total	0,723	78	9,27E-03				
Variable							
Intercept	61,097	1	61,097	4,37E+05	0,0000	1,864	2,82E-03
Time	3,66E-02	1	3,66E-02	261,476	0,0000	-3,27E-04	2,02E-05
L/W*Etot	0,395	1	0,395	2,83E+03	0,0000	-4,28E-08	8,05E-10
E Tot	6,80E-02	1	6,80E-02	486,216	0,0000	1,05E-05	4,75E-07

The algorithm chosen for the construction of the multivariate model was the Partial Least Squares (PLS). From application of the regression algorithm to the three arrays of data, three models were developed by the general formula:

$$\log \text{deg \%} = aT + bE + c \frac{\text{lux}}{W} E + d$$

Where a, b, c e d are the regression coefficients.

A procedure of full cross validation was used to validate the model. The following graphs (Fig.6) show the results obtained from the validation of the models; the comparison was made between the data calculated by using the model during the full cross validation and real values obtained from calibration set.



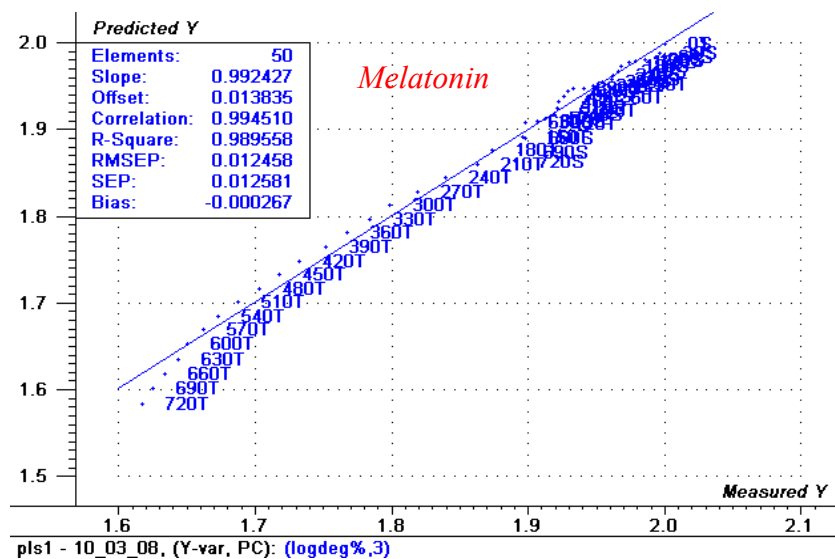


Figure 6. Graphical reports of validation on the models

Finally, the equations of the PLS models obtained for each drug are shown in the following table (Table 8).

Table 8. PLS models for the three drugs

<i>Nitrofurazone</i>		
log deg% = -3,249e-03 T – 2,216e-04 E – 1,013e-07 L/W E + 1,949		
R^2	<i>RMSEP</i>	<i>PC</i>
0,97076	0,03614	1

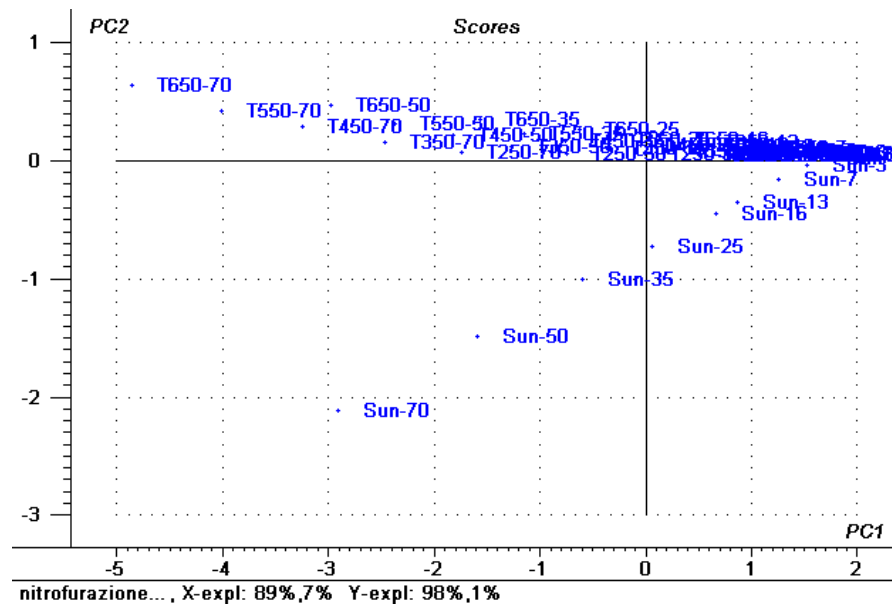
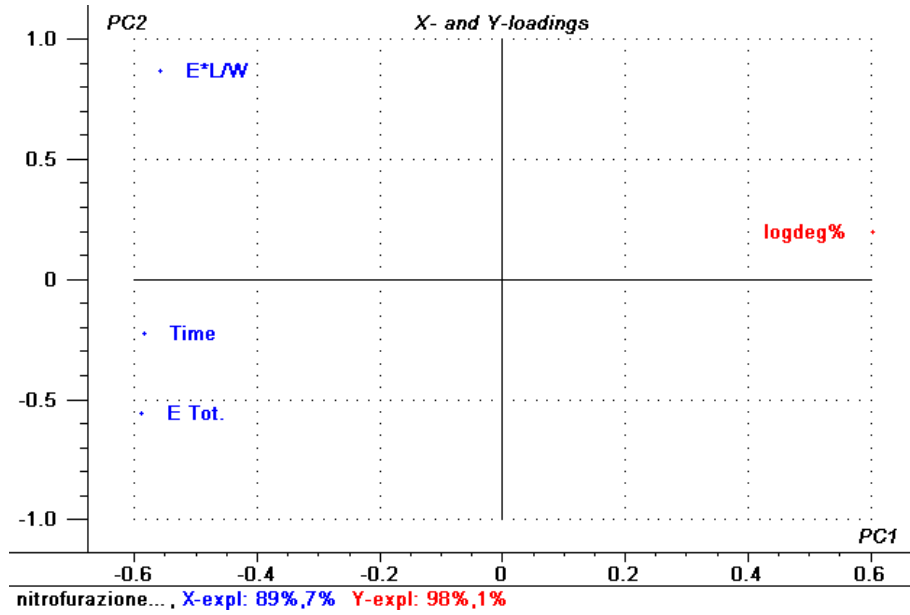
<i>Amiloride</i>		
log deg% = -5,351e-04 T – 9.658e-06 E – 1.286e-07 L/W E + 2,01		
<i>R</i> ²	<i>RMSEP</i>	<i>PC</i>
0,99234	0,029219	2

<i>Melatonin</i>		
log deg% = -4,708e-05 T + 4,079e-06 E - 4,844e-08 L/W E + 2,001		
<i>R</i> ²	<i>RMSEP</i>	<i>PC</i>
0,98955	0,012181	3

From the graphical report of X and Y loadings, it is evident the reverse correlation between Y variable (logdeg%) and L/WxE variable for all the studied drugs.

The relationships clarify that when the ratio Lux/W of the light source increases, the drug will be degraded in lower times and the comparison of the different photodegradation kinetics is possible under several photodegradation conditions. As general example the graphics of X and Y loadings and scores of NFZ is reported (Figg 7 and 8).

Nitrofurazone



Figures 7 and 8. Graphical reports of X, Y loadings and scores of NFZ

3.4. Conclusions

The work has demonstrated the ability of chemometric analysis to elaborate a very high number of analytical parameters in order to obtain a final reliable result. The correlation between two different light sources such as sunlight and artificial light was established.

The building of a model able to reproduce in laboratory the photodegradation induced by sunlight resolves the problem of the long times of irradiation under natural condition. A new variable, the ratio between illuminance and irradiation power, was found to be the connection between artificial and natural light. This permits to elaborate new models, by using data from forced or natural irradiation in the calibration set.

For more details:

[1] ICH Harmonized Tripartite Guideline, Photostability Testing of New Drug Substance and Products, Fed. Register 62 (1996) 27115-27122.

[2] Shahjahan, M., Enever, R. P., Int. J. Pharm. 143 (1996) 75-82.

[3] Li, Y.N.B., Moore, D.E. and BN Tattam,, Int J Pharm, 183 (1999) 109-116.

[4] Andrisano, V., Bertucci, C., Battaglia, A., Cavrini,V., J. Pharm. Bio. An. 23, (2000) 15-23.

[5] Greenhill, J.V. and McLelland, M.A., Photodecomposition of drugs, in Ellis, G.P. and West, G.B. (Eds.), Progress in Medicinal Chemistry, pp. 51-121. Holland: Elsevier Science Publishers, B.V. (1990)

[6] Hoeffding, A., Ann. Math. Statist. 19 (1948) 293-3251.

[7] Rabitz , H., and Alis, F., J. Mat. Chem., 25 (1999) 197--233.

[8] Carstensen, J.T. (1995) Drug Stability, 2nd ed., pp. 486-537. New York: Marcel Dekker, Inc.

4. Kinetic studies of nitrofurazone photodegradation by multivariate curve resolution applied to UV-spectral data

Nitrofurazone (2-((5-nitro-2-furanyl) methylene) hydrazinecarboxamide) (NFZ) is a well-known antibacterial agent effective against a wide variety of gram-negative and gram-positive organisms, applied to the treatment of many human and animal infections [1-3]. Nowadays, its use in medicine has become less frequent and it is above all used topically as a local anti-infective drug, prescribed in the prophylaxis and treatment of infections of the skin and mucous membranes [4].

Since the drug, when exposed to light, is susceptible to photodegradation [5,6], its use in topical preparations represents a serious problem about the loss of the pharmacological activity. In previous publications the photodecomposition of this drug under controlled conditions has been investigated, hypothesizing a very complex degradation pathway of the drug [6,7]. The photolability of NFZ was firstly reported in 1966 [8,9] but the main photoproducts were separated by HPLC and identified only in 1987 [10] as the *syn*-isomer of NFZ (*syn*-NFZ) and the bis(5-nitrofurylidene) azine (AZI), respectively. The 5-nitro-2-furaldehyde (NFA) and the hydrazone of 5-nitro-2-furaldehyde (HYD), were also reported as further potential photodegradation products but their presence was not observed.

The reaction rate of photodegradation of NFZ in solution has been reported to increase with the decrease of the drug concentration and with the increase of the illuminance power [11-

12, 7]. The influence of various factors including pH of the medium, irradiation wavelengths, presence of surfactants, metal ions or ultraviolet light absorbers has been also investigated [5,6].

Actually, the details of the photodegradation mechanism still remain unclear. The published studies are focused on the identification of the photodegradation products but do not investigate the sequential degradation steps that may take place. The prediction of the exact photochemical behaviour of a specific molecule is really difficult, as Grenhill has pointed out in his review [13]. This is due to the fact that the photodegradation mechanism depends in a complex way on the structure and on experimental conditions and then the kinetics and photoproducts distribution may vary significantly even among closely related compounds [14].

Nowadays, the spectrophotometric techniques remain largely used in the field of analytical chemistry because of the easy interpretation and handling of the spectral data. On the other hand, the conventional spectrophotometric methods use a discrete number of wavelengths that frequently are not enough to furnish the necessary information to resolve a system with severe spectra overlapping. In recent years, chemometrics approaches for the extraction of analytical information from multivariate data have been proposed [15-16]. Multivariate methods have the advantage of exploiting full spectral information, by using simultaneously all measured analytical signals.

In this work, we report the investigation on the photochemical degradation process of the NFZ drug and we give

an interpretation of the complete kinetic pathway obtained by a recently proposed hybrid hard- soft-modelling multivariate curve resolution (HS-MCR) method applied to UV spectrophotometric data. This chemometric method can be applied to the simultaneous treatment of several experiments conducted under different experimental conditions. It allows the extraction of the pure spectra of the involved components together with their concentration profiles and, at the same time, it evaluates the kinetic model and their various rate constants [17-19].

The photodegradation experiments were performed following the ICH recommendations for the drug stability tests [20]. An independent HPLC-DAD method was simultaneously developed to check the results obtained by the analysis of the UV kinetic photodegradation studies. The chromatographic data were then also analyzed by means of the same MCR approach. From the results obtained by these two approaches for synthesized and commercially obtained pure compounds, as well as for their degradation products, the chemical structure of the main photoproducts are proposed. Dependence of the kinetics pathway from sample concentrations and from different illuminance power is also verified.

4.1. Drug and Experimental Procedure

Nitrofurazone (NFZ), 5-nitro-2-furaldehyde (NFA), 2-furaldehyde (FA), 5-nitro-2-furaldehyde diacetate and hydrazine hydrate were purchased from Sigma-Aldrich Co. (Italy). The 5-nitro-2-furaldehyde azine (AZI), was prepared by condensation of 3.0 g (0.02 mol) of 5-nitro-2-furaldehyde with 0.5 g (0.01 mol) of hydrazine hydrate [21]. The hydrazone of 5-nitro-2-furaldehyde (HYD) was prepared from 2.5 g (0.01 mol) of 5-nitro-2-furaldehyde diacetate and 0.5 g (0.01 mol) of hydrazine hydrate [10].

Light exposure was performed in a light cabinet Suntest CPS+ (Heraeus, Milan, Italy), equipped with a Xenon lamp. The apparatus was fitted up with an electronic device for irradiation and temperature measuring and controlling inside the box. The system was able to closely simulate sunlight and to appropriately select spectral regions by interposition of filters.

Spectrophotometric measurements were performed using an Agilent 8453 Diode Array spectrophotometer (Agilent Technologies, USA). HPLC analysis was performed by using a chromatograph Agilent 1100 series (Agilent Technologies, CA), equipped with a binary pump delivery system and a diode array UV-Vis detector. A stock solution of NFZ (1.0 mg/ml) in ethanol was properly diluted to obtain two samples for degradation experiments: sample solution A (NFZ at 100.0 µg/ml) and sample solution B (NFZ at 20.0 µg/ml). These two samples, in quartz cells perfectly stoppered, were light irradiated directly at the wavelength range between 300 and 800 nm, by means of a glass filter,

according to the ID65 standard of the ICH rules. This light exposure was repeated by varying the irradiation power at four different levels: 250, 350, 450 and 550 W/m², corresponding to an energy value of 15, 21, 27 and 33 kJ/min/m², respectively. The solution temperature was maintained constant at 25 °C.

UV spectra were recorded in the range between 200 and 650 nm, just after preparation (t = 0) and at the following times: 1, 3, 5, 7, 10, 15, 20, 25, 30, 40, 50, 60 and 70 min. The spectra of solution B were directly recorded, while solution A needed to be diluted before analysis with ethanol to obtain a concentration of 20 µg/ml.

HPLC separations were carried out on a LC column, 5 µm C18 Gemini column (250 x 4.60 mm) (Phenomenex, Torrance, CA), by gradient elution, using water and acetonitrile as mobile phase, filtered through 0.45 µm filter before use. Mobile phase was water/acetonitrile (95:5, v/v) for 5 minutes, gradually changed to 70:30 in 10 minutes and then maintained for 10 minutes. The injection volume was 5 µl and mobile phase flow rate was 1 ml/min.

HPLC analysis was performed after irradiating a 1 mg/ml ethanolic solution of NFZ placed in a quartz cell. The irradiance power was fixed at 250 W/m², at a temperature of 25 °C. Aliquots of 5 µl of the sample were directly analyzed by HPLC after preparation (t = 0) and at the following times: 10, 20, 30, 40, 50, 60, 90, 120, 150, 180, 210, 240, 270 and 300 min.

4.2. Chemometric Techniques

4.2.1. Multivariate curve resolution-alternative least squares (MCR-ALS)

When a degradation process is monitored by UV spectroscopy, a series of spectra is collected as a function of time. Changes in these spectra can be used to extract the analytical information necessary to resolve the system, including the pure spectra and concentration profiles of the single components and the kinetics parameters.

The recorded experimental data can be ordered in a data matrix \mathbf{D} , whose rows (r) are the spectra at different times and whose columns (c) are the process signals at different wavelengths. Multivariate Curve Resolution (MCR) methods decompose mathematically these data into the contributions due to the pure components of the system [22-26], following a bilinear model derived from the generalized Lambert-Beer's absorption law.

$$\mathbf{D}_{(r \times c)} = \mathbf{C}_{(r \times n)} \mathbf{S}^T_{(n \times c)} + \mathbf{E}_{(r \times c)} \quad \text{Equation 1}$$

where \mathbf{C} is the concentration matrix of n components and \mathbf{S}^T is the matrix of their spectra. \mathbf{E} represents the unexplained variance in the data set. In MCR methods, the first step is the estimation of the number of involved components (n) in the kinetic system, which is initially obtained by application of singular value decomposition (SVD) [27]. Moreover, iterative MCR methods, like MCR-ALS, need a preliminary estimation of \mathbf{S}^T or \mathbf{C} , calculated either by evolving factor analysis (EFA) [28], by

selection of the pure variables [29-30], or by any previously estimation of them. These initial estimates are used to start the Alternating Least Squares (ALS) constrained optimization through an iterative process. At each cycle, a new estimation of \mathbf{S}^T and \mathbf{C} is calculated by solving alternatively the two following least-squares matrix equations, according to the scheme of Figure 1:

$$\mathbf{S}^T = (\mathbf{C})^+ \mathbf{D} \quad \text{Equation 2}$$

$$\mathbf{C} = \mathbf{D}(\mathbf{S}^T)^+ \quad \text{Equation 3}$$

where $(\mathbf{S}^T)^+$ and $(\mathbf{C})^+$ are the pseudoinverses of the \mathbf{S}^T and \mathbf{C} matrices (s), respectively [27, 31-32].

At every iteration, constraints like non-negativity, unimodality and concentration closure are applied to drive the optimization process towards a final solution with chemical meaning fulfilling the applied constraints [32]. This iteration procedure is stopped when convergence is achieved, by fixing a preselected number of cycles or when the value of lack of fit (LOF) does not change significantly between consecutive iterations:

$$\% \text{LOF} = 100 \times \sqrt{\frac{\sum_{ij} (d_{ij} - d_{ij}^*)^2}{\sum_{ij} d_{ij}^2}} \quad \text{Equation 4}$$

where d_{ij} and d_{ij}^* were respectively the experimental and calculated (by MCR-ALS) absorbance values. A different parameter used to indicate the quality of MCR-ALS modelling results is the percentage of explained variance (r^2):

$$r^2 = 100 \times \frac{\sum_{ij} d_{ij}^{2*}}{\sum_{ij} d_{ij}^2} \quad \text{Equation 5}$$

Another important feature of the MCR-ALS method is its possibility to perform the simultaneous analysis of multiple data sets coming from more than one experiment, using different experimental conditions and/or conducted by different analytical techniques. The whole set of photodegradation experiments performed at different NFZ initial concentrations exposed under different illuminance power conditions were arranged in a column-wise augmented data matrix and analyzed using MCR-ALS according to the extended bilinear model equation [31-32].

$$D_{\text{Aug.}} = C_{\text{Aug.}} \mathbf{S}^T + E_{\text{Aug.}} = [D_1 ; D_2 ; \dots ; D_N] = [C_1 ; C_2 ; \dots ; C_N] \mathbf{S}^T + [E_1 ; E_2 ; \dots ; E_N] \quad \text{Equation 6}$$

In this matrix equation, column wise matrix augmentation is indicated using MATLAB notation ‘;’, which indicates that every individual data block obtained in a single kinetic experiment is set on top of the other, with the same number of columns (wavelengths) in common, and consequently increasing the number of rows of the corresponding augmented matrix. As indicated in this equation, the same spectral matrix \mathbf{S}^T is resolved for all \mathbf{D}_i , $i=1, \dots, N$ matrices, i.e. the same pure spectra are resolved for the common species in the different experiments. On the contrary, the concentration profiles of the different resolved components in \mathbf{C}_i matrices are allowed to be different for the

different kinetic experiments. This is in agreement with the possibility of having degradation (concentration) profiles with different shapes in the different experimental data matrices obtained at different initial NFZ concentration and power irradiances. These degradation profiles will follow different patterns which cannot be described by the same set of concentration profiles. In contrast, however, the same chemical species will have the same characteristic UV spectrum in the different kinetic experiments. In conclusion, the model proposed in Equation 6 will fit well with the expected behaviour of the measured system if the generalized bilinear Beer's Lambert law of UV absorption holds for the system under investigation.

4.2.2 Hybrid hard- and soft-multivariate curve resolution-alternating least squares (HS-MCR) approach.

In this work, a variation of the MCR-ALS method, recently proposed and named hard–soft multivariate curve resolution (HS-MCR-ALS) modelling, was used [17]. This procedure introduces a new constraint able to force some or all concentration profiles in **C** to fit a previously selected kinetic model. At each iteration, a non-linear kinetic fitting routine handles the concentration profiles in **C** matrices to fulfil a preselected kinetic model [33-35,24, 36,19]. The resulting concentration profiles will fulfil the proposed kinetic model and the corresponding rate constants of the process will be obtained as additional information.

This HS-MCR-ALS algorithm is able to resolve some limitation of pure hard- and pure soft-modelling in the study of

photodegradation processes. On one hand, HS-MCR-ALS minimizes the rotational ambiguity associated to the estimation of concentration profiles only using non-negativity and closure constraints [31-32] and on the other hand it allows for the estimation of the best kinetics constants associated to a postulated kinetic model [34]. In comparison with hard-modelling approaches, in HS-MCR-ALS the kinetic model can be applied in a flexible way for some or all the species involved in the process, while in classical hard-modelling approaches, all contributions in the **D** matrix are constrained according to the preselected model [33,35]. This possibility can be used for instance when the absorbing species in the samples are more than those following the postulated kinetic process [17]. Furthermore the proposed HS-MCR-ALS method allows the use of different kinetic models for the simultaneous analysis of different kinetic experiments in the augmented **D** matrix. In this work, different kinetic models were considered to investigate the effects of the concentration and illumination power on the degradation process.

4.2.3 Chemometric software

The computations were performed in MATLAB environment (Mathwork Inc., version 6.5) and MCR-ALS user-friendly interface tool [37]. Hybrid hard-soft MCR-ALS (HS-MCR-ALS) has been described and used in de Juan et al. [17,24], Muñoz and de Juan [36], Mas et al. [19].

4.3. Results and Discussion

4.3.1. Photodegradation experiments

Fig. 2 shows the spectral sequence for the degradation of NFZ sample solution A (100.0 $\mu\text{g/ml}$) and sample solution B (20.0 $\mu\text{g/ml}$), both exposed to an irradiation power of 250 W/m^2 .

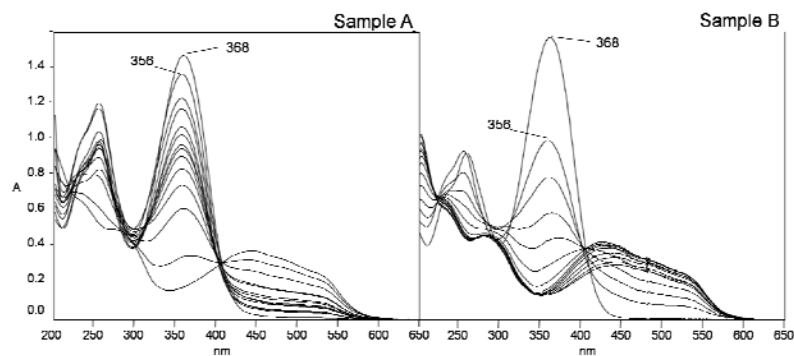


Figure 2. *UV-spectra of photodegradation experiments of NFZ sample A (100.0 $\mu\text{g/ml}$) and NFZ sample B (20.0 $\mu\text{g/ml}$), exposed under light at 250 W/m^2*

The different spectra profiles observed in these two cases confirmed the dependence of the degradation on the concentration [7]. Sample B presented a degradation process more complex than sample A with the probable formation of a higher number of photoproducts. Anyhow, a very rapid shift of the main absorbance peak from 368 to 356 nm was observed in both samples. Afterwards, this peak decreased constantly with the contemporary increase of absorbance bands above 450 nm, responsible of the rising of orange colour.

Experimental data were processed by the MCR-ALS procedure using non-negativity (concentrations and spectra of the

components must be positive), unimodality (concentration profiles in the degradation process presents only one maximum per experiment) and closure (mass balance in the kinetic process) constraints. MCR-ALS resolved three and four species for solution A and B, respectively. Fig. 3 shows the calculated concentration profiles (C) and the relative pure spectra (S^T) for both systems. Percentage of lack of fit (%LOF) values resulted to be in both cases below 1%.

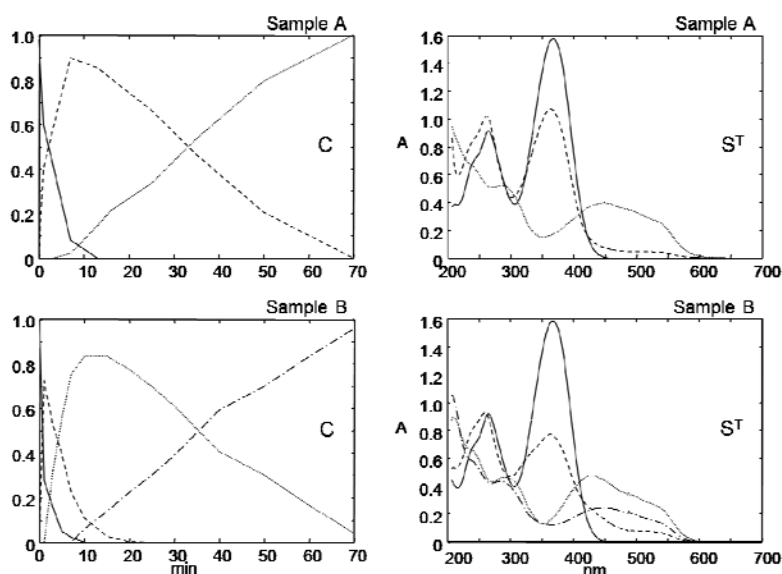
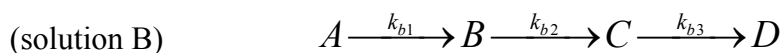


Figure 3. MCR-ALS resolved kinetic profiles and related pure spectra obtained in the analysis of individual photodegradation experiments: sample A (100.0 $\mu\text{g/ml}$) and B (20.0 $\mu\text{g/ml}$) exposed under light at 250 W/m^2 .

The spectral shapes of the common components did not show any significant difference between the two experiments. Evolution of the concentration profile plots were in agreement with kinetic

models with two and three consecutive first order reactions, respectively:



where k_{ai} are the different rate constants.

In these kinetic models, however, the possible existence of mixtures of subproducts identified as a single component (C or D) cannot be excluded. In reaction networks such as the one proposed in this work, the formation of multiple species with the same kinetic profile (for instance, in a reaction like $A \rightarrow B + C$, profiles B and C would have been exactly equal) produce the so called rank deficiency of spectral matrices measured on them [38-39]. Therefore, in this work, subproducts C and D could be considered to be a mixture of chemical compounds with different molecular structures instead of a pure chemical compound with a single molecular structure.

4.3.2. Hypothesis of photodegradation pathway

MCR-ALS analysis clearly suggested the very rapid isomerization of NFZ into its *syn*-form, as reported in previous literature [8,39], with a shift of the main peak from 368 to 356 nm and of the secondary peak from 265 to 259 nm. A significant change in the absorptivity of these peaks was also recorded, and the ratio of the first to the second peak varied from 0,587 for NFZ

to 1,485 for the isomer. Isomerisation resulted to be occurring in all the investigated cases but, in contrast, the subsequent degradation steps seemed to be strongly influenced by the NFZ initial concentration.

In sample A, the isomer degraded into a new compound characterized by an intense absorbance above 450 nm and the simultaneous disappearance of the peak at 359 nm, which is characteristic of the parent compound. This bathochromic shift of the absorption band is confirmed by the progressive colouring of the solution. Sample B at lower NFZ concentration, showed an analogous degradation pathway, but in this case MCR-ALS resolved a third photoproduct, with chromophoric features slightly different to the previously formed compound. Isolation and characterization of these two coloured photoproducts resulted very difficult, due to their simultaneous presence at high concentrations and to their further easy degradation.

In order to identify the main photoproducts of NFZ, the 5-nitro-2-furaldehyde azine (AZI) and the hydrazone of 5-nitro-2-furaldehyde (HYD) compounds were synthesized. Quilliam et al. [10] reported AZI as one of the main photodegradation products whereas HYD as a potential photoproduct. However, the recorded spectra of these two compounds demonstrated that these two compounds were not formed during the degradation process of NFZ. This was also confirmed afterwards by HPLC analysis of the NFZ photodegraded samples, which in no case did confirm the chromatographic signals of these two products. AZI (20.1 µg/ml) and HYD (20.0 µg/ml) were then exposed to light irradiation under

the same conditions adopted for NFZ, with the aim to highlight what chemical groups could be involved in the formation of the coloured photoproducts. The UV spectra of the AZI and HYD samples recorded during degradation are shown in fig. 4.

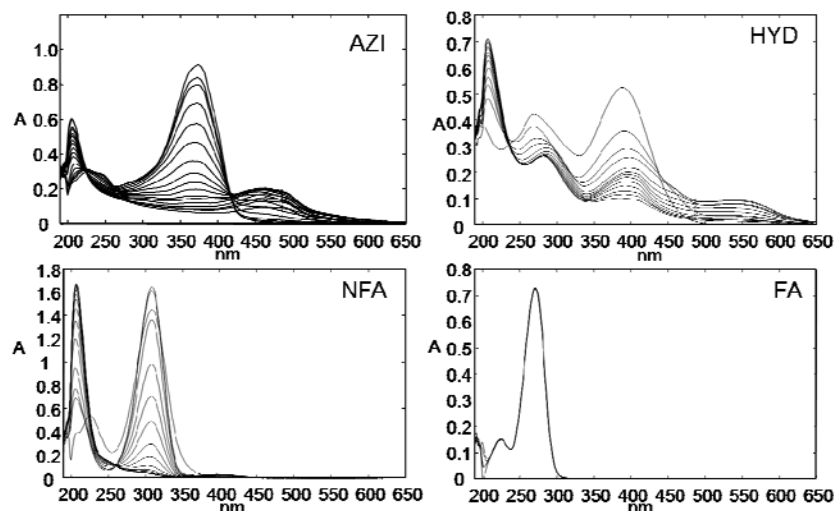


Figure 4. *UV-spectra of photodegradation experiments of solutions of AZI (20.1 $\mu\text{g/ml}$), HYD (20.0 $\mu\text{g/ml}$), NFA (20.4 $\mu\text{g/ml}$) and FA (20.0 $\mu\text{g/ml}$).*

Exposure to light of AZI and HYD gave an analogous degradation behaviour than NFZ, showing an intense colouring of their solutions and the appearance of broad bands above 450 nm. The formation of similar photodegradation compounds from NFZ, AZI and HYD demonstrated the importance of the methylene-hydrazine group in the furanic cycle. The absorbance rising in the visible region could be associated to the transformation of the nitro group into the hydroxyimminic group, in agreement with the previous results described by other authors [40-41]. Photodegradation mechanism of NFZ could be so described (Fig.5)

as a rapid isomerization to its *syn*-form that in turn undergoes degradation to a series of coloured photoproducts, highly unstable. These products could directly arise from the NFZ isomer as well as from the azine (AZI) or hydrazone (HYD) derivatives of the drug, which could be formed during degradation but they were rapidly transformed (not detected in our kinetic experiments) in the same final photoproducts as NFZ.

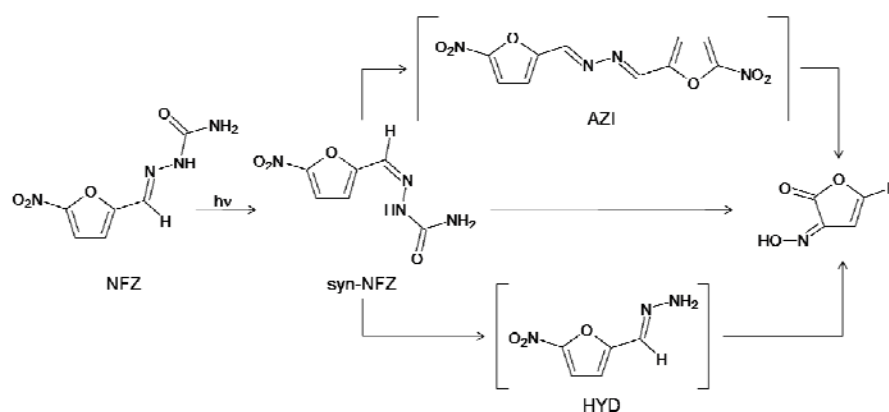


Figure 5. Scheme of the proposed degradation pathway.

Since 5-nitro-2-furaldehyde (NFA) and 2-furaldehyde (FA), were also suggested [10,7] as possible secondary photodegradation products of NFZ, they were also subjected to analogous irradiance tests. The UV spectral sequences recorded over the degradation on solutions of NFA (20.4 $\mu\text{g/ml}$) and FA (20.0 $\mu\text{g/ml}$) are also reported in figure 4. 2-furaldehyde, FA, resulted to be very stable under light exposure and no spectral changes were observed for this compound. On the other hand, UV irradiance of 5-nitro-2-furaldehyde (NFA), NFA, caused a clear decrease of its absorption

maximum peak at 309 nm. However, in both experiments, no significant absorbance above 450 nm was observed, demonstrating that they could not be the responsible for the formation of the photoproducts *C* and *D* in the photodegradation of NFZ. In fact, FA and NFA do not have this chemical group and this is the reason why they did not show the sought degradation products.

4.3.3. Hybrid hard- and soft multivariate curve resolution (HS-MCR)

In order to constrain the shape of the concentration profiles obtained by MCR-ALS analysis to fit exactly a particular kinetic model, the algorithm HS-MCR [33-35] was applied, to obtain a new set of kinetic profiles (*C*) and pure spectra (S^T) of the resolved components, as it is shown in fig. 6.

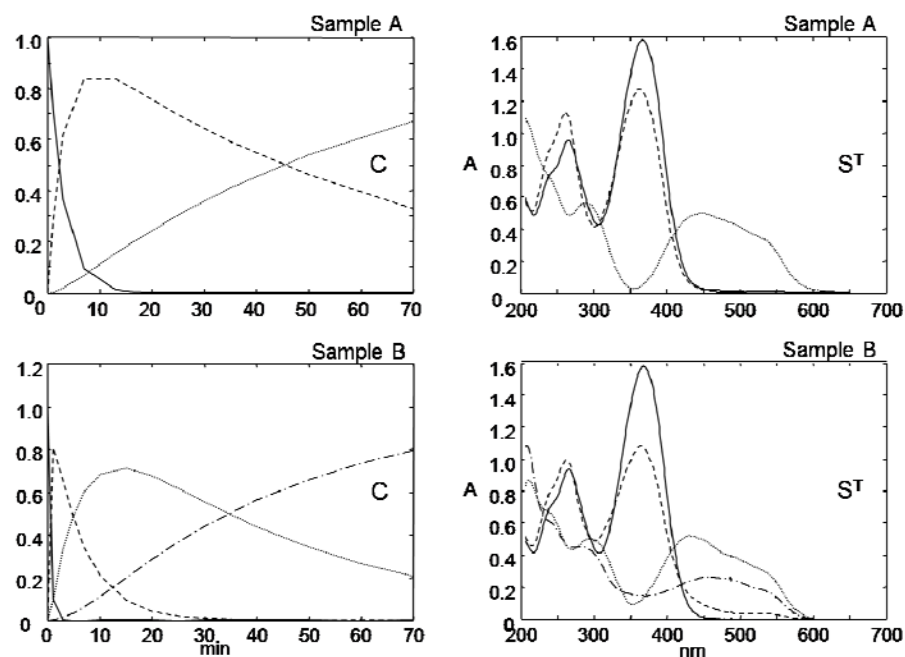


Figure 6. HS-MCR resolved kinetic profiles and related pure spectra obtained in the analysis of individual photodegradation experiments: sample A (100.0 $\mu\text{g/ml}$) and B (20.0 $\mu\text{g/ml}$) exposed under light at 250 W/m^2 .

HS-MCR analysis confirmed the pure spectra for all the components previously estimated by MCR, but a new set of concentration profiles showing now a better agreement with a particular kinetic pathway are obtained. The kinetic rate constants of the different photolysis steps in both samples A and B are listed in Table 1. The values of LOF and r^2 are also reported in this Table.

Table 1. Kinetic rates for NFZ photodegradation resulted from HS-MCR

	k_1	k_2	k_3	%LOF	r^2
Sample A (100.0 $\mu\text{g/ml}$)	8.64e-2	2.07e-2	--	1.512	99.922
Sample B (20.0 $\mu\text{g/ml}$)	4.85e-1	3.07e-1	1.143e-2	1.381	99.957

HS-MCR-ALS results confirmed the dependence of the photodegradation rate on the initial concentration of the drug. The more concentrated sample A gave a slower degradation than sample B, in agreement with previous literature results [7], furnishing a limited number of photoproducts. Indeed, the degradation process of the more diluted solution B resulted to be faster and more complex, with the formation of more photoproducts after the first common degradation steps. Nevertheless, the rate constants k_1 and k_2 , of both samples A and B, belong to the photodegradation of NFZ and syn-NFZ, while k_3 (sample B) could be considered as a composite rate constant, because the specie D could be a mixture of compounds.

4.3.4. Simultaneous MCR analysis of photodegradation experiments under various conditions

A very powerful tool in MCR analysis is the possibility of processing simultaneously multiple data sets obtained in different experiments. In the present work the spectral data from sample solutions A and B when irradiated under various illuminance power (250, 350, 450 and 550 W/m^2) were simultaneously processed by MCR-ALS and HS-MCR-ALS. The analysis of these

data sets comprised eight photolysis experiments arranged in a single column-wise augmented data matrix and modelled according to equation 6. MCR analysis was initialized, using the set of pure spectra (S^T) previously estimated in sections 4.2 and 4.3 (analysis of individual data matrices). The concentration profiles and pure spectra finally obtained from HS-MCR-ALS analysis of the augmented data matrix are shown in fig. 7.

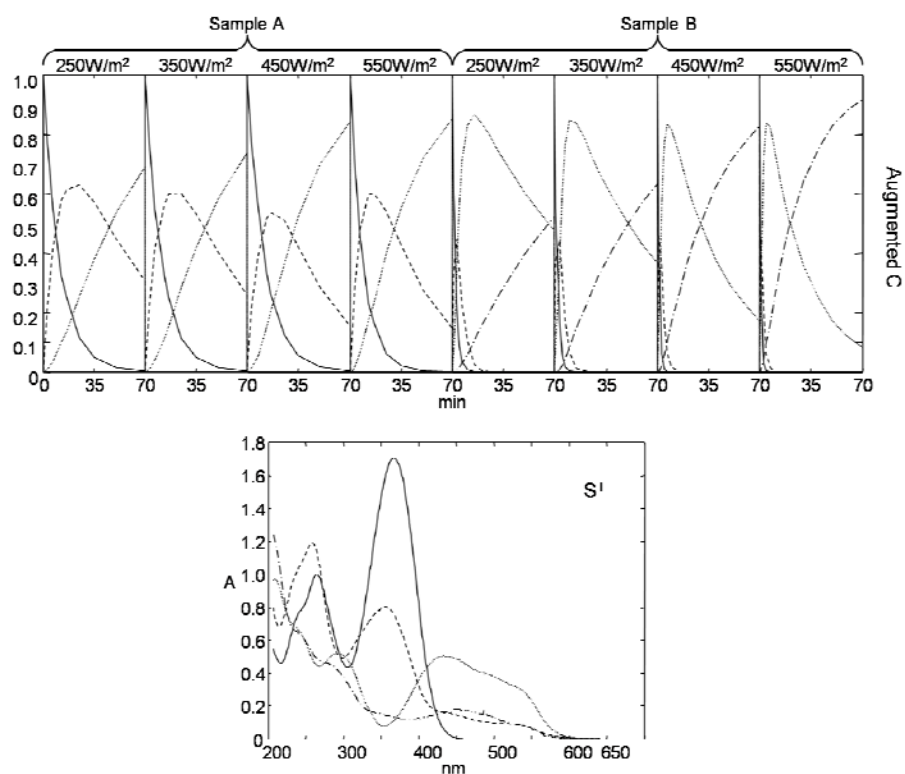


Figure 7. Simultaneous HS-MCR resolution of eight photodegradation experiments: sample A (100.0 $\mu\text{g/ml}$) and B (20.0 $\mu\text{g/ml}$) exposed under light at 250, 350, 450 and 550 W/m^2 .

The overall results were similar, as regards to both involved species and kinetic models, to the results obtained by MCR-ALS on the analysis of single degradation experiments. The final resolved pure spectra presented similar shapes. The influence of the total analyte concentration on the kinetic profiles and photodegradation rate was again confirmed, showing an increasing complexity of the degradation process in diluted solutions, at all illuminance conditions. For sample A, in fact, isomerisation of NFZ was rather constant under the different irradiance power values, whereas the formation of a secondary main photoproduct seemed to increase slightly when the irradiance also increased. In sample B (NFZ diluted), on the contrary, the disappearance of both NFZ and its isomer form resulted to be very fast. The formation of the same coloured photoproduct as in sample A was shown, but in this case it was in turn degraded to give a third photoproduct with a rate constant highly influenced by the illuminance power. Table 2 lists the rate constants for all the experiments.

Table 2. Kinetic constants for NFZ photodegradation under different conditions of irradiance power and concentration resulted from simultaneous HS-MCR analysis

	Power (W/m ²)	k_1	k_2	k_3
Sample A (100.0 μg/ml)	250	8.64e-02	2.07e-02	--
	350	8.98e-02	2.37e-02	--
	450	9.35e-02	3.39e-02	--
	550	1.12e-01	4.23e-02	--
Sample B (20.0 μg/ml)	250	4.85e-01	3.07e-01	1.14e-02
	350	5.98e-01	3.48e-01	1.53e-02
	450	9.25e-01	4.93e-01	2.64e-02
	550	1.17e+00	7.43e-01	3.69e-02

%LOF = 3.31; $r^2 = 99.95\%$

The percentage values of LOF and r^2 resulted to be 3.31% and 99.95%, respectively, which are considered very good when the amount of experiments and constraints used during the analysis are considered. The residuals in the time direction showed larger values at the beginning of the experiments, than afterwards they decreased along time; moreover, the residuals in the wavelength direction showed that they were larger when absorptions were also larger. This indicates that probably errors were proportional to absorbance intensities. In all cases, however, the residuals were small and symmetric, equally distributed in positive and negative sides, but they were not homocedastic.

4.3.5. Analysis of NFZ photodegradation by HPLC-DAD

Whit the aim to further interpret and confirm MCR-ALS results obtained in the analysis of time dependent UV data, the photodegradation of NFZ was also investigated by HPLC-DAD. Aliquot samples (0.05 ml) were taken during degradation experiments (at different times) of 1 mg/ml NFZ sample solution and analyzed by HPLC-DAD. The data set obtained in these experiments were then used to build a new set of data matrices (\mathbf{D}_{time}) and they were analyzed by MCR-ALS. Fig. 8 shows the results obtained by MCR-ALS when it was applied to this series of chromatograms runs.

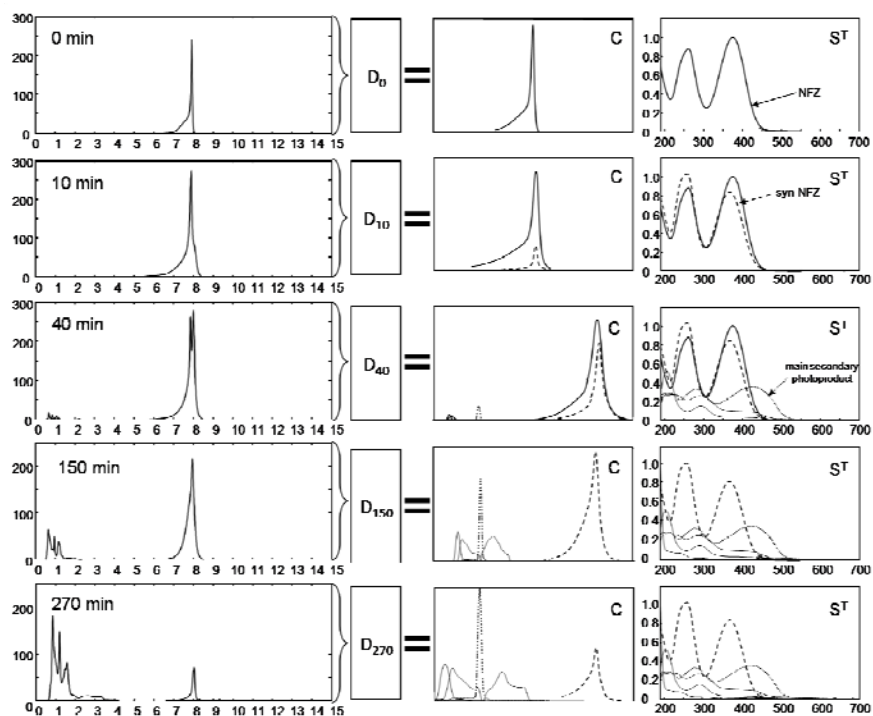


Figure 8. MCR-ALS resolution of the DAD-data from HPLC analysis of a NFZ solution (1 mg/ml), collected at different photodegradation times.

The simultaneous formation of different components in the same sequence as in previous kinetic UV spectrophotometric studies was confirmed. Although the chromatographic peak of the NFZ-isomer was highly overlapped with the NFZ drug peak, it was clearly resolved by MCR, and its formation resulted to be complete after about 1 hour of light exposure. An additional series of new chromatographic peaks were formed after about 40 minutes, all of them eluting in the first minutes of the chromatographic run and they were not further separated by chromatography. MCR-ALS achieved the resolution of at least four of these by-products, from which at least one peak presented the same spectral profile than the second photoproduct resolved in the previous spectrophotometric study.

The HPLC study confirmed therefore the intrinsic difficulties encountered in the isolation and characterization of the secondary photoproducts derived from the NFZ isomer. It is therefore concluded that the components resolved by MCR-ALS from UV kinetic spectrophotometric experiments were most probably an admixture of several related compounds rather than single distinct components with different kinetic and spectra profiles. Further investigation is needed to identify and confirm the nature of all the formed subproducts.

4.4. Conclusions

Results obtained in this work have shown the power of using multivariate curve resolution derived methods to study the degradation processes of photolabile drugs. In particular, in this work, the application of MCR-ALS and of HS-MCR-ALS methods has given an exhaustive description of the kinetic pathway involved in the photodegradation process of the NFZ drug. By using the resolution power of these two methods when they are applied to the simultaneous analysis of multiple samples at different experimental conditions, it was possible to estimate the pure spectra of the degradation products and to determine their concentration profiles and rate constants. It is concluded that NFZ is rapidly transformed into its *syn*-isomer compound which in turn undergoes further degradation to give a series of coloured compounds, unstable and difficult to characterize. Calculated rate constants were shown to depend on both drug concentration and irradiance power. An increase of the rate constants of all degradation processes was observed with the increasing of the light power and with the sample dilution (with decreasing NFZ concentration). Isolation and characterization of all the components involved in the photodegradation process of NFZ was very challenging because of the easy photodegradation of the main photoproducts. Nevertheless, the ability of MCR-ALS method to propose a pathway for the UV photodegradation of the NFZ drug from UV spectrophotometric and LC-DAD data analysis has been proved.

For more details:

- [1] Chowdhury, S.P.R., *The Lancet*. 309 (1977) 152.
- [2] Lowenthal, M.N., Jones, I.G., Kouchner, G.A., Desai, M., Chimbayo, W.A.S., Rajappan, C., *Trans. R. Soc. Trop. Med. Hyg.*, 71 (1977) 88-89.
- [3] McCalla, D.R., 1979. In: Hahn, F.E., (Ed.), *Antibiotics V-1: mechanisms of action of antibacterial agents*. Springer-Verlag, New York, p. 176.
- [4] Erdur, B., Ersoy, G., Yilmaz, O., Ozkutuk, A., Sis, B., Karcioğlu, O., Parlak, I., Ayrik, C., Aksay, E., Guryay, M., *Am. J. Emerg. Med.*, 26 (2008) 137-143.
- [5] Shahjahan, M. and Enever, R.P., *Int. J. Pharm.*, 143 (1996a) 75-82.
- [6] Shahjahan, M. and Enever, R.P., *Int. J. Pharm.*, 143 (1996b) 83-92.
- [7] Tao, L., Xian-Cheng, Z., Xiu-Cen, Y., Ning, H., Cheng-Rong, L., Lin-Li, L., *Chin. J. Chem.*, 23 (2005) 1090-1094.
- [8] Iwahara, S., Ogino, Y., Irie, T., *Shokuhin Eiseigaku Zasshi* 7, 449-454. *Through Chem. Abs.* (1966) 66, 64430k.
- [9] Uriach, J. and Pozo, A.D., *Galenica Acta*. 19 (1966) 137-151.
- [10] Quilliam, M.A., McCarry, B.E., Hoo, K.H., McCalla, D.R., *Can. J. Chem.*, 65 (1987) 1128-1132.

[11] Lin, S. and Lachman, L., Bull. Parent. Drug Assoc., 23 (1969) 149-165.

[12] Allowood, M.C. and Plane, J.H., Int. J. Pharm., 31 (1986) 1-7.

[13] Greenhill, J.V., 1995. In: Horspool, W.H. and Song, P.S., Handbook of organic photochemistry and photobiology, CRC Press, Boca Raton, p. 83.

[14] Albini, A. and Fasani E., 1997. Photochemistry of drugs: an overview and practical problems. In Albini, A. and Fasani E. (Ed), Drugs: photochemistry and photostability, The Royal Society of Chemistry, Cambridge, pp. 1-73.

[15] Massart, D., Vandeginste, B., Buydens, L., De Jong, S., Lewi, P., Smeyers-Verbeke, J., 1998. Handbook of Chemometrics and Qualimetrics, Elsevier, Amsterdam.

[16] Brereton, R., 2003. Chemometrics, Data Analysis for the Laboratory and Chemical Plant, Wiley, Chichester.

[17] de Juan, A., Maeder, M., Martínez, M., Tauler, R., Chemom. Intell. Lab. Syst., 54 (2000) 123-141.

[18] Amigo, J.M., de Juan, A., Coello, J., MasPOCH, S.A., Anal. Chim. Acta, 567(2006) 245-254.

[19] Mas, S., de Juan, A., Lacorte, S., Tauler, R., Anal. Chim. Acta, 618 (2008) 18-28.

- [20] ICH Harmonized Tripartite Guideline, 1996. Photostability Testing of New Drug Substance and Products. Fed. Register 62, 27115-27122.
- [21] Bird, R.F. and Stevens, S.G.E., *Analyst*, 87 (1962) 362-365
- [22] Lawton, W.H. and Sylvestre, E.A., *Technometrics*, 13 (1971) 617-633.
- [23] Sylvestre, E.A., Lawton, W.H., Maggio, M.S., *Technometrics*, 16 (1974) 353-368.
- [24] de Juan A., Maeder, M., Martínez, M., Tauler, R., *Anal. Chim. Acta*, 442 (2001) 337-350.
- [25] Hamilton, J.C., and Gemperline, P.J., *J. Chemom.*, 4 (1990) 1-13.
- [26] Jiang, J.H., Liang Y., Ozaki, Y., *Chemom. Intell. Lab. Syst.*, 71 (2004) 1-12.
- [27] Golub, G.H. and Van Loan, C.F., 1989. *Matrix Computations*, 2nd Ed., The John Hopkins University Press, London.
- [28] Gampp, H., Maeder, M., Meyer, C.J., Zuberbuehler, A.D., *Anal. Chim. Acta*, 193 (1987) 287-293.
- [29] Windig, W. and Guilment, J., *Anal. Chem.*, 63 (1991) 1425-1432.
- [30] Sánchez, F.C., Toft, J., van den Bogaert, B., Massart, D.L., *Anal. Chem.*, 68 (1996) 79-85.

- [31] Tauler, R., *Chemom. Intell. Lab. Syst.*, 30 (1995) 133-146.
- [32] Tauler, R., Smilde, A.K., Kowalski, B.R., *J. Chemom.*, 9 (1995) 31-58.
- [33] Maeder, M. and Zuberbuhler, A.D., Nonlinear least-squares fitting of multivariate absorption data. *Anal. Chem.*, 62 (1990) 2220-2224.
- [34] de Juan, A., Casassas, E., Tauler, R., 2000. Soft modeling of analytical data. In: *Encyclopedia of Analytical Chemistry: Instrumentation and Applications*, Wiley, New York.
- [35] Maeder, M. and Neuhold, Y.M., 2007. *Practical data analysis in chemistry*, Elsevier Ltd., Netherlands.
- [36] Muñoz, G. and de Juan, A., *Anal. Chim. Acta*, 595 (2007) 198-208.
- [37] Jaumot, J., Gargallo, R., de Juan, A., Tauler, R., *Syst.*, 76 (2005) 101-110.
- [38] Izquierdo-Ridorsa, A., Saurina, J., Hernández-Cassou, S., Tauler, R., *Chemom. Intell. Lab.*, 38 (1997) 183-196.
- [39] Saurina, J., Hernández-Cassou, S., Tauler, R., Izquierdo-Ridorsa, A., *J. Chemom.*, 12 (1998) 183-203.
- [40] Borodulin, V.B., Shebaldova, A.D., Kornienko, G.K., Kravtsova, V.N., *Pharm. Chem. J.*, 33 (1999) 44-46.

[41] Edhlund, B.L., Arnold, W.A., McNeill, K., Environ. Sci. Technol., 40 (2006) 5422-5427.

5. Application of multivariate curve resolution (MCR) to the spectrophotometric study of the melatonin photodegradation

The photostability of drugs represents an important field in the pharmaceutical research and a high number of compounds have been discovered to be photolabile [1-5]. A complete knowledge of the drug photo-reactivity is effectively essential for a correct pharmaceutical formulation and its packaging. A protocol for testing the photostability of new drugs is described in the ICH Guideline and recommended in the pharmaceutical industry as a key testing of the drugs [6].

Melatonin (N-acetyl-5-methoxytryptamine) (ML) is a neurohormone produced mainly by the vertebrate pineal gland and it's synthesized from L-tryptophan [7-8]. ML is an important component of the body's internal time keeping system and it is involved in important physiological events, as circadian rhythms (sleep wake cycle). Alterations in ML metabolism have been demonstrated in circadian rhythm sleep disorders, Alzheimer's and Parkinson's diseases, glaucoma, depressive disorder, breast and prostate cancer, hepatoma and melanoma [9-15]. In pharmaceutical therapy, ML is used to balance possible metabolic disorders or to regulate circadian rhythm, sleep disorders, insomnia in blind people, intercontinental flight disrhythmia (jet-lag syndrome) and insomnia in elderly patients [16].

ML is known as a photolabile drug and its exposure to light causes a deep transformation of the chemical structure with a

probable loss of the therapeutic activity. The photodegradation process (Fig. 1), described in previous publications, consists in the oxidation of the indole ring to give the N-{3-[2-(formylamino)-5-methoxyphenyl]-3-oxopropyl}acetamide (MLD) through an endoperoxide intermediate [17].

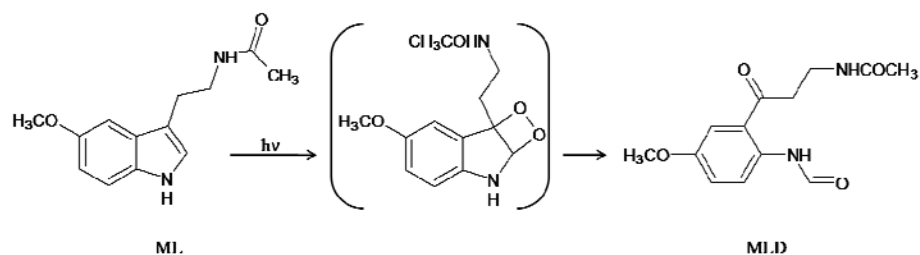


Figure 1. Hypothesis of photodegradation mechanism

Actually, the spectrophotometric methods are widely used in analytical chemistry because of the easy manipulation and interpretation of the spectral data. Nevertheless, the traditional spectrophotometric methods use few wavelengths that frequently are not enough to furnish the necessary information to resolve a system with components presenting spectra overlapping. In recent years, multivariate approaches for the extraction of a largest analytical information from UV spectra have been proposed [18]. Multivariate methods have the advantage of exploiting full spectral data points, by using simultaneously a very high number of analytical signals.

Multivariate curve resolution approach is one of the most recent chemometric techniques for elaborating the UV spectrophotometric data [19-20]. It allows to extract the pure spectra and concentration of the components in a mixture from a

set of spectra with different composition. Its application is particularly useful to study a chemical transformation, allowing to estimate the single spectra and the concentration profiles of all the involved species. When the matter is a kinetic study, it is besides possible to obtain the rate constants (k) of the reactions.

This work aims to describing the kinetic pathway of ML photodegradation by MCR approach, applied on spectral data from analysis of the drug when exposed under different illuminance power. The influence of the changing exposure conditions on the photodegradation rate was also investigated.

5.1. Drug and Experimental Procedures

Melatonin (ML), (N-acetyl-5-methoxytryptamine) was purchased from Sigma-Aldrich Co. (Italy).

Light exposure was performed in a light cabinet Suntest CPS+ (Heraeus, Milan, Italy), equipped with a Xenon lamp. The apparatus was fitted up with an electronic device for irradiation and temperature measuring and controlling inside the box. The system was able to closely simulate sunlight and to appropriately select spectral regions by interposition of filters.

Spectrophotometric measurements were recorded using an Agilent 8453 Diode Array spectrophotometer (Agilent Technologies. USA).

Chemometric elaboration was performed in MATLAB environment (Mathwork Inc., version 6.5) and MCR-ALS user-

friendly interface tool [21]. Hybrid hard-soft MCR-ALS (HSMCR-ALS) has been described and used in previous works [19, 22-24].

All the photodegradation experiments were performed following the ICH recommendations for the drug stability tests [6].

A stock solution of ML (1 mg/ml) in ethanol was properly diluted to obtain a series of 20 $\mu\text{g/ml}$ samples for degradation experiments. These solutions, in quartz cells perfectly stoppered, were directly light irradiated according to the ID65 standard of the ICH rules. The wavelength range was set between 300 and 800 nm, by means of a glass filter, and the irradiation power at four different levels: 250, 350, 450 and 550 W/m^2 , corresponding to an energy value of 15, 21, 27 and 33 $\text{kJ}/(\text{min}\cdot\text{m}^2)$, respectively. The inner temperature was maintained constant at 25 $^{\circ}\text{C}$ in all the experiments.

UV spectra were recorded in the wavelength range between 200 and 450 nm, just after preparation ($t = 0$) and at the following times: 20, 40, 60, 80, 100, 120, 140, 160, 180, 200, 220, 240, 260, 280, 300, 320, 340 and 360 min.

5.2. Applied Chemometry

5.2.1. Multivariate curve resolution – Alternative least squares (MCR-ALS)

When a degradation process is studied by UV spectroscopic analysis, a series of spectra is stored, recording the temporal variation of the system. All the collected UV data contain the information about all species involved in the chemical process. The characterization of the various components in a chemical process

represents a serious analytical problem and their resolution depends on the complexity of the transformation and on the number of the degradation products. These difficulties increase when some components are only intermediate compounds and are in their turn rapidly transformed. In the last years the chemometric methods imposed themselves as very powerful tools to resolve multicomponent mixture systems.

MCR-ALS modelling provides to decompose mathematically the analytical data into the contributions due to the pure components, describing at the same time the evolution of the process [25-26]. This approach describe the system as a bilinear model of pure component contributions, (Fig. 2a).

$$1) \quad D = C S^T + E$$

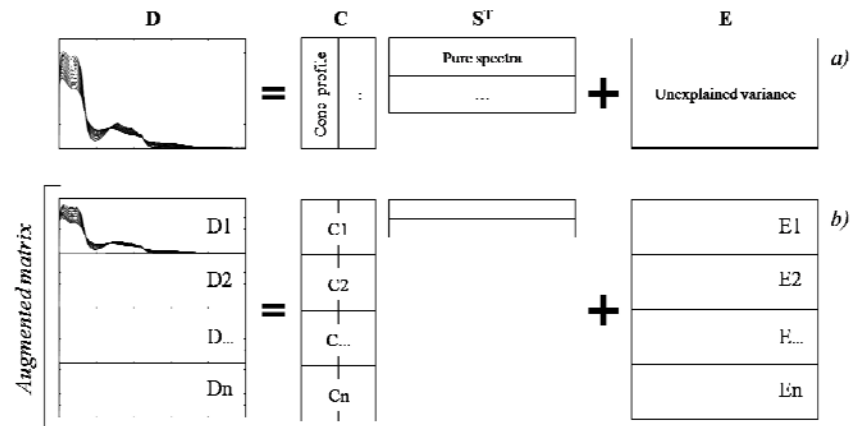


Figure 2. (a) MCR-ALS resolution applied on a single data matrix D (b) MCR-ALS resolution applied to the column-wise augmented data matrix

The experimental data are disposed in a D matrix, where the rows are the spectra at different times and the columns represent the process signals at different wavelengths, C is the concentration matrix of the n components involved in the process, S is the spectra matrix of the pure components and E represents the unexplained variance in the data set. The model appears equivalent at the general law of Lambert-Beer, therefore is well fit in elaborating an UV data matrix.

In MCR application, the first step is the estimation of the number of components, which is performed through the rank analysis on D matrix. Principal component analysis (PCA) and singular value decomposition (SVD) [27] are two of the most used methods for this aim. MCR-ALS algorithm requires an estimate of the S^T or C matrix, that can be obtained by application of evolving factor analysis (EFA) for C_{estimate} [28] or selection of the pure variables (PUREST) for S_{estimate} [29-30]. Afterward, the initial results are used to perform the alternative least square algorithm in such a way to optimize them through an iterative process. At each cycle, a new estimation of S^T and C is calculated by solving alternatively the two following least-squares matrix equations:

$$2) \quad S^T = (C)^+ D$$

$$3) \quad C = D(S^T)^+$$

where $(S^T)^+$ and $(C)^+$ are the pseudoinverse of the S^T and C matrices, respectively [31-32].

Optimization of the resolution can be obtained through the application of the constraints in such a way to drive the final solution towards a chemical meaning and reduce so the intrinsic

ambiguity of the resolution. *Non-negativity* constraint forces the concentrations and the spectra of the components so that must be positive; the concentration profiles in the degradation process are forced to give only one maximum per experiment by *unimodality* constraint; in the kinetic process the mass balance is assured by applying the *closure* constraint [32].

The iteration procedure is stopped when convergence is achieved, by fixing a preselected number of cycles or by evaluating the value of lack of fit (LOF):

$$4) \quad \%LOF = 100 \times \sqrt{\frac{\sum_{ij} (d_{ij} - d_{ij}^*)^2}{\sum_{ij} d_{ij}^2}}$$

where d_{ij} is the experimental absorbance at reaction time i and wavelength j and d_{ij}^* is the absorbance obtained by the MCR-ALS model. Another parameter used to indicate the quality of MCR-ALS modelling is the percentage of explained variance (r^2):

$$5) \quad r^2 = 100 \times \frac{\sum_{ij} d_{ij}^{2*}}{\sum_{ij} d_{ij}^2}$$

An important feature of MCR-ALS is the possibility of the simultaneous data handling with more than one experiment, by adopting various experimental conditions and/or conducted by different analytical techniques. For this aim, the dataset can be represented by row-wise augmented matrices, column-wise augmented matrices or row- and column-wise augmented matrices.

In the photodegradation studies, the analytical data can be carried out from samples under different experimental conditions,

e.g. the illuminance power. In such case, it is possible to use column-wise augmented matrices, obtaining so a change of the ALS modelling and the extension of the bilinear equation [33-34], according to equation 6 (Fig. 2b):

$$6) D_{Aug.} = C_{Aug.} S^T + E_{Aug.} = [D_1 ; D_2 ; \dots ; D_n] = [C_1 ; C_2 ; \dots ; C_n] S^T + [E_1 ; E_2 ; \dots ; E_n]$$

In agreement with this equation, a single S^T is resolved for all the D_n matrices and the same pure spectra are resolved for the common species in the different experiments. On the contrary, the C_n matrices of concentration profiles are calculated for each experiment.

5.2.2. Hybrid hard- and soft-multivariate curve resolution (HS-MCR)

A development of MCR-ALS (also called soft MCR-ALS) modelling was used to improve the kinetic study of the photodegradation process. Hybrid hard and soft multivariate curve resolution (HS-MCR) procedure [19] introduces a new constraint, a non-linear kinetic fitting routine. This constraint forces the concentration profiles (C matrices) to follow a kinetic model [35-36]. The fitted kinetic profiles complete the simple MCR-ALS and supply the rate constants of the process. Furthermore, HS-MCR modelling permits the simultaneous use of different kinetic models, in such a way to resolve an augmented D matrix obtained from different experiments [23-24].

In this work, different kinetic models have been considered to investigate the effects of the illuminance power on the degradation process.

5.3. Results and Discussion

5.3.1. Photodegradation experiments and MCR analysis

The UV spectra of four ML solutions (20 $\mu\text{g/ml}$) under different conditions of light irradiance were recorded along an exposure time of 360 min. In particular, light power was set at 250, 350, 450 and 550 W/m^2 , respectively. Fig. 3 shows the spectral sequence from all photodegradation experiments.

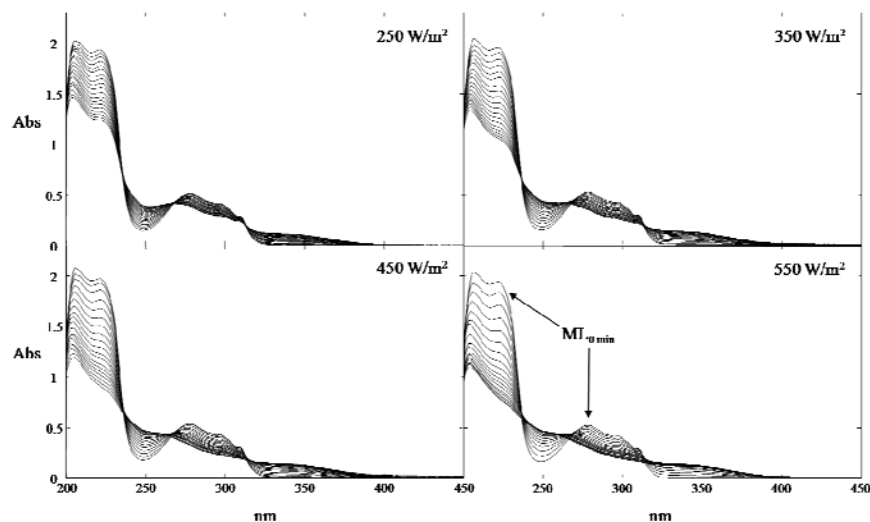


Figure 3. UV-spectra of photodegradation experiments of ML (20.0 $\mu\text{g/ml}$), exposed under light at 250, 350, 450 and 550 W/m^2

The different graph profiles confirmed the dependence of the degradation from experimental conditions, with a significant

increase of the photodegradation rate when the irradiation power rose.

The rank analysis (SVD) carried out a kinetic system of two species for all the experiments and the estimate of the pure spectra was calculated by purest method. The spectra were identified to be ML and MLD, whereas the peroxide intermediate was never found. The spectral data were processed by MCR procedure, by applying non-negativity (both concentrations and spectra), unimodality (only concentrations) and closure (only concentrations) as constraints. Fig. 4 shows the calculated concentration profiles (C) and the relative pure spectra (S^T) for the experiment executed with the irradiation power fixed to 250 W/m².

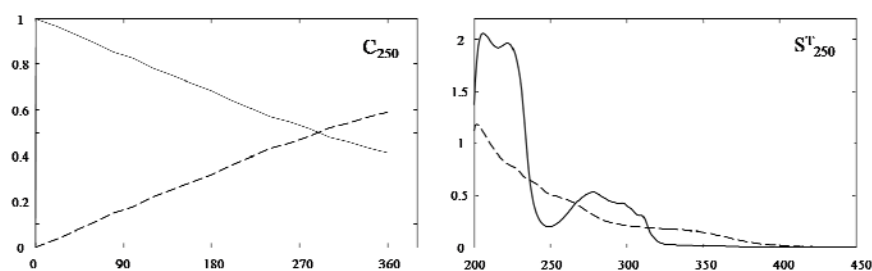


Figure 4. MCR-ALS resolved kinetic profiles and related pure spectra of ML photodegradation process at 250 W/m², ML (—) and MLD (---).

The values of %LOF resulted in any case below 1%. The absorption shapes of the components did not show very significant differences in all the experiments and the variation of the concentration profile plots was in agreement with the kinetic model explained by a first order reactions (ML→MLD).

With the aim to drive spectra and concentration profiles to fit the kinetic model, the algorithm HS-MCR was then applied, obtaining the new kinetic profiles (C) and pure spectra (S^T) of the components. HS-MCR analysis confirmed the spectral curves estimated by simple MCR but the concentration profiles of the new plots showed a better fitting to the defined kinetic pathway.

5.4.2. MCR analysis on augmented matrix from photodegradation under various conditions

At last, the simultaneous HS-MCR was performed on the augmented matrix consisting of the various photodegradation experiments. So the spectral data from ML solution when irradiated under illuminance power of 250, 350, 450 and 550 W/m^2 were simultaneously processed by HS-MCR-ALS. The concentration profiles and the pure spectra carried out from the

augmented analysis are shown in fig. 5.

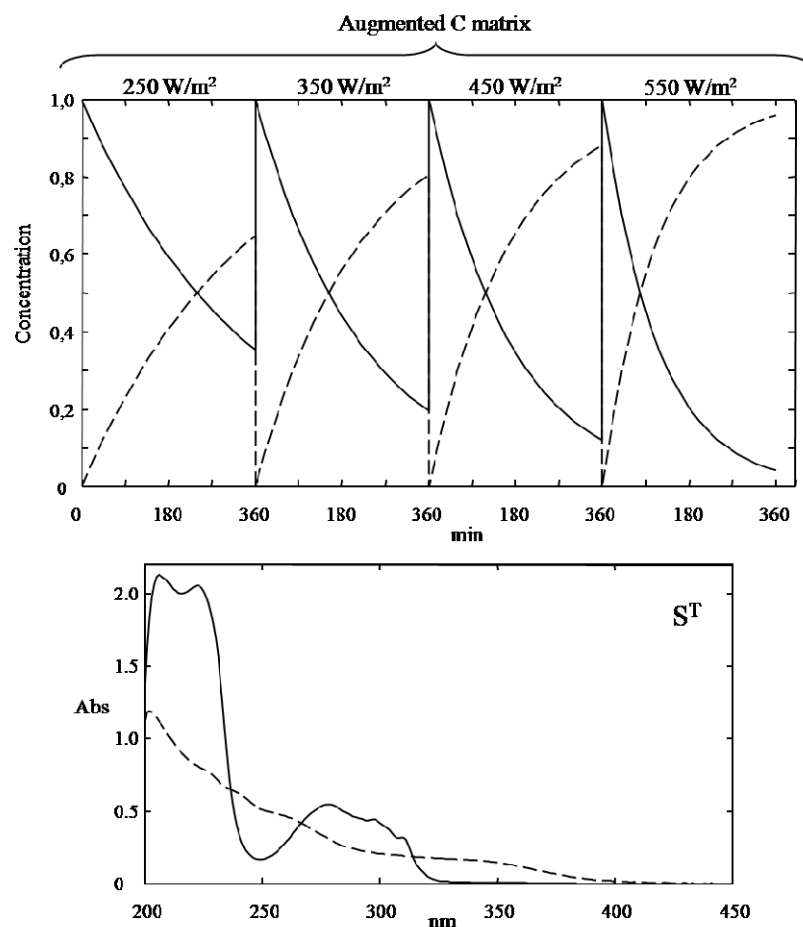


Figure 5. Simultaneous HS-MCR resolution with the four models of photodegradation experiments of ML solution (20.0 $\mu\text{g/ml}$) exposed under light at 250, 350, 450 and 550 W/m^2 , ML (—) and MLD (---).

Table 1 lists the rate constants relative to all the experiments. The percentage values of LOF and r^2 resulted to be 2.13% and 99.94%, respectively.

Table 1. Kinetic constants for ML photodegradation under different conditions of irradiance power

<i>Power (W/m²)</i>	<i>k</i>
250	3.185E-03 ± 2.121E-05
350	4.351E-03 ± 2.859E-05
450	6.460E-03 ± 6.828E-05
550	1.008E-02 ± 6.737E-05

These results agreed, as regards both involved species and kinetic models, with the results obtained by MCR on the single degradation experiments. In fact, the final pure spectra presented very similar shapes to the ones carried out in the previous analysis.

The results from MCR-ALS analysis pointed out a significant dependence of the photodegradation kinetics by the illuminance power, as it is evident from the graph of fig. 6.

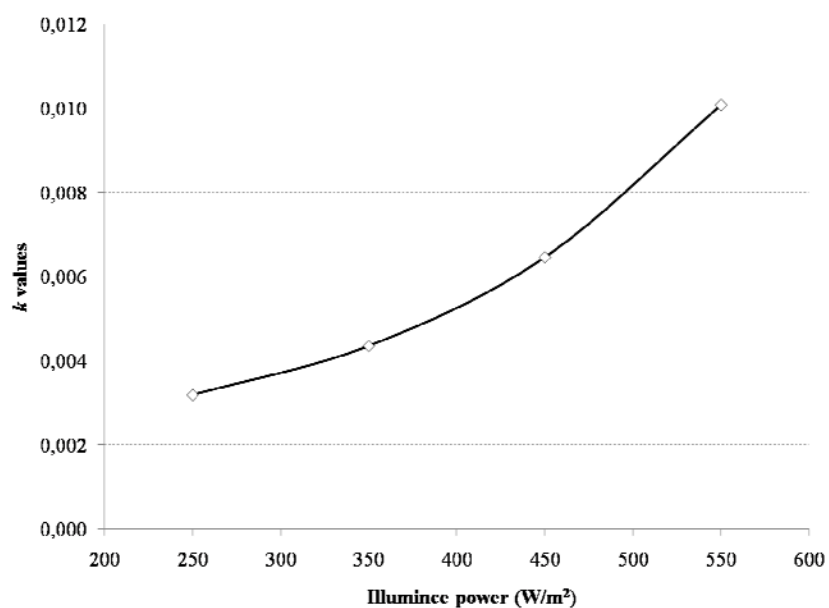


Figure 6. *Dependence of the kinetic constants from the illuminance power*

All the rate constants increased with the increase of the light power, following an exponential tendency.

5.4.3. Simultaneous determination of ML and its photoproduct by MCR

The graph of the concentration profiles (C matrix) can be also used to carry out quantitatively, in terms of relative or absolute values, the concentration of both the components, ML and MLD, after a certain time of light exposure. By applying the equation 3, it is possible to obtain the concentration of each component. In fact, the product of the pseudoinverse S^T matrix with a recorded spectrum (D_x), at a degradation time x , gives the C_x matrix (Eq. 7) that coincides with the concentrations of ML and MLD in the mixture, expressed as relative content.

$$7) \quad C_x = D_x(S^T)^+$$

With the aim to validate this determination procedure, a series of ML solutions was exposed to light, at different irradiance power values and for different times, and then analyzed by UV spectroscopy. Their spectra were computed in according to equation 7 and the respective percentage concentrations were so predicted. Table 2 summarizes the calculated concentrations of ML and MLD.

Table 2. *Composition predicted for ML samples photodegraded at various times*

Sample	Irradiance power (W/m ²)	Exposure time x (min)	Relative concentration $C_x = D_x(S^T)^+$	
			<i>ML</i>	<i>MLD</i>
1	250	55	0,870	0,130
2	250	124	0,725	0,275
3	350	32	0,870	0,130
4	350	162	0,494	0,506
5	450	46	0,748	0,252
6	450	138	0,488	0,512
7	550	12	0,913	0,087
8	550	95	0,477	0,524

These results demonstrate the ability of the proposed method in calculating the composition of a mixture arisen from degradation of a photosensitive drug.

5.4. Conclusions

Application of MCR methods has demonstrated good ability in extracting the useful information from a set of UV spectral data in order to give an exhaustive description of the kinetic pathway involved in the photodegradation process of ML. By using the resolution power of MCR modelling at different experimental conditions, it was possible to estimate the spectra of the degradation products and to determine the rate constants of the degradation transformations.

The kinetic model was demonstrated to depend on irradiance power and an increase of the rate of all the degradation processes was observed with the increasing of the light power. This approach demonstrates the substantial power of the multivariate curve resolution techniques as a method to study in depth the degradation process of photolabile drugs.

The ability of the MCR procedure as an analytical method for quantitative analysis was also demonstrated through the determination of the composition of ML samples variously photodegraded.

For more details:

- [1] Cornelissen, P.J.G., Beijersbergen van Henegouwen, G.M.J. , Photochem. Photobiol. 30 (1979) 337.
- [2] De Villiers, M.M., van der Watt, J.G., Lotter, A.P. , Int. J. Pharm. 88 (1992) 275.
- [3] Tønnesen, H.H., Int. J. Pharm. 225 (2001) 1.
- [4] Beijersbergen van Henegouwen, G.M.J., Adv. Drugs Res. 29 (1997) 79.
- [5] Albini, A., Fasani, E. Drug Photochemistry and Photostability, The Royal Society of Chemistry, Cambridge, 1998.
- [6] ICH Harmonized Tripartite Guideline, Photostability Testing of New Drug Substance and Products. Fed. Register 62, 27115-27122, 1996.
- [7] Pandi-Perumal, S.R., Trakht, I., Srinivasan, V. , Spence, D.W., Maestroni, G.J.M. , Zisapel, N., Cardinali, D.P., Prog. Neurobi. 85 (2008) 335.
- [8] Axelrod, J. , Wurtman, R.J., Adv. Pharmacol. 6 (1968) 157.
- [9] Dahlitz, M., Alvarez, B., Vignau, J., English, J., Arendt, J., Parkes, J.D., Lancet 337 (1991) 1121.

- [10] Folkard, S., Arendt, J., Clark, M., *Chronobiol. Int.* 10 (1993) 315.
- [11] Hagan, R.M., Oakley, N.R., *Trends Pharmacol. Sci.* 16 (1995) 81.
- [12] Brugger, P., Marktl, W., Herold, M., *Lancet* 345 (1995) 1408.
- [13] Pandi-Perumal, S.R., Zisapel, N., Srinivasan, V., Cardinali, D.P., *Exp. Gerontol.* 40 (2005) 911.
- [14] Bartsch, C., Bartsch, H., *Cancer Causes Control* 17 (2006) 559.
- [15] Stevens, R.G., *Cancer Causes Control* 17 (2006) 501.
- [16] Leger, D., Laudon, M., Zisapel, N., *Am. J. Med.* 116 (2004) 91.
- [17] Andrisano, V., Bertucci, C., Battaglia, A., Cavrini, V., *J. Pharm. Biomed. Anal.* 23 (2000) 15.
- [18] Massart, D., Vandeginste, B., Buydens, L., De Jong, S., Lewi, P., Smeyers-Verbeke, J., *Handbook of Chemometrics and Qualimetrics*, Elsevier, Amsterdam, 1998.
- [19] de Juan, A., Casassas, E., Tauler, R., *Soft modeling of analytical data*. In: *Encyclopedia of Analytical Chemistry: Instrumentation and Applications*, Wiley, New York, 2000.
- [20] Amigo, J.M., de Juan, A., Coello, J., MasPOCH, S.A., *Anal. Chim. Acta* 567 (2006) 245.

- [21] Jaumot, J., Gargallo, R., de Juan, A., Tauler, R., *Chemom. Intell. Lab. Syst.* 76 (2005) 101.
- [22] de Juan, A., Maeder, M., Martínez, M., Tauler, R., *Chemom. Intell. Lab. Syst.* 54 (2000) 123.
- [23] Muñoz, G., de Juan, A., *Anal. Chim. Acta* 595 (2007) 198.
- [24] Mas, S., de Juan, A., Lacorte, S., Tauler, R., *Anal. Chim. Acta* 618 (2008) 18.
- [25] de Juan, A., Tauler, R., *Anal. Chim. Acta* 500 (2003) 195.
- [26] Jiang, J.H., Liang, Y., Ozaki, Y., *Chemom. Intell. Lab. Syst.* 71 (2004) 1.
- [27] Golub, G.H., Van Loan, C.F., *Matrix Computations*, 2nd Ed., The John Hopkins University Press, London, 1989.
- [28] Gampp, H., Maeder, M., Meyer, C.J., Zuberbuehler, A.D., *Anal. Chim. Acta* 193 (1987) 287.
- [29] Windig, W., Guilment, J., *Anal. Chem.* 63 (1991) 1425.
- [30] Sánchez, F.C., Toft, J., van den Bogaert, B., Massart, D.L., *Anal. Chem.* 68 (1996) 79.
- [31] Tauler, R., *Chemom. Intell. Lab. Syst.* 30 (1995) 133.

- [32] Tauler, R., Smilde, A.K., Kowalski, B.R., *J. Chemom.* 9 (1995) 31.
- [33] Leger, M.N., Wentzell, P.D., *Chemom. Intell. Lab. Syst.* 62 (2002) 171.
- [34] Garrido, M., Larrechi, M.S., Rius, F.X., Tauler, R., *Chemom. Intell. Lab. Syst.* 76 (2005) 111.
- [35] Maeder, M., Zuberbuhler, A.D., *Anal. Chem.* 62 (1990) 2220.
- [36] Maeder, M., Neuhold, Y.M., *Practical data analysis in chemistry*, Elsevier Ltd., Netherlands, 2007.

6. Multivariate calibration techniques applied to derivative spectroscopy data for the analysis of pharmaceutical mixtures

In recent years, chemometric techniques are playing a very important role in the multicomponent analysis of pharmaceutical mixtures [1-4]. Multivariate calibrations are widely applied to the elaboration of analytical data obtained from many instrumental assays [5-8]. The most adopted multivariate methods in pharmaceutical analysis are principal component regression (PCR) and partial least-squares (PLS), whose theory has been fully described by several authors [9-13]. They are factor analysis methods which allow to build a mathematical model by using the matrices of spectral and concentration data from a series of reference samples. This model is used in a second step to predict the composition of a sample containing the same components with unknown concentrations.

Spectrophotometry in particular has benefited from the combination with the chemometric procedures and several applications have been reported for the simultaneous analysis of drugs in pharmaceutical formulations containing two or more compounds with overlapping spectra (14-16). PCR and PLS are calibration methods effective for the resolution of mixtures presenting serious spectral overlapping and non-linear absorbance additivity. The main advantage of a multivariate calibration when applied on spectral data is the high speed in

processing both absorbance and concentrations values. At the same time, the errors in model calibration are minimized by using the absorbances of the full spectrum or selected wavelength regions.

Despite the success in the field of pharmaceutical analysis, the methods based on the ordinary spectrophotometry have proved to be often unsatisfactory for the analysis of multicomponent mixtures, owing to their low resolution power [17-18]. In contrast, derivative spectrophotometry has reached a large success in resolving complex mixtures because of its ability in extracting high analytical information from spectra composed of overlapped bands. This technique provides a better resolution of the spectral overlap by magnifying small differences between the spectral curves [19-23]. Moreover, minimization of the nonspecific matrix interference is reached by elimination of baseline drifts [24-26]. A very recent review describes derivative spectrophotometry as a powerful tool in pharmaceutical analysis [27].

The combined use of derivative spectrophotometry and chemometric techniques has demonstrated to be a highly convenient choice in the determination of multicomponent matrices presenting serious spectra overlapping, thanks to their common potential ability to exploit minor spectral features [28-31].

In this work three multivariate procedures, based on PCR, PLS1 and PLS2 algorithms, have been applied on absorbance data of a ternary mixture of drugs. The main goal of the work

was a detailed comparison between the regression methods when they are applied on ordinary or derivative spectral data. The influence of the derivative order from zero to four on the prediction ability of the methods was investigated.

Design of experiments (DOE) and calibration optimization were used as chemometric tools to assist the development of the analytical methods. The impact of DOE on the prediction ability of multivariate calibration methods is well known [36-39]. In this work a suitable mixture design associated with response surface methodology was defined, able to build a calibration set covering an experimental domain which reflects the drug combination in the pharmaceutical specialties.

Validation of the models was performed by full cross-validation procedure, providing to select the optimal number of factors. In the optimization step, the wavelength regions containing the most useful information were also selected and all the useless signals, due to interferences or noise, were discarded. For this aim, we have developed a novel mathematical procedure, based on the absolute values of the component regression coefficients. This procedure was compared with other ones reported in literature, by evaluating the application easiness and the improvement of the predictive ability of the models.

In order to test the proposed methods, they were applied to the simultaneous determination of a ternary mixture containing Paracetamol (PAR), Propiphenazone (PRO) and

Caffeine (CAF), that are combined in various analgesic and antipyretic commercial formulations. The content of CAF is usually very low with respect to the other two components in pharmaceuticals, making so its determination the most difficult to carry out.

The most recent methods for the determination of the studied drugs are based on spectrophotometric [32-33] or chromatographic techniques [34-35], but, for their large usage in pharmaceutical formulations, simultaneous multicomponent analysis by rapid but reliable methods are preferred. The procedures herein proposed present execution speed, due to the exclusion of pre-separation steps, and satisfactory prediction performance.

The optimized models were compared by application to the analysis of synthetic mixtures and commercial pharmaceutical formulations, in order to establish their reliability in terms of accuracy and precision.

6.1. Drugs and Experimental Method

PAR and CAF were generous gifts from Onga SpA, Italy; PRO was courteously provided from Montefarmaco SpA, Italy. The pharmaceutical specialties Neoptalidon[®] (Novartis Consumer Health SpA), Saridon[®] (Roche SpA) and Veramon[®] (Sofar SpA) were obtained commercially.

Absorption spectra were recorded on a λ range of 200–400 nm in a 10 mm quartz cell, by a Perkin-Elmer Lambda 40P spectrophotometer at the following conditions: scan rate 1 nm

s^{-1} ; time response 1 s; spectral band 1 nm; data density 1 point nm^{-1} . Derivative spectra were elaborated by the Savitzky-Golay algorithm with a $\Delta\lambda$ value fixed at 6 nm for the first-order, and 10 nm for the other orders. The software

UV Winlab 2.79.01 (Perkin-Elmer) was used for spectral acquisition and elaboration.

Application of PCR, PLS1 and PLS2 algorithms was supported by the software package “The Unscrambler 9.7[®]” (Camo Process As., Oslo, Norway). The software is dedicated to both multivariate analysis and experimental design and is equipped with several multivariate methods. It allows to optimize the calibration models and to develop validation procedures.

In order to obtain the calibration set, stock solutions of PAR (4 mg ml⁻¹), PRO (4 mg ml⁻¹) and CAF (0.5 mg ml⁻¹) in ethanol were used. Stock solutions were appropriately diluted with the same solvent to give reference mixtures with concentration values within the range 0.0–30.0 $\mu g ml^{-1}$ for PAR and PRO, and 0.0–4.5 $\mu g ml^{-1}$ for CAF. These values were chosen in agreement with the concentration ratios present in the commercial formulations.

Sample solutions were obtained from pharmaceutical formulations. They were assayed by weighing the content of five tablets and reducing them to a fine powder. An amount exactly corresponding to the average tablet weight was suspended in ethanol and made up to a volume of 10 ml. The suspension was sonicated for 10 min and then filtered through a

PTFE 0.45 μm membrane filter. Samples for analysis were obtained after serial dilution 1:1000 (10^3) of this filtrate with ethanol and analyzed.

6.2. Chemometric Techniques

6.2.1. Design of experiments DOE

Prediction ability of a regression model is largely affected by the mixture design in building the calibration set. A careful selection of the reference solutions increases the chances of improving quality of information from the calibration set. Statistical DOE is a powerful technique for choosing the component concentrations so that to minimize the total number of samples in covering the defined experimental region. The region defined by the reference solutions was represented by means of a Simplex-lattice design as a triangular surface [40]. The simplex contained all possible drug combinations distributed on five levels, within the concentration ranges above described, generating so a representative and balanced calibration data set.

6.2.2. Multivariate analysis

PCR and PLS are factor analysis methods, based on a two-stage procedure: a calibration step, in which a mathematical model is built by using component concentrations and spectral data from a set of references, followed by a prediction step in which the model is used to calculate the

concentrations of an unknown sample from its spectrum. Both algorithms transform the original variables into a smaller number of orthogonal variables called factors or principal components (PCs), which are linear combinations of the original variables.

When multivariate calibration approaches are applied in spectrophotometric multicomponent analysis, a relationship between spectral and concentration data from reference samples, representing the variables of the system, is established. A new matrix constituted by the new variables PCs and scores is built. The calculation of this new matrix is planned by an algorithm specific to the regression method adopted. PCs represent the absorptivity values of the samples at the various concentration and wavelength values, whereas the scores represent the numerical coefficients. Their combination allows to build the mathematical model representing the reference spectra and able to predict the component concentrations of new samples.

6.2.3. Determination of PC number

The optimal number of principal factors is essential in building multivariate models. The prediction error decreases with the number of PCs used until to reach an optimal value. Most information is usually contained in the first PCs but it is not assured that the useful information is exclusively reserved to these factors. Full cross-validation is the most used validation method, in which one reference at a time is removed from the calibration set,

after that the same sample is predicted by using the calibration built with the others references. Several tests have been proposed to select the number of PCs. The Root Mean Square Error of Prediction (RMSEP) was chosen to express the prediction error when PCR and PLS procedures were applied. This parameter represents an estimate of the error when other samples are predicted with that model. The best prediction ability of the models is reached when the prediction error is at its lowest value.

$$RMSEP = \sqrt{\frac{\sum_{i=1}^n (\hat{c} - c_i)^2}{n}}$$

where \hat{c} is the predicted value for the references; c_i is the real value for the references; n is the number of references.

Another important statistical parameter in evaluating the model quality is R^2 . It represents an index of quality in fitting all data to a straight line and represents the fraction of total variance explained by the model. It is computed as:

$$R^2 = \frac{\sum_{i=1}^N (\bar{c} - c_i)^2}{\sum_{i=1}^N (c_i - \bar{c})^2}$$

where \bar{c} represents the mean of the true concentrations in the prediction set.

6.3. Results and Discussion

6.3.1. Data processing and model building

The absorption UV spectra of pure PAR, PRO, CAF in ethanol are shown in fig. 1.

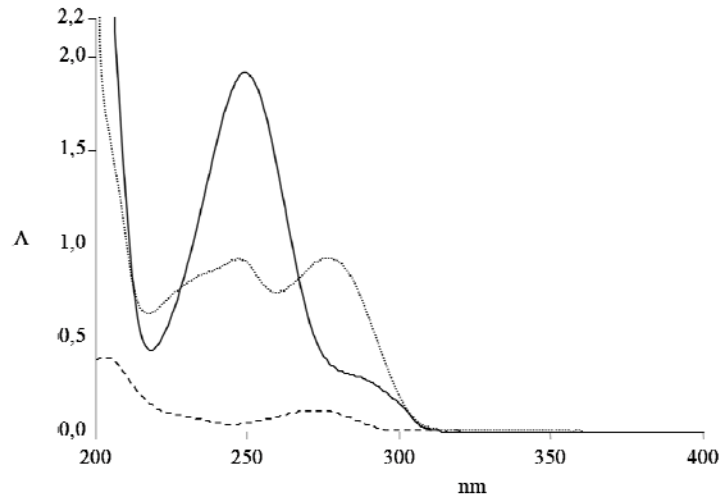


Figure 1. Absorbance spectra in ethanol of $20.41 \mu\text{g ml}^{-1}$ PAR (—), $19.85 \mu\text{g ml}^{-1}$ PRO (⋯), $2.25 \mu\text{g ml}^{-1}$ CAF (---).

The drugs are in a concentration ratio equivalent to the content of the commercial pharmaceutical specialties. The wavelength range 200-350 was throughout considered because the absence of absorbance after 350 nm for all the drugs. Quantitative determination by ordinary spectrophotometry, which uses measurements at discrete wavelengths, was proved to be inaccurate because of the extensive overlap of the spectral curves. Quantification of CAF, which is present in a very low

content in comparison with the other two drugs, gave the worse results.

With the aim to extract the most significant analytical information from the spectral data, the mathematical derivatives of the absorbance values against wavelengths ($dA/d\lambda$) were calculated. Fig. 2a-d shows the first-to-fourth order derivative spectra of the three drugs. The wavelength interval ($\Delta\lambda$) used to calculate the derivative spectra was optimized for each order. Accordingly, a value of 6 nm for the first order and 10 nm for the other orders, which gave the best signal-to-noise ratio, were selected.

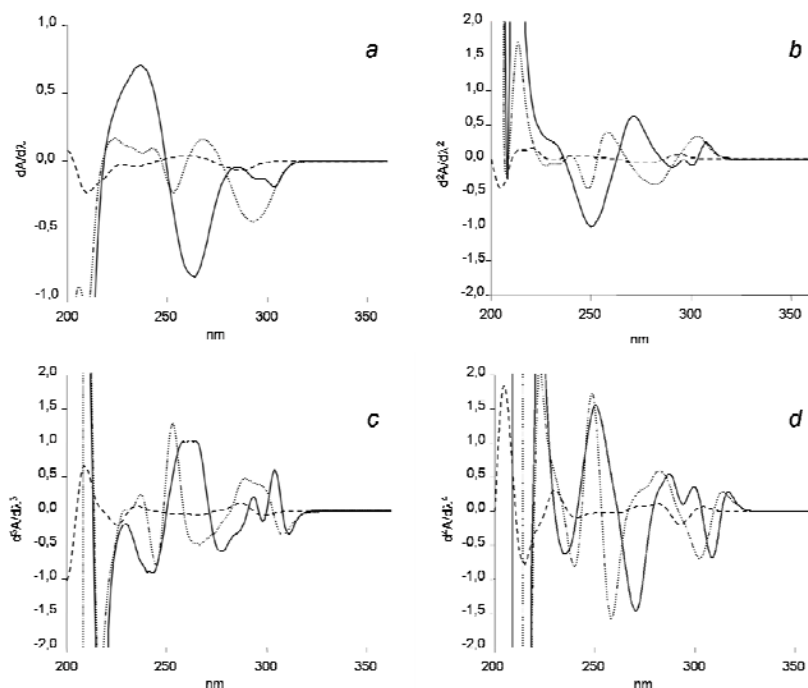


Figure 2. First-order (a), second-order (b), third-order (c), fourth-order (d) derivative spectra in ethanol of $20.41 \mu\text{g ml}^{-1}$ PAR (—), $19.85 \mu\text{g ml}^{-1}$ PRO (⋯), $2.25 \mu\text{g ml}^{-1}$ CAF (---).

A clear overlap between the curves is evident for all the derivative orders too. A deep examination of all the spectra was done but no signal proportional to the components was singled out. Multivariate calibration methods appeared to be ideal in order to overcome such a drawback as they allow to extract analytical information from the full-spectra, providing significant improvements over methods that are restricted to a small number of wavelengths. Moreover, the chemometric models can be optimized by a further selection of the wavelength regions providing the most useful information.

An appropriate design of the calibration set to be used in modeling was taken in great consideration because it can largely affect the prediction ability of a multivariate model. DOE associated with response surface methodology is an excellent tool for successfully carrying out the calibration set of multicomponent matrices [40-41]. In the present work, a simplex centroid mixture design was applied, in order to select a series of reference mixtures covering the entire experimental domain centered on the content of the commercial pharmaceutical specialties (Fig. 3).

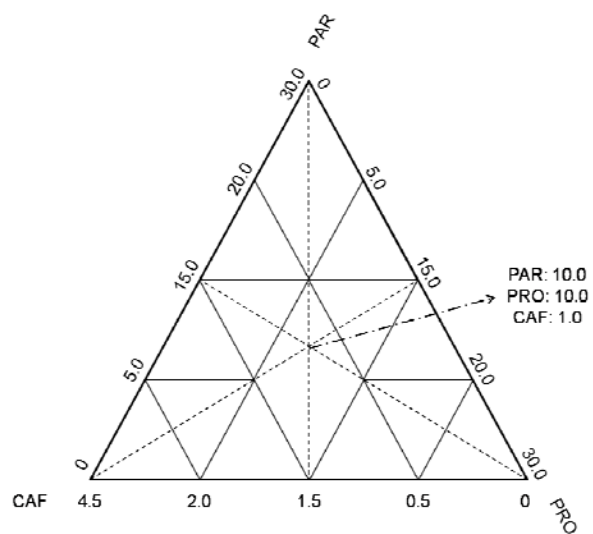


Figure 3. Simplex centroid design for building the calibration set.

DOE comprised seventeen solutions on five concentration levels, summarized in Table 1.

Table 1. Calibration set from Simplex centroid mixture design. Concentrations are expressed as $\mu\text{g ml}^{-1}$.

Sample	PAR	PRO	CAF
1	0.00	30.00	0.00
2	0.00	20.00	0.50
3	0.00	15.00	1.50
4	0.00	5.00	2.00
5	0.00	0.00	4.50
6	5.00	20.00	0.00
7	5.00	15.00	0.50
8	5.00	5.00	1.50
9	5.00	0.00	2.00
10	10.00	10.00	1.00
11	10.00	10.00	1.00
12	15.00	15.00	0.00
13	15.00	5.00	0.50
14	15.00	0.00	1.50
15	20.00	5.00	0.00
16	20.00	0.00	0.50
17	30.00	0.00	0.00

For all the mixtures, the contribution of each component was ensured to be additive without ever exceeding the linear range of the spectrophotometer.

PCR, PLS1 and PLS2 calibration models were firstly developed on data from the full-range spectra of zero-to-four derivative orders and a comparative study of the three chemometric approaches was undertaken. The models were validated by full cross-validation and the statistical parameters RMSEP and R^2 were recalculated when a new factor was added to the models. Table 2 lists the optimal PCs and the corresponding statistical parameters.

Table 2. Statistical parameters calculated from application of PCR and PLSs methods to full spectra of calibration samples

		PCR					PLS1					PLS2				
		⁰ D	¹ D	² D	³ D	⁴ D	⁰ D	¹ D	² D	³ D	⁴ D	⁰ D	¹ D	² D	³ D	⁴ D
PAR	PC	3	4	4	6	6	3	3	3	4	4	4	4	4	4	4
	RMSEP	0,9387	0,1146	0,2191	0,1648	0,1797	0,7693	0,4841	0,5104	0,4369	0,5798	0,0897	0,1144	0,2191	0,4406	0,5822
	R ²	0,9908	0,9998	0,9994	0,9996	0,9996	0,9923	0,9970	0,9962	0,9974	0,9955	0,9999	0,9998	0,9994	0,9974	0,9954
PRO	PC	4	5	5	5	5	4	4	4	4	4	5	4	4	4	4
	RMSEP	0,7595	0,1762	0,2719	0,2660	0,2535	0,6637	0,8309	0,6467	0,7970	0,6939	0,1703	0,8318	0,6477	0,8982	0,6892
	R ²	0,9925	0,9996	0,9990	0,9991	0,9991	0,9941	0,9907	0,9944	0,9915	0,9935	0,9996	0,9907	0,9900	0,9906	0,9936
CAF	PC	6	5	5	7	5	5	5	5	6	5	5	5	5	7	7
	RMSEP	0,2763	0,4499	0,5153	0,5291	0,5033	0,4683	0,4573	0,5082	0,5357	0,5004	0,2263	0,4531	0,5130	0,5295	0,5048
	R ²	0,9494	0,8372	0,7900	0,7769	0,7980	0,8236	0,8317	0,7928	0,7682	0,7989	0,9585	0,8349	0,7902	0,7745	0,7948

RMSEP values were satisfactory for all the models in the different derivative orders. PCs resulted ranging between 3 and 7, showing the higher values in correspondence of CAF determination. Analogously, the values of R^2 could be considered good for PAR and PRO, all over the value of 0.99, whereas lower values were carried out for CAF. These worse results could be imputed to the relative low content of CAF in the mixtures. The internal validation so demonstrated a preliminary substantial equivalence between the models built by using data from both ordinary or derivative UV spectra.

6.3.2. Recovery study

In order to test the prediction ability of the constructed models, a series of synthetic mixtures involving binary or ternary mixtures of PAR, PRO and CAF were analyzed. A prediction set of sixteen samples, containing the drugs in the same concentration ranges used for the calibration set, was randomly prepared. The above defined PCR and PLSs calibrations were applied to the prediction set and the models were tested by comparing accuracy and precision, in terms of percentage recovery and standard deviation, reported in Table 3.

Table 3. Accuracy (recovery%) and precision (SD) results from application of PCR and PLSs models to full spectra of the prediction set samples

		⁰ D	¹ D	² D	³ D	⁴ D	Mean A	SD
PCR	PAR	103.08	99.28	99.12	98.85	98.24	99.72	1.92
	PRO	128.66	128.66	98.03	103.03	100.84	111.84	15.45
	CAF	107.84	100.32	107.32	106.24	105.05	105.35	3.01
	Mean B	113.19	109.42	101.49	102.71	101.38		
	SD	13.60	16.67	5.08	3.70	3.44		
PLS1	PAR	100.06	104.14	97.95	100.29	100.96	100.68	2.24
	PRO	122.20	121.69	119.48	128.52	99.45	118.27	11.05
	CAF	122.23	87.64	105.20	98.85	103.39	103.46	12.52
	Mean B	114.83	104.49	107.54	109.22	101.27		
	SD	12.79	17.03	10.95	16.73	1.99		
PLS2	PAR	101.98	99.68	98.88	98.80	100.01	99,87	1,29
	PRO	108.57	121.72	97.74	105.44	109.75	108,64	8,68
	CAF	68.77	86.28	104.65	105.96	105.37	94,21	16,44
	Mean B	93,11	102,56	100,42	103,40	105,04		
	SD	21,33	17,89	3,71	3,99	4,88		

With the aim to study the influence of the spectral derivative elaboration on the models power, this table also shows the mean recoveries, and relative precision, of the single drugs for each multivariate method (Means A) and cumulative recoveries, and relative precision, for each derivative order (Means B). Means A allow to compare the power of the multivariate methods in predicting the single drugs; Means B allow to evaluate the influence of the derivative order in the resolution of the mixture.

Unfortunately, the agreement between experimental and predicted values was not very satisfactory. PAR quantification resulted good for all the methods and derivative orders, showing recovery within the range 97.95 - 104.14% and cumulative SD under 2.24. In contrast, determination of PRO gave worse results in terms of both recovery (97.74 – 128.66%) and SD (until to 15.45), in spite of its relative high content in the mixtures. CAF analysis showed the highest dependence from the derivative elaboration, yielding recovery values improving with the increase of the derivative order. Since CAF content is very lower than that of the other drugs, the increase of variance in the high derivative orders seemed to provide more useful information about CAF in building the multivariate models.

6.3.3. Optimization of the models by wavelength selection

A selection of wavelength subsets was investigated in order to emphasize the spectral characteristics of the single components with the aim to optimize the prediction power of the chemometric models. In this work, we have developed a simple but powerful technique for choosing those wavelength regions optimal for the quantitative resolution of complex systems.

A number of approaches to wavelength selection has been proposed for multicomponent systems presenting severe spectral overlapping. In some cases, the selection is simply based on spectral features of the analytes; in others, statistical parameters carried out from the validation procedure [42] or graphs relative to the calibration [39], have been proposed.

Some Authors have described the use of genetic algorithms or artificial neural networks [43-45].

The procedure herein proposed is based on the use of the regression coefficients calculated in a multivariate method for each component. In contrast with the above cited procedures, the selection uses objective parameters inherent the same calibration model and requires simple computer procedures.

The regression coefficients correlate the wavelengths (predictors) with the concentration of one component (analytical response) through the following equation:

$$C = b_0 + b_1 \lambda_1 + b_2 \lambda_2 + \dots + b_n \lambda_n$$

where C is the analyte concentration, b the regression coefficients and λ the wavelengths. Usually, the wavelengths presenting a value of b higher than 0.2 can be considered rich in useful information, whereas those having values under 0.1 can be discarded because their contribution is considered negligible [46]. Fig. 4 shows the distribution of the regression coefficients of the drugs in the range 200-350 nm.

As an example, this graph is referred to the model PCR applied on the zero-order derivative spectra.

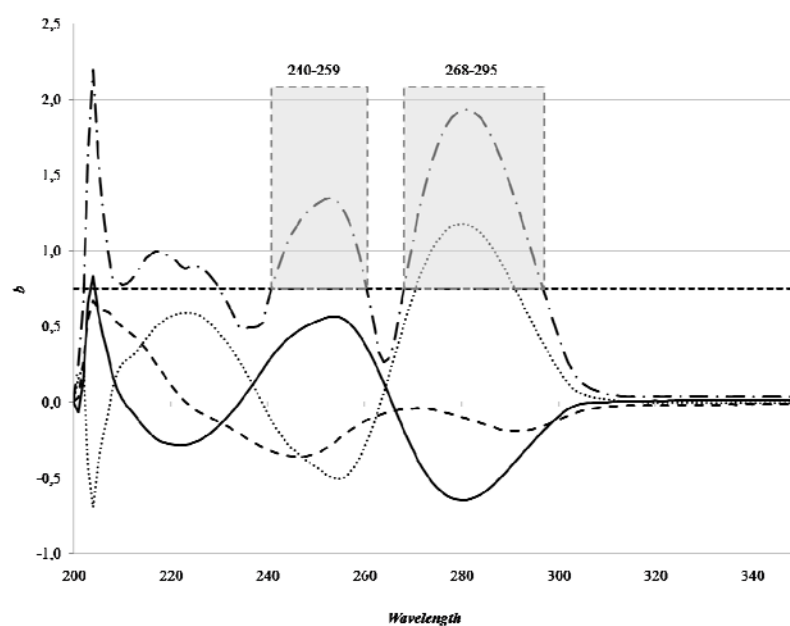


Figure 4. Distribution of regression coefficients (b) for PAR (—), PRO (·····), CAF (---) in the PCR model applied on zero-order derivative spectra. The curve of the cumulative coefficients B (-·-·-) and the cutoff line (- - -) corresponding to \bar{B} are plotted.

In Table 4 the matrix of the regression coefficients b is represented.

Table 4. Matrix of the regression coefficients (*b*)

	λ_1	λ_2	...	λ_n
Component 1 (<i>b</i> ₁)	$b_{1\lambda_1}$	$b_{1\lambda_2}$...	$b_{1\lambda_n}$
Component 2 (<i>b</i> ₂)	$b_{2\lambda_1}$	$b_{2\lambda_2}$...	$b_{2\lambda_n}$
...
Component <i>m</i> (<i>b</i> _{<i>m</i>})	$b_{m\lambda_1}$	$b_{m\lambda_2}$...	$b_{m\lambda_n}$
Sum	B_{λ_1}	B_{λ_2}	...	B_{λ_n}
	$B_{\lambda_j} = \sum_{i=1}^m b_i $		$\bar{B} = \frac{1}{n} \sum_{j=1}^n B_j$	

In our procedure, the absolute values of *b*, for every wavelength, obtained from the components equations were summed, obtaining so the cumulative coefficients B.

$$B_{\lambda_j} = \sum_{i=1}^m |b_i|$$

The curve resulting from plotting the values of B against wavelengths was added in Figure 4. After that, the mean of all the B values (\bar{B}) was calculated and this value was plotted as a cutoff line on the same graph. Finally, the wavelengths having a value of B over the cutoff line set at \bar{B} were selected.

$$\bar{B} = \frac{1}{n} \sum_{j=1}^n B_j$$

The selected wavelengths are clearly highlighted in the graph of Fig. 4. For this example, the most useful wavelengths

resulted to be ranging in the regions 240-259 and 268-295 nm. The wavelengths under 230 nm were discarded because affected by high noise that made unstable the model.

6.3.4 Analysis of the prediction set

All the multivariate models were re-built by using just the wavelength regions selected by the above defined procedure and listed in Table 5.

Table 5. *Wavelengths regions selected for PCR and PLSs models*

<i>Model</i>	<i>Selected wavelengths (nm)</i>
PCR	⁰ D 240-259, 268-295
	¹ D 250-252, 258-275, 283-303
	² D 244-250, 253-264
	³ D 235-240, 249-271, 285-307
	⁴ D 230-232, 239-262, 266-278
PLS1	⁰ D 267-296
	¹ D 233-239, 249-275, 283-303
	² D 240-263, 268-289
	³ D 234-245, 250-270, 285-306
	⁴ D 250-303
PLS2	⁰ D 243-259, 267-295
	¹ D 258-275, 283-303
	² D 241-263, 268-306
	³ D 237-271, 284-307
	⁴ D 230-242, 253-277, 298-305

The number of PCs and the statistical parameters RMSEP and R^2 carried out by full cross-validation are summarized in Table 6.

Table 6. Statistical parameters calculated from PCR and PLSs methods after wavelength selection procedure.

		PCR					PLS1					PLS2				
		⁰ D	¹ D	² D	³ D	⁴ D	⁰ D	¹ D	² D	³ D	⁴ D	⁰ D	¹ D	² D	³ D	⁴ D
PAR	PC	2	2	2	2	2	2	1	1	2	2	2	2	2	2	2
	RMSEP	0,1912	0,3685	0,3488	0,3485	0,3422	0,1911	0,2460	0,5936	0,3223	0,3525	0,1909	0,2672	0,34872	0,3183	0,3418
	R ²	0,9995	0,9991	0,9984	0,9987	0,9985	0,9995	0,9993	0,9955	0,9986	0,9983	0,9992	0,9990	0,99844	0,9987	0,9985
PRO	PC	3	2	2	2	2	2	2	2	2	2	3	2	2	2	2
	RMSEP	0,2859	0,4297	0,1873	0,2225	0,2641	0,6380	0,4500	0,1902	0,2222	0,2648	0,2823	0,4499	0,1870	0,2222	0,2637
	R ²	0,9989	0,9976	0,9995	0,9994	0,9991	0,9945	0,9973	0,9995	0,9993	0,9991	0,9989	0,9973	0,9995	0,9994	0,9991
CAF	PC	4	3	3	5	3	5	3	3	5	3	4	3	3	3	3
	RMSEP	0,1541	0,2151	0,2133	0,2569	0,1780	0,3976	0,2119	0,2118	0,1460	0,1804	0,1553	0,2125	0,2126	0,2787	0,1788
	R ²	0,9851	0,9693	0,9713	0,9608	0,9808	0,8746	0,9701	0,9718	0,9879	0,9803	0,9849	0,9700	0,9715	0,9530	0,9807

It is evident the remarkable decreasing of PCs used in these optimized models in comparison with the old models based on the full spectra (Table 2). The statistical parameters RMSEP and R^2 resulted analogously improved. These results demonstrated that the wavelength selection had provided to select a limited number of predictors but very rich in useful information.

The samples of the prediction set were assayed again by applying the optimized PCR and PLSs models, giving the results summarized in Table 7.

Table 7. Accuracy (recovery%) and precision (SD) results from application of optimized PCR and PLSs models on the prediction set

		⁰ D	¹ D	² D	³ D	⁴ D	Mean A	SD
PCR	PAR	100,95	100,56	100,09	99,79	99,51	100,18	0,58
	PRO	106,62	102,85	101,86	100,99	101,62	102,79	2,24
	CAF	96,92	111,88	102,87	98,59	107,52	103,55	6,21
	Mean B	101,50	105,10	101,60	99,79	102,88		
	SD	4,87	5,98	1,41	1,20	4,15		
PLS1	PAR	96,09	100,70	100,34	99,82	100,28	99,44	1,90
	PRO	121,82	100,27	98,19	100,96	106,06	105,46	9,59
	CAF	109,72	112,49	101,51	99,77	107,84	106,27	5,43
	Mean B	109,21	104,49	100,01	100,18	104,73		
	SD	12,87	6,94	1,68	0,67	3,95		
PLS2	PAR	95,98	100,58	100,12	99,38	99,52	99,11	1,82
	PRO	106,23	106,65	101,71	101,08	104,62	104,06	2,55
	CAF	93,07	112,36	101,35	100,24	107,77	102,96	7,41
	Mean B	98,42	106,53	101,06	100,23	103,97		
	SD	6,91	5,89	0,83	0,85	4,16		

Whatever model was employed, very good values of both accuracy and precision were carried out for PAR assay. The

high absorptivity values of this drug was surely essential in the success of its determination. On the contrary, analysis of PRO and CAF gave conflicting results, as the application of a number of PCR and PLS models resulted unsatisfactory.

The results were compared with those carried out by using the wavelength zones selected by other procedures above cited. The selection proposed by Linares et al. [42], using the relative standard error of prediction (RSEP), selects a wavelength range of 220-280 nm, while the use of leverage graph, proposed by De Luca et al. [39], singles out a wide range between 218 and 302 nm. When the calibration models based on these ranges were applied to the samples of the prediction set, the results were worse than those carried out by the method herein proposed. Both accuracy and precision resulted unsatisfactory, giving recovery values within the range 88.15 and 116.56% and RSD higher than 10%. The better performance of the models using the selection procedure proposed in this paper could be ascribed to the ability in selecting narrow spectral zones in which is contained the most useful analytical information.

With the aim to investigate the weight of the spectral derivatization on the prediction power of the multivariate models, the influence of the different derivative orders was compared. Generally, the use of the data from ordinary spectra gave bad recoveries in determination of both PRO and CAF. In contrast, accuracy considerably improved when higher derivative orders were used, reaching the best performance with the third-order derivative spectra. The next models based on the

fourth-order derivative spectra became inaccurate again. The notable increase in the absorbance variance with the derivative order probably furnished reliable information for the mixture resolution, but the associate noise became so high in the fourth derivative to cause instability of the models.

Recovery values from the application of the models using the full spectra and the optimized models using selected wavelength regions are compared in fig. 5.

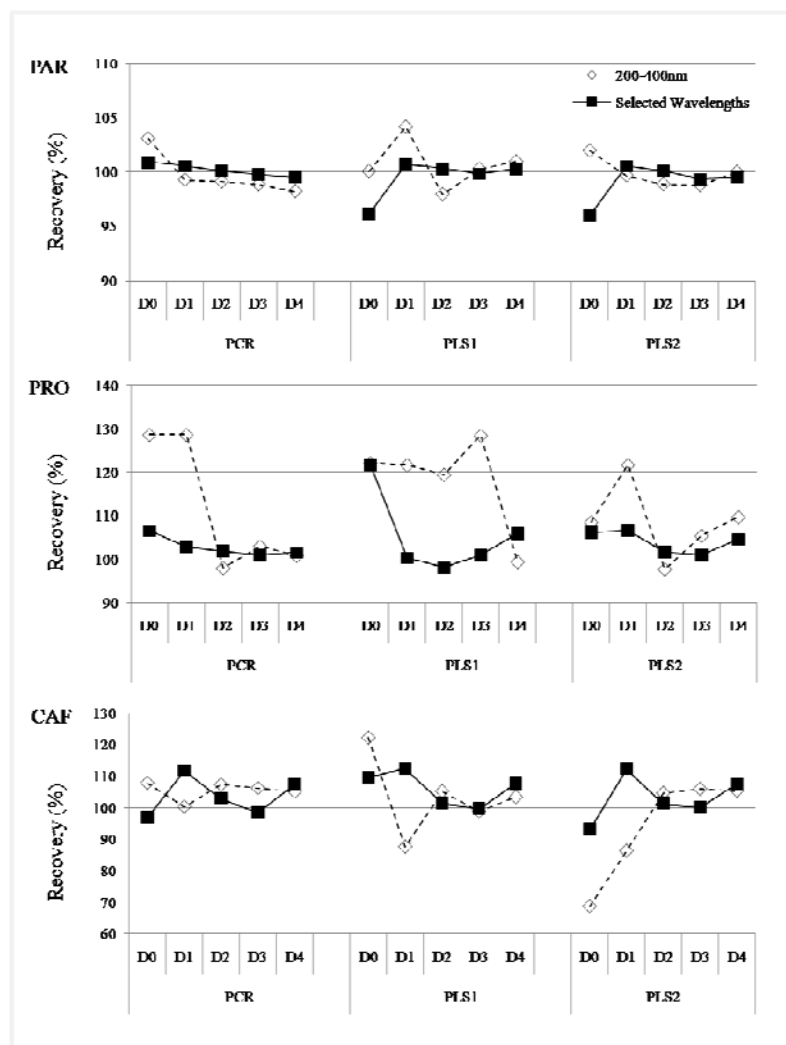


Figure 5 Comparison of recovery from PCR, PLS1, PLS2 models using the full spectra (◇) and the optimized models using selected wavelengths (■).

4.5 Analysis of commercial formulations

The final PCR and PLSs models were applied to the assay of binary and ternary pharmaceutical specialties. The assay results are summarized in Table 8.

Table 8. Assay results from application of optimized PCR and PLSs models on the pharmaceuticals. Drugs content is expressed as mg.

		Nominal									Found		
					PCR			PLS1			PLS2		
		PAR	PRO	CAF	PAR	PRO	CAF	PAR	PRO	CAF	PAR	PRO	CAF
NeoOptalidon	⁰ D	200	125	25	211,31	142,33	25,37	210,15	131,82	31,71	210,42	130,47	26,58
	¹ D				212,91	145,53	24,83	210,37	134,18	26,90	211,01	131,39	27,90
	² D				210,56	136,01	26,03	211,06	132,98	25,76	209,66	133,04	26,01
	³ D				208,81	128,88	25,03	208,21	126,58	26,01	207,36	125,94	26,00
	⁴ D				208,05	153,57	24,33	208,45	144,54	24,33	207,62	145,60	22,39
Saridon	⁰ D	250	150	25	255,99	176,75	25,88	257,64	159,94	32,37	254,69	160,88	27,08
	¹ D				254,72	169,56	24,62	253,71	154,86	24,90	252,88	153,40	26,10
	² D				255,38	166,00	29,35	255,76	158,19	30,30	254,76	161,26	29,71
	³ D				257,59	155,94	26,09	258,46	151,69	26,47	257,49	153,21	25,35
	⁴ D				256,09	174,21	26,61	255,70	155,32	27,69	254,99	155,05	29,05
Veramon	⁰ D	200	285	--	191,57	281,84	4,03	191,78	252,14	3,14	195,70	254,45	3,51
	¹ D				195,19	275,00	-10,06	192,66	246,16	-9,79	193,89	247,12	-6,71
	² D				196,93	274,20	-3,94	195,91	260,57	0,33	196,61	267,29	-2,45
	³ D				190,64	280,52	1,39	193,50	278,32	1,45	198,82	279,83	5,13
	⁴ D				192,72	258,94	-0,40	191,51	250,05	1,43	191,01	240,38	1,56

A good coincidence was observed between experimental results and label claim of the commercial formulations. Recovery values for PAR were in the range 95.32 – 106.46% and precision was calculated within 3.14 – 3.75 for all the multivariate methods. For PRO and CAF analysis, application of the models based on third-order derivative spectra gave recovery between 96.21 and 105.86% and SD not above 2. No interference from the excipients used in the dosage forms was observed.

6.4. Conclusions

Ultraviolet-visible spectral data can be transformed in increasing derivative orders so to obtain more useful information. Application of chemometric methods to derivative UV spectra can magnify the prediction ability of this spectrophotometric technique. A comparative study on the application of the multivariate calibration methods PCR, PLS1 and PLS2 on zero-to-fourth order derivative spectra of ternary mixtures of Paracetamol, Propiphenazone and Caffeine has been accomplished.

In general terms, the best assay results were carried out from the application of PCR and PLSs models to the third-order derivative spectra, being they rich in useful information but bearing a limited signal noise. A careful procedure to select the optimal wavelengths to be used in building the models was defined, based on the use of the regression coefficients as a discriminant factor. Very satisfactory results were obtained when the optimized models were applied to the analysis of synthetic mixtures and commercial drug formulations.

According to these studies, multivariate calibration methods (PCR, PLS1, PLS2) coupled with derivative spectral data can be recommended as a very suitable choice to resolve severe overlapped absorption spectra of drug mixtures. This approach is simple in application, inexpensive, requires an easy treatment of the samples and provides reliable analytical results.

For more details:

- [1] Wold, S., Sjöström, M., Eriksson, L., *Chemom. Intell. Lab. Syst., Lab. Inf. Manag.*, 58 (2001) 109-130.
- [2] Wold, S., Trygg, J., Berglund, A., Antti, H., *Chemom. Intell. Lab. Syst., Lab. Inf. Manag.*, 58 (2001) 131-150.
- [3] Massart, D., Vandeginste, B., Buydens, L., De Jong, S., Lewi, P., Smeyers-Verbeke, J., *Handbook of Chemometrics and Qualimetrics*, Elsevier, Amsterdam, 1998.
- [4] Brereton, R., *Chemometrics, Data Analysis for the Laboratory and Chemical Plant*, Wiley, Chichester, 2003.
- [5] Ragno, G., Ioele, G., Risoli, A., *Anal. Chim. Acta*, 512 (2004) 173-180.
- [6] Ragno, G., Vetuschì, C., Risoli, A., Ioele, G., *Talanta*, 59 (2003) 357-382.
- [7] Ni, Y., Qi, Z., Kokot, S., *Talanta*, 65 (2005) 36-47.
- [8] Lemus Gallego, J.M., Pérez Arroyo, J., *Anal. Chim. Acta*, 460 (2002) 85-97.
- [9] Martens, H., Naes, T., *Multivariate Calibration*, Wiley, Chichester, 1989.

- [10] Wold, H., *Research Papers in Statistics*, Wiley, New York, 1996, p. 411.
- [11] Wold, H., Martens, H., Wold, S., in A. Ruhe and B. Kagstrom (Ed.), *Multivariate Calibration Problems in Chemistry Solved by PLS*, Heidelberg, 1983, pp. 286-293.
- [12] Beebe, K.R. Kowalski, B.R., *Anal. Chem.*, 59 (1987) 1007-1017.
- [13] Wold, S., Geladi, P., Esbensen, K., Ochaman, J., *J. Chemom.*, 41 (1987) 1-24.
- [14] Ghasemiu, J., Niazi, A., *Microchem J.*, 68 (2001) 1-11.
- [15] Berzas Nevado, J.J., Rodriguez Flores, J., Villaseñor Llerena, M.J., Rodriguez Farinas, N., *Talanta*, 48 (1999) 895-903.
- [16] Dinç, E., Özdemir, A., Baleanu, D., *Talanta*, 65 (2005) 36-47.
- [17] Bosh Ojeda, C., Sanchez Rojas, F., *Anal. Chim. Acta*, 518 (2004) 1-24.
- [18] Karpinska, J., *Talanta*, 64 (2004) 801-822.
- [19] Tena, R.C., Delgado, M.A.R., Sanchez, M.J., Montelongo, F.G., *Talanta*, 44 (1997) 673-683.
- [20] Pappano, N.B., De Micalizzi, Y.C., Debattista, N.B. Ferretti, F.H., *Talanta*, 44 (1997) 633-639.

- [21] Erk, N., J. Pharm. Biom. Anal., 23 (2000) 1023-1031.
- [22] Dinç, E., Baleanu, D., J. Pharm. Biom. Anal., 31 (2003) 969-978.
- [23] Karljikovic-Rajic, K., Novovic, D., Marinkovic, V. Agbaba, D., J. Pharm. Biom. Anal., 32 (2003) 1019-1027.
- [24] Bosh Ojeda, C., Sanchez Rojas, F., Cano Pavon, J.M., Talanta, 42 (1995) 1195-1214.
- [25] Popović, G., Čakar, M., Agbaba, D., J. Pharm. Biomed. Anal., 33 (2003) 131-136.
- [26] L. Wang, M. Asgharnejad, J. Pharm. Biomed. Anal., 21 (2000) 1243-1248.
- [27] P.C. Damiani, G.M. Escandar, A.C. Olivieri and H.C. Goicoechea, Curr. Pharm. Anal., 1 (2005) 145-154.
- [28] Ferraro, M.C.F., Castellano, P.M., Kaufman, T.S., J. Pharm. Biomed. Anal., 34 (2004) 305-314.
- [29] Abbaspour, V, Mirzajani, R., J. Pharm. Biomed. Anal., 38 (2005) 420-427.
- [30] Afkhami, A., Bahram, M., Spectrochim. Acta Part A, 61 (2005) 869-877.
- [31] Markopoulou, C.K., Malliou, E.T., Koundourellis, J.E., Il Farmaco, 59 (2004) 627-636.

- [32] Dinç, E., Kökdil, G., Onur, F., *J. Pharm. Biomed. Anal.*, 26 (2001) 769-778.
- [33] Dinç, E., Baleanu, D. Aboul-Enein, H.Y., *Il Farmaco*, 59 (2004) 335-342.
- [34] Emre, D., Özaltın, N., *J. Chromat. B*, 847 (2007) 126-132.
- [35] Dimitrov, B., Doytchinov, I., Zlatkov, M., *J. Pharm. Biomed. Anal.*, 23 (2000) 955-964.
- [36] Filho, H.A.D., Galvão, R.K.H., Araújo, M.C.U., da Silva, E.C., Saldanha, T.C.B., José, G.E., Pasquini, C., Raimundo Jr., I.M., Rohwedder, J.J.R., *Chemom. Intell. Labor. Syst.*, 72 (2004) 83-91.
- [37] Bernaerts, K., Gysemans, K.P.M., Nhan Minh, T. Van Impe, J.F., *Intern. J. Food Microbiol.*, 100 (2005) 153-165.
- [38] Pronzato, W.E., *Identification of Parametric Models from Experimental Data*, Springer, Masson, 1997, pp. 413.
- [39] De Luca, M., Ioele, G., Risoli, A., Ragno, G., *Microchem. J.*, 83 (2006) 24-34.
- [40] Myers, R.H., Montgomery, D.C., *Response surface methodology. Process and product optimization using designed experiments*, New York, John Wiley & Sons, Inc., 1995.
- [41] Chasalow, S., *J. Applied Statist.*, 44(4) (1995) 534-545.

- [42] Linares, M.S., Fraga, J.M.G., Jimenez, A.I., Jimenez, F., Arias, J.J. , Anal. Lett., 32 (1999) 2489-2505.
- [43] Todeschini, R., Galvegni, D., Vilchez, J.L., del Olmo, M., Navas, N., Trends Anal. Chem., 18 (1999) 93-98.
- [44] Broadhurst, D., Guodacre, R., Jones, A., Rowland, J.J., Kell, B., Anal. Chim. Acta, 348 (1997) 71-86.
- [45] Arcos, M.J., Ortiz, M.C., Villahoz, B., Sarabia, L.H., Anal. Chim. Acta, 339 (1997) 63-77.
- [46] Esbensen, K.H., Multivariate Data Analysis in practice, CAMO Software AS, Oslo, 2006.

7. Artificial neural network combined with principal component analysis (ANN-PCA) for resolution of complex pharmaceutical formulations

Multivariate calibration methods, e.g. CLS (Classical Least Squares), ILS (Iterative Least Squares), PCR (Principal Component Regression) and PLS (Partial Least Squares), have represented in the last years a valid answer to the multicomponent determination of several drugs in the absence of interferences from excipients. Nevertheless, these classical chemometric methods show some difficulties in the resolution of complex samples, especially when the number of components increases, owing to the above mentioned problems.

Several analytical applications indicate that the combination of mathematical techniques provides more accurate results than those obtained by the application of single classical methods [1-2]. In recent years, the hyphenated methods based on principal component analysis and artificial neural network (PCA-ANN) regression have been proposed as calibration tools for the analysis of mixtures when spectral data were complex or when noise interference, nonlinear and interaction interferences were present [3-6]. Although the ANN methods have found greater application in nonlinear calibration systems, they have the ability to model also linear relationships [7-9]. A neural network is composed of an input layer and an output layer with one or several hidden layers of neurons. In the ANN model, neurons are used to calculate coefficients or relationships between input and output layers by

means of transfer functions. In a network, input and output correspond to the entry data and quantitative outcome, respectively [10-12]. The combined use of PCA and ANN usually improves the training speed, enhances the robustness of the model and reduces the calibration errors. Since the ratio between samples and variables in the ANN should be kept as high as possible, PCA is widely used in chemometrics to reduce the number of variables in a data matrix. Several ANN applications in quantitative analysis use PC scores obtained from PCA, as input variables [13-14].

In this work, a new hyphenated chemometric approach based on PCA and ANN was developed for the simultaneous determination of caffeine (CAF), mepyramine (MEP), phenylpropanolamine (PPA) and pheniramine (PNA) in pharmaceutical formulations without any separation step. The drugs are combined all together only in one pharmaceutical specialty but they are also present in many analgesic and antipyretic formulations in different combination as ternary, binary or single-component mixtures.

CAF is a psychoactive stimulant drug having the effect of temporarily warding off drowsiness and restoring alertness. It has diuretic properties too, at least when administered in sufficient doses to subjects who do not have a tolerance for it [15]. MEP is a first generation antihistamine, targeting the H1 receptor. However, it rapidly permeates the brain often causing drowsiness. It is used in combination products to treat the common cold and menstrual symptoms [16]. PPA, also known as norephedrine or oxyamphetamine, is a psychoactive drug of the phenethylamine

and amphetamine chemical classes which is used as a stimulant, decongestant and anorectic agent [17-18]. It is commonly used in prescription and over-the-counter cough and cold preparations. PNA is an antihistamine used to treat allergic conditions such as hay fever or urticaria. It has relatively strong sedative effects, and may sometimes be used off-label as an over-the-counter sleeping pill. Usually, it's used in combination with other drugs [19]. The above drugs have been analyzed in previous studies by using different spectrophotometric [20-22] and chromatographic methods [23-27]. CAF and MEP have been also quantified in pharmaceuticals by multivariate procedures [28-30].

UV analysis of the quaternary mixture showed an extensive overlap of the drug spectra. The spectral interference resulted very critical for PPA and PNA, because of their low absorptivity and, at the same time, the relatively higher absorptivity of the other two components. For this reason PPA and PNA could more suffer by interference from excipients or instrumental noise. ANN approach appeared so useful to minimize noisy and nonlinear interferences in such a way to obtain a more robust model.

Performance of ANN-PCA was compared with a simple ANN calibration, to investigate the ability of the PCA in extracting the most useful information from the raw data set and with a classical linear calibration technique such as PLS2. PLS2 was preferred to PLS1 because the data processing is made contemporarily for all the components and only one ANN PCA model is used to predict all four drugs at once. It results extremely effective when applied to systems with component presenting not very different

concentrations. On the contrary, PLS1 processing is made for one constituent at a time and is preferable when the concentrations of the components present a high difference.

Validation of all the calibration models was performed by analysis of synthetic mixtures of the target compounds added with tablets excipients, to verify their prediction ability in terms of accuracy and precision. The models were finally applied to the simultaneous quantitative prediction of the four studied compounds in commercial tablets.

7.1. Chemometric Techniques

7.1.1. Principal component analysis (PCA)

Principal component analysis (PCA), also named eigenvector-based multivariate analysis, is widely used in statistics to reduce the number of the variables of a data matrix. Usually, one of the main problems in modern data analysis is precisely the reduction of dimensionality. In fact the multidimensional data sets are difficult to interpret, and their structure cannot be directly visualized.

PCA transforms a number of correlated variables into a smaller number of uncorrelated variables called principal components (PCs), or factors, which can explain sufficiently the data structure. The main idea of PCA is to project the data from a high dimensional space in a lower dimensional space. In addition, PCA helps to find out in what respect one sample is different from another and which variables contribute most to this difference. The

data structure so obtained can be visualized directly in a graphical way by projection of objects onto the space defined by the selected PCs. The first PC contains most of the variability in the data and the succeeding PCs that are uncorrelated to former ones carry the remaining variability. The details about this argument is well described in literature [31-32].

7.1.2. Artificial neural network (ANN)

Artificial neural networks (ANN), also known as “neural networks” (NNs), is among the most widely used mathematical algorithms for overcoming non-linearity [30, 33]. In the last time, ANN has demonstrated high ability in acquiring useful information from complex systems, in presence of noise or instrumental fluctuations, providing robust models [34-35].

Usually, ANN is a computer system able to establish relationships between independent and dependent variables directly from raw data and can be used to model complex relationships between inputs and outputs or to find patterns in data. A number of different ANN structures have been proposed [3-4]. The structure adopted in this study was the Multilayer Perceptron (MLP) with back propagation. This technique has demonstrated to be a very powerful data modeling tool, able to capture and represent complex input/output relationships and has been already employed in pharmaceutical analysis [36-37]. MLP is a group of highly interconnected neurons arranged in layers with a feed forward structure. ANN architecture is based on input and output layers, named nodes, interconnected via one or more hidden layers.

The nodes in the input and output layers represent the independent and dependent variables, respectively.

MLP operation is divided into two steps. In a first step of training, the analytical data are presented as input parameters. These data are transformed by a weighting factor and the output values are iteratively fed to the hidden layers. During this step, termed 'learning', the MLP algorithm learns to associate the inputs with the expected outputs. In the last step, called 'testing', MLP generates an output signal as a response to previously unknown inputs. The network so develops a model capable to predict the properties of the analytical system.

7.1.3. Partial least squares 2 (PLS2)

PLS2 is a factor method, that defines a linear relationship between a set of dependent (response) variables and a set of predictor variables. The processing of data is made contemporarily for all the components and the regression simultaneously uses spectral and concentration data. It is an evolution of PLS1 in which, on the contrary, the data processing is made for one constituent at a time. The original variables are transformed into a smaller number of PCs and a new matrix constituted by the new variables PCs and scores allows to build the model for the prediction of the component concentrations of new samples.

The number of PCs must be optimized because the prediction error decreases with the number of PCs used until to reach an optimal value. The most used validation method is the full cross-validation, in which one reference at a time is removed from the

calibration set, after that the same sample is predicted by using the calibration built with the others references. The selection of number of PCs can be performed by adopting the minimum SEP, which represents an estimate of the error when other samples are predicted with that model. Detailed description of the PLS technique can be found in literature [38-39].

7.2. Drug and Experimental Method

Ethanol 95% was of spectrophotometric grade (J.T. Baker, Holland). PTFE 0.45 μm membrane filters were purchased from Supelco (Milan, Italy). CAF was a generous gift from Ognà SpA, Italy; MEP, PPA and PNA were generous gifts from Novartis SpA, Italy.

The pharmaceutical specialty (Triaminic® Tablets, Novartis Consumer Health SpA, Italy) was obtained commercially. This formulation contained 25.00 mg CAF, 25.00 mg MEP, 25.00 mg PPA and 25.00 mg PNA per tablet. Absorption spectra were recorded on a wavelength range of 220–300 nm in a 10 mm quartz cell, by a Perkin-Elmer Lambda 40P spectrophotometer at the following conditions: scan rate 1 nm/s; time response 1 s; spectral band 1 nm; data density 1 point/nm. The software UV Winlab 2.79.01 (Perkin-Elmer) was used for spectral acquisition and elaboration. The data were computed with programs written in MATLAB 7.0 (Mathworks). Application of PLS2 algorithm was supported by the software package “The Unscrambler 9.7®” (Camo Process As., Oslo, Norway).

Stock solutions of the studied compounds were separately prepared dissolving in ethanol nearly 20.00 mg of CAF, MEP, PPA and PNA in 100 ml calibrated flasks. A calibration set of 16 mixture solutions consisting of the drugs in the concentration range of 2.52-20.16 $\mu\text{g/ml}$ for CAF, 2.53-20.24 $\mu\text{g/ml}$ for MEP, 2.48-19.84 $\mu\text{g/ml}$ for PPA and 2.60-20.80 $\mu\text{g/ml}$ for PNA was randomly prepared from the stock solutions. In order to optimize the building of the ANN methods, an independent validation set consisting of 12 synthetic mixtures of the four compounds in the above concentration ranges was prepared. A similar second validation set consisting of 12 samples was prepared by adding excipients in order to reproduce as closely as possible the composition of the commercial specialities. The following excipients were used: sodium chloride, polyethylene glycol 4000, sucrose magnesium stearate microcrystalline cellulose and starch. This dataset was used for the external validation of the ANN and PLS2 models.

Pharmaceutical formulations were assayed by weighing the content of five tablets and reducing them to a fine powder. An amount exactly corresponding to the average weight was suspended in ethanol and made up to a volume of 10 ml. The suspension was sonicated for 10 min and then filtered through a PTFE 0.45 μm membrane filter. Samples for analysis were obtained after serial dilution 1:10 of this filtrate with ethanol until to reach the concentration ranges above reported and then analyzed. The developed PLS2, ANN and PCA-ANN calibrations were applied to the spectral data so obtained and the predicted amounts of CAF, MEP, PPA and PNA in tablets were carried out.

7.3. Results and Discussion

7.3.1. Building of ANN and PLS2 models

The UV spectra of pure CAF, MEP, PPA and PNA were individually recorded in the spectral region between 200-300. A first examination of these spectra pointed out a significant instability of the spectral signals in the region under 220 nm. The study was so pursued by using just the wavelength region between 220 and 300 nm. Fig. 1 shows the single spectra of the drugs, at the same concentration ratio of the pharmaceutical tablets, and the mixture spectrum resulting from their sum.

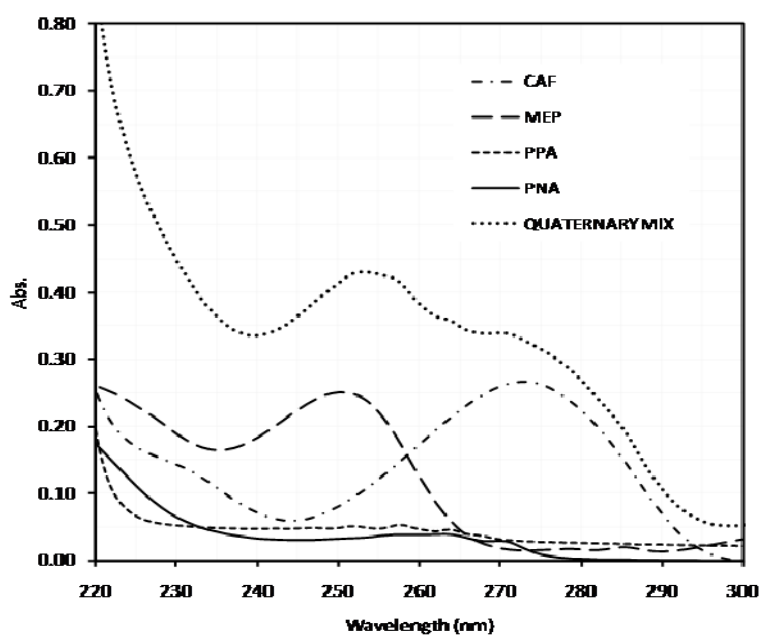


Figure 1. Absorption spectra in ethanol of 4.92 $\mu\text{g/ml}$ CAF, 5.02 $\mu\text{g/ml}$ MEP, 5.32 $\mu\text{g/ml}$ PPA, 5.50 $\mu\text{g/ml}$ PNA and their quaternary mixture.

As can be seen in this figure, the spectra of all the compounds overlap along the entire spectral range. Moreover, the absorptivity values of PPA and PNA along the full wavelength range result much lower than the other two components, making so their determination even more difficult to carry out.

The complexity of the studied multicomponent system reduced the chances of success in the simultaneous determination of the components by classical spectroscopy methods, which use measurements at discrete wavelengths. On the contrary, the multivariate methods can provide a greater resolution power because they use simultaneously a large number of signals, allowing so to extract more analytical information.

In this paper, the possibility of predicting the concentration of the four components by UV spectroscopy was studied through the non-linear calibration technique ANN and compared with the linear method PLS2. The ANN approach was also coupled with a PCA procedure in such a way to reduce the number of variables in the data matrix.

A calibration set consisting of 16 quaternary mixture solutions in ethanol with drugs at different concentrations was prepared. This training set is summarized in Table 1.

Table 1. Calibration set consisting of quaternary mixtures^a

Sample	CAF	MEP	PPA	PNA
1	2.52	5.06	4.96	20.8
2	2.52	10.12	9.92	20.8
3	2.52	5.06	19.84	5.02
4	2.52	10.12	19.84	10.4
5	5.04	20.24	2.48	20.8
6	5.04	10.12	9.92	5.2
7	5.04	20.24	2.48	2.6
8	5.04	10.12	19.84	10.4
9	10.08	2.53	2.48	20.8
10	10.08	20.24	4.96	5.2
11	10.08	2.53	19.84	5.2
12	10.08	20.24	9.92	2.6
13	20.16	2.53	2.48	10.4
14	20.16	5.06	4.96	10.4
15	20.16	2.53	9.92	2.6
16	20.16	5.06	9.92	5.2

^aConcentration is expressed as $\mu\text{g/ml}$

The absorbance values of these solutions in the wavelength set 220-300 nm were collected to build a data set consisting of a 16x81 (samples x wavelengths) dimension matrix. PLS2, ANN and PCA-ANN procedures were performed on these data. Special care was taken to ensure that, in the concentration ranges studied and for all the mixtures, either the total absorbance did not exceed the

linear range of the spectrophotometer and the contribution of each component was additive.

ANN and PCA-ANN methods with different input sets were executed. Table 2 indicates the topology of these networks.

Table 2. ANN topologies in the applied networks

	ANN	PCA-ANN
Input	81	4
Hidden	10	5
Output	4	4
Transfer functions	Tansig/purelin	Tansig/purelin

In a first stage, based on the use of the raw spectral data, ANN was directly applied to concentration and absorbance data. The dataset having dimension 16x81 was presented as an input vector to the ANN algorithm. A validation set with dimension 12x81 was also supplied during the training phase for early stopping of the training so to prevent over-fitting. A two layer ANN was built with tansig activation function in first hidden layer and purelin activation function in output layer. By using this structure, a rapid convergence of the inputs was reached and a linear mapping of the outputs provided to decrease the generalization error.

In applying the PCA-ANN approach, the calibration and validation datasets were reduced by PCA and three outputs were gathered. The first output was a loading matrix having size 81x4 (wavelengths x loadings), each column consisting of coefficients for one PC. The columns were made in order of decreasing component variance. The second output was the matrix of the

principal component scores having size 16x4 (samples x scores). The scores were the data obtained from the transformation of the original data into the space of the PCs. The third output was a vector containing the 4 eigenvalues of the covariance matrix of input. The first four PCs were observed to represent 99.9% of the total variance. Therefore, the first four columns of the score matrix were used to compose new datasets for learning and testing. Both calibration and validation datasets were so presented to the PCA-ANN, which was a two-layered neural network with tansig and purelin activation functions in hidden and output layers, respectively.

Performance of the two neural networks were compared by generalization accuracy and convergence speed. Figg. 2 and 3 point out the calculated errors versus the number of iterations for the training step of the neural networks.

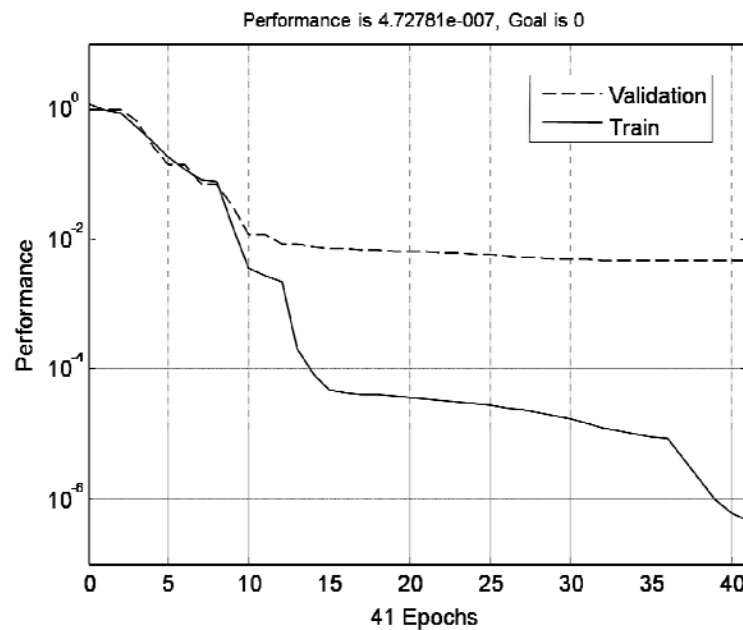


Figure 2. Error performance for training of ANN with raw data inputs

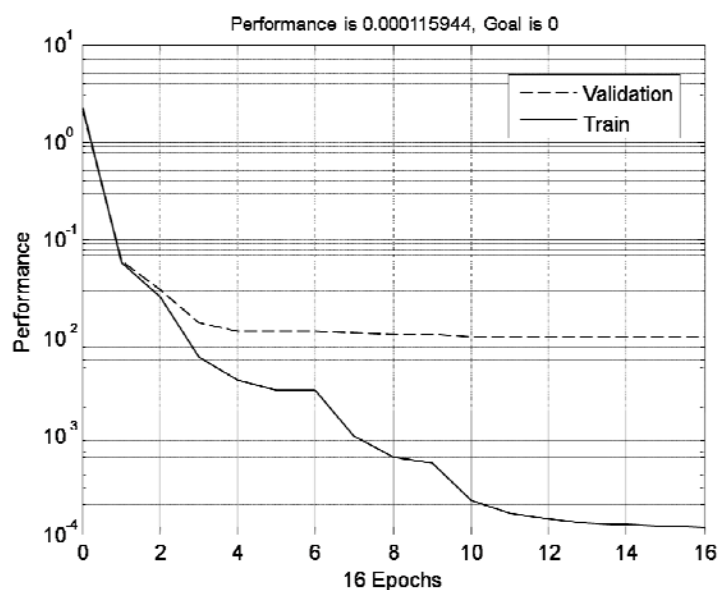


Figure 3. Performance (mean square error) for training of ANN with PCA applied inputs

Validation was performed by adopting the standard error of calibration (SEC) as a criterion to estimate the error when the samples are predicted.

A third calibration model was defined by PLS2 algorithm, by using concentration values and spectral data in the range 220-300 nm. The model was then validated by full cross-validation and the SEP values calculated each time after a new factor was added to the model. The optimum number of factors was found to be 4.

Validation furnished reliable assay results with SEC values for ANN and PCA-ANN methods not over 0.8 and SEP values for PLS2 not over 0.4. Table 3 shows SEC and SEP values and the statistical parameters from the regression analysis on the nominal and predicted concentrations.

Table 3. Statistical data obtained from internal validation on the reference samples by ANN, PCA-ANN and PLS2

Method	Parameter	CAF	MEP	PPA	PNA
ANN	SEC	0.735	0.620	0.724	0.619
	Slope	0.998	1.000	1.007	1.014
	Intercept	0.001	-0.001	0.001	0.000
	Correlation	0.993	0.992	0.998	0.993
PCA-ANN	SEC	0.156	0.098	0.035	0.123
	Slope	1.004	0.984	1.010	0.993
	Intercept	0.001	-0.002	-0.001	-0.000
	Correlation	0.999	1.000	0.989	0.979
PLS2	SEP	0.219	0.243	0.360	0.262
	Slope	1.007	1.042	1.050	0.997
	Intercept	0.002	-0.003	-0.003	-0.002
	Correlation	0.993	0.999	0.998	0.990

7.3.2. External validation of the models

The defined chemometric models were validated through analysis of an external prediction set consisting of 12 quaternary mixtures with the same concentration ranges adopted in the calibration samples and spiked with excipients commonly used in tablet formulations. The values of SEP were calculated for all the methods and components and summarized in Table 4.

Table 4. Statistical data obtained from external validation of ANN, PCA-ANN and PLS2 methods

Parameter	ANN				PCA-ANN				PLS2			
	CAF	MEP	PPA	PNA	CAF	MEP	PPA	PNA	CAF	MEP	PPA	PNA
SEP	0.148	0.308	0.295	0.323	0.094	0.130	0.216	0.194	0.153	0.076	0.279	0.253
Slope	1.011	1.016	1.032	1.027	0.998	0.992	1.028	1.021	1.049	0.972	0.955	0.968
Intercept	0.004	-0.028	-0.565	-0.058	0.065	0.029	-0.067	-0.058	-0.032	-0.057	0.075	-0.027
Correlation	1.000	0.999	1.000	0.998	1.000	0.999	0.999	1.000	0.999	0.999	0.998	0.999
Recovery	101.48	101.21	102.41	102.22	100.74	99.27	101.34	101.08	101.48	101.72	100.64	102.02
SD	1.93	2.07	1.93	2.43	1.35	1.46	2.08	1.21	1.63	1.05	2.12	1.53
RSD	1.90	2.05	1.88	2.37	1.34	1.47	2.05	1.20	1.28	1.72	1.84	2.68

^aConcentration is expressed as µg/ml; SD: Standard deviation; RSD: Relative standard deviation

The parameters from the regression analysis between nominal and predicted concentrations, mean recoveries and relative standard deviations were also calculated and listed in the same table. Mean accuracy, expressed as % recovery (\pm RSD), was found to be 101.58 (\pm 2.05), 100.61 (\pm 1.52) and 99.72 (\pm 2.42) for ANN, PCA-ANN, and PLS2, respectively.

A good coincidence was observed among the results obtained by the application of all the models in the estimation of CAF and MEP. PCA-ANN gave brilliant determination results also in the assay of PPA and PNA, slightly better than the results obtained by application of the simple ANN. Probably, the reduction of dimensionality of the input data allowed a selection of the most useful analytical information. In contrast, a significant difference between nominal amounts and predicted values were obtained in the prediction of PPA and PNA when the model PLS2 was applied. This inaccuracy was supposed due to the low absorptivity of these components, which made them more sensitive to instrumental noise or to interferences caused by some excipients. PCA-ANN gave the best results presumably because this method is particularly well suited to account for any non-linear information from a such complex analytical system.

7.3.3. Application of the models to the assay of pharmaceuticals

The above defined PLS2, ANN and PCA-ANN models were applied to the determination of CAF, MEP, PPA and PNA content in the commercial tablets, following the procedure above reported.

The obtained results are shown in Table 5, also listing some statistical parameters, as standard deviation, percent relative standard deviation and standard error.

Table 5. *Statistical results by applying ANN and PCA-ANN methods to the analysis of pharmaceutical formulations*

	ANN				PCA-ANN				PLS2			
	CAF	MEP	PPA	PNA	CAF	MEP	PPA	PNA	CAF	MEP	PPA	PNA
Mean ^a	25.74	25.82	24.38	24.12	24.92	25.45	25.82	24.03	24.53	26.24	27.53	23.87
SD	0.53	0.66	0.58	0.65	0.32	0.43	0.41	0.33	0.52	0.42	1.15	1.35
RSD	2.06	2.56	2.90	3.24	1.28	1.69	1.49	1.57	2.12	1.60	3.89	4.06
Recovery	102.96	103.28	97.52	96.48	99.68	101.8	103.28	96.12	98.12	104.96	110.12	95.48

^aResults are expressed as mg/tablet and are referred to average of four replicates (n=4); SD: Standard deviation;
RSD: Relative standard deviation

The measurements and the statistical parameters confirmed the results carried out in the external validation on the synthetic mixtures. A satisfactory coincidence between labeled and predicted amounts was observed in the estimation of all the drugs by applying the model PCA-ANN. Slightly less accurate results were obtained from application of the ANN model and significant errors were recorded in the prediction of PPA and PNA when the model PLS2 was used.

7.4. Conclusions

In this work, ANN and PCA-ANN multivariate methods demonstrated high resolution power in assaying a very complex pharmaceutical mixture, consisting in four drugs presenting a severe overlapping of their UV spectra. Great advantages of these methods are simplicity, rapidity and low cost, requiring neither sophisticated instrumentation nor any prior separation procedure. The ANN models were compared with a PLS2 model. The statistical parameters showed that both the ANN models were reliable, but PCA-ANN demonstrated a better performance in the prediction of the validation set samples, showing lower residual errors. Moreover, convergence speed for PCA-ANN was shorter than ANN, as verified in the training graphs. PLS2 also gave satisfactory results for the assay of CAF and MEP but proved to be less accurate in assaying PPA and PNA, probably for the non-linear interferences due to instrumental noise or the presence of excipients from tablet extraction. The successful application of the proposed methods to the quality control analysis of quaternary pharmaceutical preparations, demonstrated that the ANN procedures can be a valid alternative to the classical instrumental or multivariate procedures also for linear data systems.

For more details:

- [1] Dinç, E., Ragno, G., Ioele, G., Baleanu, D., J. AOAC Int., 89, (2006) 1538-1546.
- 2) Dinç, E., Kanbur, M., Baleanu, D., Spectrochim. Acta A Mol. Biomol., 68, (2007) 225-230.
- 3) Jin-Mei, X., Xiao-Jian, W., Ying-Jin, Y., Metabolomics, 3, (2007) 531-537 .
- 4) Forshed, J., Andersson, F.O., Jacobsson, S.P., J. Pharm. Biomed. Anal., 29, (2002) 495-505.
- 5) Yin, C., Shen, Y., Liu, S., Yin, Q., Guo, W., Pan, Z., Comput. Chem., 25, (2001) 239-243 .
- 6) Absalan, G., Soleimani, M., Anal. Sci., 20, (2004) 879-882 .
- 7) Khanchi, A.R., Mahani, M.K., Hajhosseini, M., Maragheh, M.G., Chaloosi, M., Bani, F., Food Chem., 103, (2007) 1062-1068 .
- 8) Guiberteau, A., Galeano, T., Mora, N., Salinas, F., Ortiz, J.M., Virè, J.C., Comput. Chem., 25, (2001) 459-473.
- 9) Ni, Y., Zhang, G., Kokot, S., Food Chem., 89, (2005) 465-473.
- 10) Agatonovic-Kustrin, S., Beresford, R., J. Pharm. Biomed. Anal., 22, (2000) 717-727.

- 11) Tominaga, Y., *Chemom. Intell. Lab. Syst.*, 49, (1999) 105-115.
- 12) Plumb, A.P., Rowe, R.C., York, P., Brown, M., *Eur. J. Pharm. Sci.*, 25, (2005) 395-405.
- 13) Gemperline, P.J., Long, R., Gregoriou, V.G., *Anal. Chem.*, 63, (1991) 2313-2323.
- 14) Zarei, K., Atabati, M., Kazemi, L., *Il Farmaco*, 60, (2005) 37-42.
- 15) Maughan, R.J., Griffin, J., Hum, J., *Nutr. Diet.*, 16, (2003) 411-420.
- 16) Parsons, M.E., Ganellin, C.R., *Br. J. Pharmacol.*, 147, (2006) 127-135.
- 17) Flavahan, N.A., *J. Pharmacol. Exp. Ther.*, 313, (2005) 432-439.
- 18) Kernan, W.N., Viscoli, C.M., Brass, L.M., Broderick, J.P., Brott T., Feldmann, E., Morgenstern, L.B., Wilterdink, J.L., Horwitz, R.I., *N. Engl. J. Med.*, 343, (2000) 1826-1832.
- 19) Korduba, C.A., Veals, J., Symchowicz S., *Life Sci.*, 13, (1973) 1557-1564.
- 20) Abbaspour, A., Mirzajani, R., *J. Pharm. Biomed. Anal.*, 38, (2005) 420-427.
- 21) Dinç, E., Kökdil, G., Onur, F., *J. Pharm. Biomed. Anal.*, 26, (2001) 769-778.

- 22) Shama, S.A., Amin, A.S., *Spectrochim. Acta A Mol. Biomol.*, 60, (2004) 1769-1774.
- 23) Kartal, M., *J. Pharm. Biomed. Anal.*, 26, (2001) 857-864.
- 24) Abbasi, K., Bhanger, M.I., Khuhawar, M.Y., *J. Pharm. Biomed. Anal.*, 41, (2006) 998-1001.
- 25) Ferreyra, C., Ortiz, C., *J. Pharm. Biomed. Anal.*, 25, (2001) 493-499.
- 26) Louhaichi, M.R., Jebali, S., Loueslati, M.H., Adhoum, N., Monser, L., *Talanta*, 78, (2009) 991-997.
- 27) Mikus, P., Valásková, I., Havránek, E., *J. Pharm. Biomed. Anal.*, 38, (2005) 442-448.
- 28) Ragno, G., Ioele, G., Risoli, A., *Anal. Chim. Acta*, 512, (2004) 173-180.
- 29) De Luca, M., Oliverio, F., Ioele, G., Ragno, G., *Chemom. Intell. Lab. Syst.*, 96, (2009) 14-21.
- 30) Aksu, Ö., Bozdogan, A., Kunt, G., *Anal. Lett.*, 39, (2006) 751-761.
- 31) Meloun, M., Militký, J., Forina, M., "Chemometrics for analytical chemistry", Vol. 1, PC-Aided Statistical Data Analysis, Ellis Horwood, Chichester, 1992.

- 32) Beebe, K.R., Pell, R.J., Seasholtz, M.B., "Chemometrics: a practical guide", Wiley-Interscience Ed., New York, 1998.
- 33) Dinç, E., Baleanu, D., Ioele, G., De Luca, M., Ragno, G., J. Pharm. Biomed. Anal., 48, (2008) 1471-1475.
- 34) Sun, Y., Peng, Y., Chen, Y., Shukla, A. J., Adv. Drug Deliv. Rev., 55, (2003) 1201-1215.
- 35) Takayama, K., Fujikawa, M., Obata, Y., Morishita, M., Adv. Drug Deliv. Rev., 55, (2003) 1217-1231.
- 36) Hussain, A.S., Yu, A., Johnson, R.D., Pharm. Res., 8, (1991) 1248-1252.
- 37) Chen, Y., Jiao, T., McCall, T.W., Baichwal, A.R., Meyer, M.C., Pharm. Dev. Technol., 7, (2002) 373-379.
- 38) Geladi, P., Kowalski, B.R., Anal. Chim. Acta, 185, (1986) 1-17 .
- 39) Wold, S., Sjöström, M., Eriksson, L., Chemom. Intell. Lab. Syst., 58, (2001)109-130.

8. Naproxen as a Photoactive Probe within Liposomes Microenvironment. Retarded Photooxidation by Included Cholesterol.

Liposomes are the smallest artificial vesicles of spherical shape that can be produced from natural phospholipids and cholesterol (Ch). They are very versatile tools in biology, biochemistry and medicine [1-5] and have attracted attention as potential vehicles for drug delivery to selected cells or tissues *in vivo* and as carriers of drugs including proteins, hormones and diagnostic agents [6-7]. Although most of this interest has focused on drug delivery, a variety of other applications can be considered in cosmetics, cleansing, ecology, and food technology [8]. Liposomes have also been shown to be effective as simple biomimetic models for cell membranes in photoinduced electron transfer reactions [9] and for the study of lipid peroxidation [10-11].

Inclusion of photosensitizers used in photodynamic therapy within liposomes has been studied, and a good correlation between the physicochemical features of formulations and their efficiency as photosensitizers has been found [12]. Moreover, photosensitive liposomes offer an appropriate tool for selective drug release. In addition, interaction of light with photosensitive bilayers may cause membrane reorganization, with possible applications in imaging, sensing as well as therapeutics [13].

Naproxen (NPX, Fig. 1) is widely used as a highly effective nonsteroidal anti-inflammatory drug. Although NPX is rather safe

and tolerable, serious gastrointestinal side effects, and in some cases skin photosensitivity, may appear after oral administration [14-16]. Besides, it exhibits red blood cells photohaemolytic activity and causes photocleavage of DNA [17].

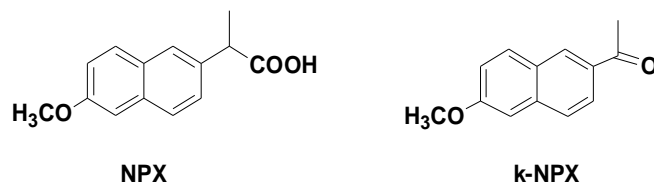


Figure 1. Structures of naproxen (NPX) and its ketonic photoproduct (k-NPX).

It is known that NPX may undergo photodegradation in aqueous solutions under aerobic and anaerobic conditions. Decarboxylation seems to be the main process, which leads to photoproducts formation (see structure of the ketonic photoproduct in Fig. 1) [18-19]. The photophysical properties and photochemical degradation mechanism of NPX have been studied theoretically [20]. A major photochemical pathway of NPX is known to be singlet oxygen generation, which can produce deleterious effects on biomolecules, for instance, lipid peroxidation [21]. In this context, it has been reported that cyclodextrin complexation of NPX results in a reduced photohaemolytic activity; however, this microenvironment does not increase drug photostability [19].

In this context, the goal of the present work has been to study the photophysical and photochemical behavior of the liposome-encapsulated drug. In this context, a point of special interest is the possibility that liposome microenvironment protects against photooxidative degradation.

8.1. Drug and Experimental Procedures

(S)- and (R)-NPX, Ch, 1,2- dioleoyl-sn-glycero-3-phosphocholine (PC) were purchased from Sigma–Aldrich (Steinheim, Germany) and > 99% grade of purity. Chloroform and methanol were of HPLC grade from Scharlab (Sentmenat, Spain) and were used without further purification. Phosphate buffered saline solution (PBS) (pH = 7.4, 0.01 M) was prepared by dissolving Sigma tablets in the appropriate amount of purified water (Milli-Q system, Millipore). Lipids were stored as purchased at -20°C.

Liposomes including (S)- and (R)- NPX with and without cholesterol were prepared by thin layer evaporation (TLE) method according to standard conditions [22-23]. Liposomes solutions were obtained dissolving 12.1 mg of PC in 10 mL of chloroform containing NPX (*ca.* 2×10^{-3} M) in a 50 mL round-bottomed flask. In order to prepare liposomes with cholesterol, the same amount of phosphatidylcholine and 3.6 mg of Ch were dissolved in 10 mL of a 9:1 chloroform:methanol solution containing NPX as above. Drug-free liposomes were prepared as blank. The solutions were submitted to evaporation at 58 °C with a vacuum rotary evaporator for ten minutes, to eliminate the organic solvents. Then, the solvent was completely removed by drying under vacuum for 2 hours. The lipid film obtained was hydrated with 2 mL of PBS, leading to a liposomal emulsion. Large unilamellar liposomes (LUV) were produced starting from multilamellar ones by sonication in an ultrasonic bath for 30 min at 50 °C. In this way, more homogeneous size vesicles were obtained; they were kept under

controlled temperature (4 °C) until their use within three days. Immediately before use, 0.5 mL of liposome suspension were added to the same amount of PBS and purified by centrifugation at 14000 x g during 10 min for three times at room temperature in a HERAUS Pico 21 centrifuge (Thermo electron corporation, Germany).

For size analysis, liposomes were analyzed using transmission electronic microscopy (TEM) and cryoscopic scanning electronic microscopy (CryoSEM). TEM observation of liposomes was carried out by a JEOL2010-FEG TEM/STEM microscope, equipped with a field emission electron source and an objective lens with Cs value of 0.5 mm. The images were digitally recorded on a 1024 x 1024 CCd camera. Image analysis was performed using routines implemented in the software plugins of Digital Micrograph. For TEM measurements 5 µL of purified liposomes were put on a holey-carbon coated 3-mm Cu-grid and dried at room temperature under a cabinet equipped with an aspiration system. After complete evaporation of the solvent, the sample was ready for direct observation. SEM images were obtained using a JEOL JSM-6300 microscope operating at 20 kV. For CryoSEM analysis samples were frozen, and thin frozen sections were imaged without staining. For both microscopic analysis liposomes were rehydrated with Millipore water instead of PBS, in order to avoid the optical interference of saline crystal in the medium.

The encapsulation efficiency (EE) of NPX was determined using equation 1 [24]; it is expressed as the percentage of the drug trapped in purified liposomes referred to the non purified solutions.

$$\text{Encapsulation efficiency (\%)} = \frac{C_t - C_o}{C_t} \times 100 \quad (\text{Equation 1})$$

where C_o is concentration in the supernatant diluted with PBS and C_t refers to the liposome suspension diluted with warm ethanol (70°C), for disruption of the liposomes and release of the included drug to the solvent. The amount of entrapped drug was determined from absorbance of the samples with UV-Vis spectrophotometry at the maximum (230 nm). Encapsulation efficiency was verified at each preparation of new batch of liposomes.

About the spectroscopic measurements, irradiations of the solutions were performed using a Photon Technology International (PTI, Germany) LPS-220B spectrofluorometer equipped with a monochromator in the wavelength range of 200-700 nm. The samples were placed in a 10 x10 mm² quartz cells of 4 mL capacity with a septum cap. The experiments were carried out using air-equilibrated and oxygen-purged PBS solutions with absorbance in the range 0.60–0.70 at 230 nm. All the UV visible spectra were recorded after irradiation at 230 nm every 5 minutes using a spectrophotometer Cary Varian 300 (Varian, Spain) on the λ range of 200 – 400 nm, at time response 1 s and spectral band 1 nm. The software Cary UV Scan (Varian) was used for spectral acquisition and elaboration. Steady state fluorescence experiments were

carried out using the spectrofluorometer above described and preparing the solutions at the absorbance of 0.1 at excitation wavelength ($\lambda = 330$ nm) in the quartz cells. Emission spectra were recorded after excitation at 330 nm, using a personal computer equipped with Felix Program (PTI) for spectral acquisition and elaboration.

Lifetimes evaluation was carried out with a Time Master fluorescence lifetime spectrometer TM-2/2003 from PTI by means of the stroboscopic technique. Hydrogen/nitrogen flash lamp was used as excitation source. Felix software (PTI) was used for data elaboration (fitting by exponential functions), and a deconvolution procedure was needed to separate the sample kinetic traces from the lamp pulse profile. For both experimental procedures, solutions were nitrogen-purged and prepared at the absorbance of 0.1 at excitation wavelength ($\lambda = 330$ nm). Fluorescent quantum yield measurements were obtained with nitrogen-bubbled PBS solutions; the absorbance was adjusted at the excitation wavelength ($\lambda = 330$ nm) using (*S*)- or (*R*)- NPX as standard ($\phi_f = 0.4$). All experiments were conducted at room temperature and were run in triplicate.

Laser flash photolysis (LFP) studies were carried out with a pulsed XeCl excimer laser ($\lambda_{exc} = 308$ nm, ca. 17 ns pulse width, < 100 mJ per pulse). A pulsed Lo255 Oriel xenon lamp was used as detecting light source. The observation wavelength was selected with a 77200 Oriel monochromator, and the signal was amplified by an Oriel photomultiplier tube (PMT) system made up of a 77348 side-on PMT tube, 70680 PMT housing and a 70705 PMT power supply. The signal was registered with a TDS-640A

Tektronix oscilloscope and subsequently transferred to a personal computer. All transient spectra were recorded using 10 x 10 mm² quartz cells with 4 mL capacity. In general, solutions were nitrogen-purged for 10 min before acquisition, and the decays were registered at 440 and 650 nm. Samples were prepared in PBS, and the absorbance was kept at *ca.* 0.15 in order to obtain transparent solutions and to avoid non-linear effects like self-absorption or inhomogeneous transient distribution. All measurements were performed at room temperature. Solutions of (*R*)- and (*S*)- NPX in PBS, treated in the same way as liposomes solutions, were used as reference. LFP analyses were run in triplicate.

8.2. Results and Discussion

Photophysical and photochemical studies were performed on NPX entrapped within liposomes, in order to establish the influence of this microenvironment on drug photobehavior. The presence of Ch was also investigated as a potential protector against photooxidative NPX damage.

8.3.1. Entrapment of naproxen within liposomes

Large unilamellar liposomes (LUV) have been reported since 1965 as membrane biomimetics [25]. Addition of cholesterol (Ch) to phosphatidylcholine (PC) in liposomes bilayer increases the hydrophobicity of the interfacial region, influencing drug incorporation within the lipidic membrane [26]. In this work, liposomes with and without Ch were prepared. Optimization of the classical method of TLE was performed in an attempt to increase

the encapsulation efficiency (EE) and to obtain liposomes with homogeneous size. Different amounts of Ch in the range between 10 and 50 % (w/w) were added to PC; the best results were obtained with a content of *ca.* 30% Ch.

Under these conditions, the EE was *ca.* 40 % for (*S*)- and (*R*)-NPX. Moreover, this parameter appeared to be very sensitive to the storage of liposomes. In fact, maintenance at room temperature caused a progressively decrease of EE, which dropped to 15 % after several days, with an important transfer of NPX from liposomes to the PBS solution.

The obtained solutions were characterized using TEM and CryoSEM microscopy (Figure 1). Both techniques are suitable to investigate the size and external features of liposomes. In particular, TEM analysis is widely used in this field [27] because it can offer an unrefined image of the liposomal profile and permits size measurements. The diameter of prepared liposomes was in the range of 100-260 nm corresponding to LUV, which makes them appropriate as biomimetic models (Fig. 1A). On the other hand, CryoSEM analysis shows liposome morphology in the hydrated state: in general the expected spheroidal shape was observed. Uniform and compact bilayers, a typical mark of unilamellar liposomes, are clearly identified; smaller liposomes were rarely observed (Fig. 1B). In some cases, small inclusions on the surface were found, probably lipids from disrupted liposomes at the moment of analysis in contact with the same surface.

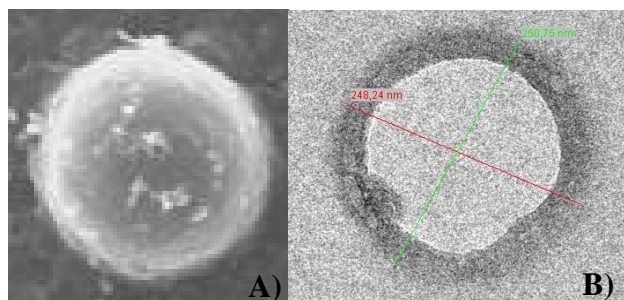


Figure 2. Images of liposomes prepared by thin layer evaporation (TLE). **A)** cryoscopic scanning electronic microscopy (CryoSEM) and **B)** transmission electron micrograph (TEM) respectively.

8.3.2. Photophysics of naproxen within liposomes.

The emission spectra of NPX in homogeneous medium and incorporated within liposomes were recorded at room temperature, using 330 nm as the excitation wavelength (see Figure 2). Solutions of NPX outside and inside liposomes showed the same spectrum, with a maximum at 355 nm. The shape and position of the main bands of excitation spectra were essentially coincident with those of the absorption spectra. From the intersection between normalized excitation and emission traces, a singlet energy (E_s) of *ca.* 85 kcal/mol was obtained for all systems. Fluorescence quantum yields inside liposomes with or without Ch ($\phi_f = 0.4$) were similar to the value obtained for free NPX. In order to detect a possible dynamic quenching, time resolved fluorescence studies were carried out; they showed similar lifetimes of the singlet excited state (τ_s *ca.* 10 ns) for (*S*)- and (*R*)- NPX in the bulk solution and within liposomes, either without or with Ch. Thus, both static and dynamic fluorescence quenching inside the liposomes can be safely ruled out.

Table 1. Photophysical parameters of (S)- and (R)-NPX outside and inside liposomes with or without Ch.

Sample	τ_s (ns) ^a	E_s (Kcal/mol) ^b	K_{fq} (M ⁻¹ sec ⁻¹) ^c	τ_t (μ s) ^d
(S)-NPX	9.9	85	1×10^9	15
(S)-NPXLiposomes	10.1	85	7×10^9	18
(S)-NPXLiposomesCh	9.9	85	7×10^9	17
(R)-NPX	9.9	85	1×10^9	15
(R)-NPXLiposomes	10.2	85	7×10^9	18
(R)-NPXLiposomesCh	9.9	85	7×10^9	17

^a Singlet lifetime. ^b Singlet energy. ^c Fluorescence quenching rate constant for oxygen. ^d Triplet lifetime.

The rate constant of singlet excited state quenching by oxygen in PBS was determined using time-resolved fluorescence spectroscopy, recording decays under N₂, air, and O₂ atmosphere. The lifetimes of NPX within liposomes were more sensitive to the presence of oxygen than those of free NPX in solution. From these data the apparent quenching rate constant by oxygen was determined by means of the Stern-Volmer relationships and found to be $1 \times 10^9 \text{ M}^{-1} \text{ s}^{-1}$ for the free drug and $7 \times 10^9 \text{ M}^{-1} \text{ s}^{-1}$ for liposome-encapsulated drug. However, it has to be considered that effective oxygen concentration within liposomes may be much higher than in solution (typically 3-4 times) [28]. Hence, the corrected values in the different reaction media would be much closer to each other than the trend reflected in Table 1.

In addition to fluorescence measurements, laser flash photolysis (LFP) experiments were carried out in the nanosecond-microsecond timescale, using a 308 nm XeCl excimer laser for excitation. The transient absorption spectra in PBS were similar to that previously described for NPX [16]. Two transient species were observed 300 ns after the laser pulse, which decayed with different kinetics (see Figure 3, for the *S* enantiomer): an earlier intermediate assigned to the solvated electron (maximum *ca.* 700 nm and lifetime shorter than 1 μ s) and a triplet-triplet absorption showing typical band at 440 nm. The triplet state was quenched by oxygen leading to formation of singlet oxygen [21]. The triplet lifetime was in the range 15-18 μ s, depending on the employed media (see Fig. 3B and Table 1). Although within liposomes the signal was noisier, the triplet lifetime appeared to be somewhat higher.

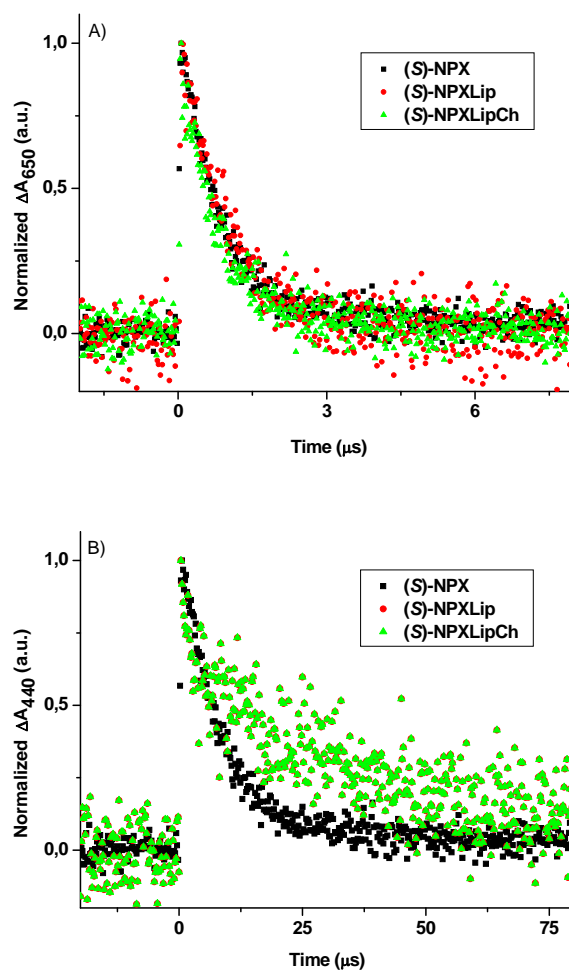


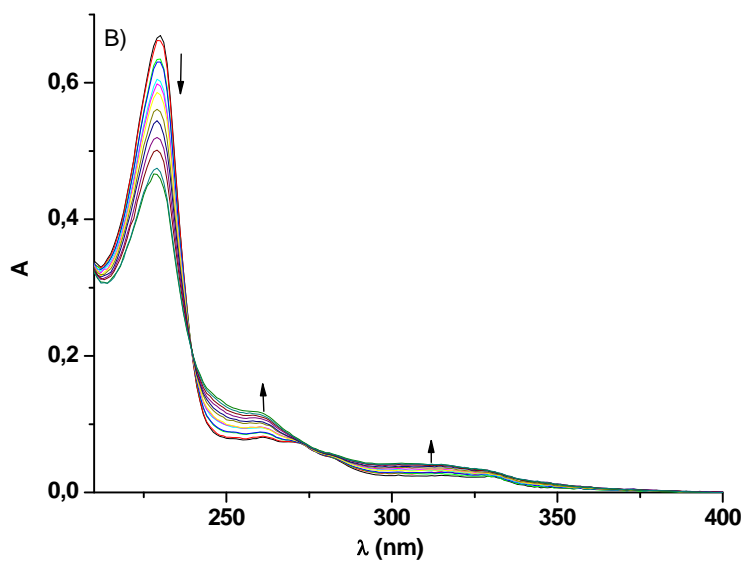
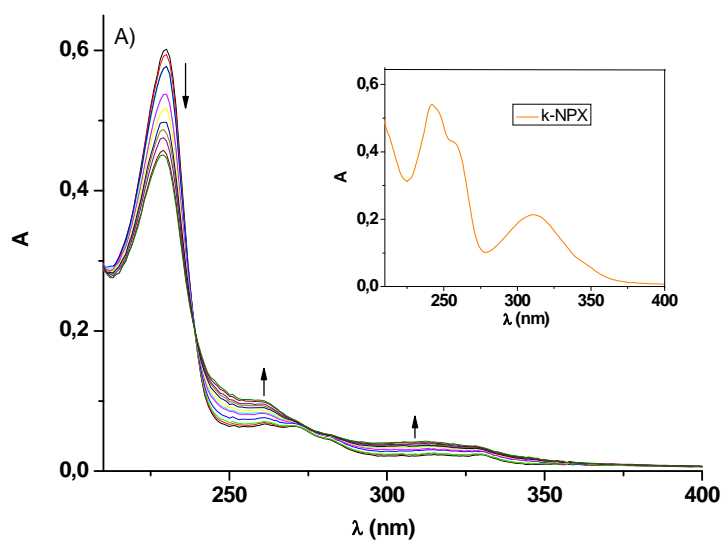
Figure 3. **A)** Decays of the solvated electrons generated from NPX, NPX within liposomes (NPXLip) and NPX within liposomes with Ch monitored at 650 nm. **B)** Decays of the triplets generated from NPX, NPXLip and NPXLipCh monitored at 440 nm.

8.3.3. Antioxidant activity of cholesterol in liposomes.

Aerated and oxygenated solutions of (S)- and (R)- NPX outside and inside liposomes were irradiated with monochromatic light at $\lambda = 230$ nm in PBS, where NPX shows four bands with

maxima at 230, 270, 320 and 330 nm [29]. The irradiation wavelength was selected because it corresponds to an absorption maximum of the drug at which it is possible to avoid turbidity of liposomal preparations. The results are displayed in fig. 4. Irradiations were monitored by UV-spectrophotometry, following the decrease in the absorption at 230 and the concomitant increase at 315 nm and 250 nm, correspond to the ketonic photoproduct (k-NPX). This observation is in agreement with the results obtained by irradiation of NPX under aerobic conditions in aqueous solutions.

Photodegradation profile was nearly the same for (*S*)- and (*R*)- NPX. No important differences were noted between (*S*)-NPX photodegradation in PBS and in liposomal formulation without cholesterol, where a linear increment of the absorbance at 250 and 315 nm was found. The same trend was observed under oxygen atmosphere. By contrast, photodegradation of liposomes containing cholesterol was clearly slower, indicating that Ch acts as a protector of NPX against oxidation, in spite of the higher concentration of oxygen within liposomes. Probably, Ch plays a sacrificial role, undergoing oxidation itself (and consuming available oxygen) to prevent photooxidative damage of the encapsulated drug.



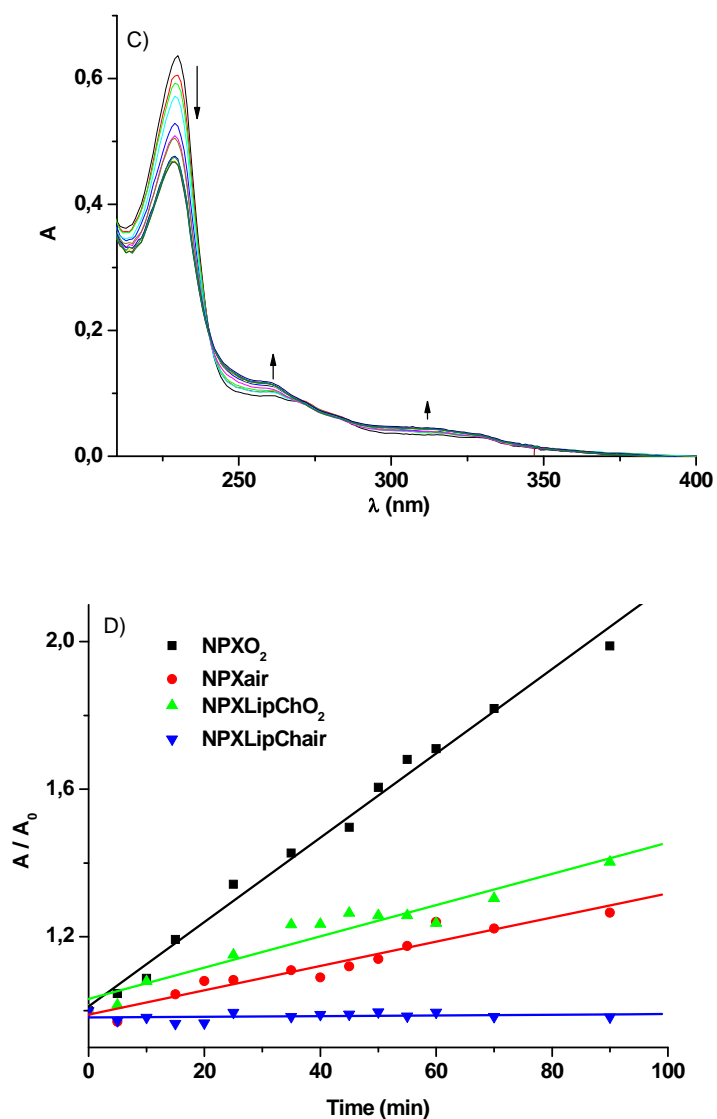


Figure 4. A), B) and C) UV spectra of oxygenated PBS solutions of NPX, NPXLip and NPXLipCh, respectively, after increasing irradiation times (every 5 minutes). **Inset:** UV spectrum of *k*-NPX. **D)** Increase of the absorbance at 250 nm for NPX and NPX within liposomes with Ch under air and O_2 atmosphere as a function of the irradiation time.

8.3. Conclusions

The present work has revealed a different behavior between NPX entrapped in liposomes with and without Ch under aerobic conditions. Inclusion of the drug in supramolecular complexes as liposomes appears interesting in connection with oxidative damage in a cell-membrane like system. Steady state studies show that encapsulation of NPX in liposomes does not constitute a physical barrier for the interaction with light; however, the presence of Ch in these biomimetic systems is a relevant parameter for photostability, providing protection against oxidative photodegradation.

For more details:

- [1] Lasic, D. D.; Papahadjopoulos D. *Science* 1995, 267, 1275-1276.
- [2] Chetanachan, P.; Akarachalanon, P.; Worawirunwong, D.; Dararutana, P.; Bangtrakulnonth, A.; Bunjop, M.; Kongmuang, S. *Adv. Mater. Res.* 2008, 55-57, 709-711.
- [3] Liang, X. F.; Wang, H. J.; Luo, H.; Tian, H.; Zhang, B. B.; Hao, L. J.; Teng, J. I.; Chang, J. *Langmuir* 2008, 24, 7147-7153.
- [4] Sharma, A.; Sharma, U. S. *International Journal of Pharmaceutics* 1997, 154, 123-140.
- [5] Mulder, W. J. M.; Strijkers, G. J.; Tilborg, G. A. F.; Griffioen, A. W.; Nicolay, K. *NMR Biomed.* 2006, 19, 142-164.
- [6] Lasic, D. D. In *Vesicles*; Rosoff, M.; Ed.; Marcel Dekker: New York, 1987; Vol. 62, p 447.
- [7] *Liposomes as drug carriers: Recent Trends and Progress*; Gregoriadis, G.; Ed.; John Wiley & Sons: New York, 1988.
- [8] Lasic D. D. *Trends in Biotechnology* 1998, 16, 307-321.
- [9] Armitage, B.; O'Brien, D. F. J. *Am. Chem. Soc.* 1992, 114, 7396-7403.
- [10] Chatterjee, S. N.; Agarwal, S. *Free Radic. Biol. Med.* 1988, 4, 51-72.

[11] Xu, L.; Davis, T. A.; Porter, N. A. J. *Am. Chem. Soc.* 2009, 131, 13037-13044.

[12] Bombelli, C.; Caracciolo, G.; Profio, P.; Diociaiuti, M.; Luciani, P.; Mancini, G.; Mazzuca, C.; Marra, M.; Molinari, A.; Monti, D.; Toccaceli, L.; Venanzi, M. *J. Med. Chem.* 2005, 48, 4882-4891.

[13] Bennett, D. E.; Lamparski, H.; O'Brien D. F. *J. Lipo. Res.* 1994, 4, 331-348.

[14] Stuttgen, G. *Drugs* 1988, 36, 43-48.

[15] Partyka, M.; Au, B. H.; Evans, C. H. *J. Photochem. Photobiol. A-Chem.* 2001, 140, 67-74.

[16] Boscá, F.; Marín, M. L.; Miranda, M.A. *Photochem. Photobiol.* 2001, 74, 637-655.

[17] Costanzo, L. L.; De Guidi, G.; Condorelli, G. *J. Photochem. Photobiol. B: Biol.* 1989, 3, 223-235.

[18] Boscá, F.; Miranda, M. A.; Vaño, L.; Vargas, F. *J. Photochem. Photobiol. A: Chem.* 1990, 54, 131-134.

[19] Jiménez, M. C.; Miranda, M. A.; Tormos, R. *J. Photochem. Photobiol. A: Chem.* 1997, 104, 119-121.

[20] Musa, K. A. K.; Eriksson, L. *A. J. Phys. Chem. A.* 2008, 112, 10921-10930.

[21] De la Peña, D.; Martí, C.; Nonell, S.; Martínez, L. A.; Miranda, M. A. *Photochem. Photobiol.* 1997, 65, 828-832.

[22] Soichiro, W.; Michiko, I. *J. Org. Chem.* 1997, 62, 8616-8617.

[23] Tavano, L.; Muzzalupo, R.; Cassano, R.; Trombino, S.; Ferrarelli, T.; Picci, N. *Colloid Surfaces (B)* 2010, 75, 319-322.

[24] Nii, T.; Ishii, F. *Int. J. Pharm.* 2005, 298, 198-205.

[25] Bangham, A.D.; Standish, M.M.; Watkis, J.C. *J. Mol. Biol.* 1965, 13, 238-252.

[26] Bernsdoff, C.; Wolff, A.; Winter, R.; Gratton, E. *Biophys. J.* 1997, 72, 1264-1277.

[27] De Rosa, G.; De Stefano, M.; Ungaro, F.; La Rotonda, I.M. *Int. J. Pharm.* 2008, 362, 189-192.

[28] Möller, M.; Botti, H.; Batthyany, C.; Rubbo, H.; Radi, R.; Denicola, A. *J. Biol. Chem.* 2005, 280, 8850-8854.

[29] Moore, D. E.; Chappuis, P.P. *Photochem. Photobiol.* 1998, 47, 173-180.